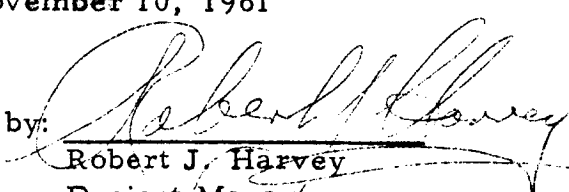FINAL REPORT

for

PHASE I

SET GENERATOR PROGRAM

TEE-4013-8

Submitted by

Thermo Electron Engineering Corporation

November 10, 1961

Approved by:

Robert J. Harvey

Project Manager

LEGAL NOTICE

FOREWORD

This report is the final report summarizing work performed during Phase I of the SET Generator Program, extending from May 22 through October 20, 1961. This report is submitted in compliance with the requirements of paragraph 4, Article IV, of Contract No. 11483 with Electro-Optical Systems, Inc.; subcontract on JPL's Contract No. 950109.

SUMMARY

Phase I of the SET Generator Program has been completed, the results of which are contained in this report.

The design and analysis of the SET Generator have been completed. A thermal test model generator to verify cavity design was designed, fabricated, and delivered to EOS for testing. Eighteen diodes were fabricated, of which eight were extensively tested. Three diode test devices were designed, fabricated, and used for diode testing. An electron-bombardment heater for the SET Generator was designed, and parts were fabricated. The proceedure for conducting the diode sublimation test was written and approved. The test set-up was assembled and used in diode life testing. The JG-P generator was designed, parts were fabricated, and all sub-assemblies were completed. The completion awaits only the selection of a representative diode and the final assembly of the JG-P generator. The fixture for assembling the SET generator was designed, fabricated, assembled, and successfully checked out, using the JG-P generator. The brazing fixture for the final assembly of the diode support structure was designed, fabricated, and successfully used on the brazing of the JG-P diode support structure.

The principal problem encountered on the SET program was mechanical difficulty with the SET diode. The solution of this problem delayed the program, and required sacrificing diode performance for life and reliability. The final diodes fabricated during phase I have shown that the diode design is such that it (a) can be reliably fabricated to give excellent reproducibility from diode to diode, (b) has a long life (greater than 600 hours), and (c) is capable of withstanding at least 20 thermal cycles.*

SET generators, based on the present diode design, can now be fabricated. To meet the JPL specification for the SET generator, diode performance must be raised back to and beyond their former levels, without jeopardizing the life and reliability established thus far.

---

*One diode successfully withstood over 115 thermal cycles.

TABLE OF CONTENTS

LIST OF ILLUSTRATIONS

LIST OF TABLES

LIST OF TABLES (continued)

I. INTRODUCTION

A program to develop a solar thermionic generator for use as a power supply for interplanetary space missions was initiated by the Jet Propulsion Laboratory in May 1961. Electro-Optical Systems, Inc., was selected as the prime contractor with Thermo Electron Engineering Corporation as the principal subcontractor to supply the thermionic generator for the solar-energized space power system. The undertaking was designated as the SET program, the first phase of which was to be completed by November 1961. The SET system was tentatively being considered for the Mariner Spacecraft.

The objective of Phase I of the generator program at Thermo Electron was to deliver two test model generators and two SET generators to Electro-Optical Systems, Inc., for further testing.

The original specifications for the SET generator are summarized in Table I-1. These specifications were to be met at the end of Phase II of the program. The performance objectives of Phase I were not specifically established, the general guideline being to approach these alternate specifications as closely as possible.

The general objectives of the program were divided into two groups, according to order of importance. These are:

Group I:

    (a) Reliability,

    (b) Life in Space

    (c) Efficiency.

Group II:

    (a) Weight,

    (b) Size,

    (c) Cost.

The two test model generators were to verify specific design features of the SET generator. The first of these was designated as the dummy cavity, the purpose of which was to corroborate the thermal design of the cavity for the SET generator;

in particular, it was to determine temperature differences over the cavity surface. The second of the test model generators, designated as generator JG-P, was to be fabricated as a means of checking the ability of the SET diode, while mounted in the SET generator configuration, to withstand the dynamic environmental conditions encountered during a missile launch.

The two complete SET generators were designated as JG-1 and JG-2. JG-1 was to be thoroughly tested at Thermo Electron, including a 1000-hour life test, and then delivered to EOS. JG-2 was to be delivered to EOS for system testing, after qualification testing at Thermo Electron.

To complete the requirements of the program, work was needed in the following areas:

    (1) SET generator design,

    (2) SET diode,

    (3) cesium reservoir temperature control,

    (4) diode test devices,

    (5) electron-bombardment heater,

    (6) diode sublimation test,

    (7) dummy cavity,

    (8) JG-P generator,

    (9) SET generator assembly fixture, and

  (10) brazing fixture for the support structure.

This report is organized into individual sections according to the breakdown described above.

II.   SET GENERATOR DESIGN

A.   Configuration

1.   General

The thermionic generator required to convert the thermal energy of
concentrated solar flux to electrical energy consists of five diodes arranged
to form the five faces of a cube, with the cavity entrance located on the sixth
face (see Fig. II-1). Thermal energy is focused at the entrance of the cavity
by the solar concentrator. As the solar flux passes through the cavity entrance
into the cavity proper, it diverges since it has already passed through the image.
However, even with this dispersion, a disproportionate amount of flux falls
directly on the rear diode. Therefore, the rear diode (see Fig. II-2) has been
specifically designed to reflect a considerable portion of the incident flux to
the four adjacent side diodes instead of absorbing the total. The diode cavity
faces of the side diodes (see Fig. II-3) are designed to absorb as much of the
incident and reflected flux as possible. The intersection of these five cylindrical
diodes forms the thermal cavity of the generator (see Fig. III-4).

_II - 4_

2.   Generator Performance and Materials

PROPOSED

The performance of the thermionic generator is shown in Table II-1. The
performance cited in this table is based on analytically determined values. How-
ever, the analytical methods have been tempered by previous experimental
experience at Thermo Electron and are expected to agree quite closely with the
actual generator performance.

The materials to be used in various parts of the thermionic diode are
described in Section III. The choice of electrical lead materials was made with the
aid of the information presented in Table II-2. Because of the low emissivity of
rhodium and its relatively low evaporation rate, it was decided to plate the inner
walls of the diode support structure and portions of the front cone with rhodium.
After several unsuccessful attempts to obtain satisfactory rhodium plating at an
electroplating firm, the following tests were run in an attempt to obtain a

satisfactory method of rhodium plating.

Several 1-in^2 test pieces were prepared from 0.005-in. molybdenum sheet stock. They were ultrasonically degreased with trichlorethylene and boiled for 5 minutes in a 20% KOH solution to remove oxide films. These pieces were then electroplated in a solution of rhodium sulfate at various current densities (from 7 ma/m^2 to 2 amp/m^2) and for times ranging from 10 sec to 1 hour. In all cases, the adherence of the rhodium was very poor; flaking occurred as the deposit built up. The surfaces of several pieces were roughened with sand paper; in these cases the rhodium plated well, with no apparent limit to the thickness of the plate that could be deposited. However, the finished surface was quite rough. Polishing would only result in bare spots where the molybdenum high spots existed. Therefore, additional work was done.

Rhodium plating was also attempted on test pieces cut from sheet stock that had been hydrogen- or vacuum-fired at 1400°C for 30 minutes and immediately placed in acetone to prevent oxidation upon removal from the furnace. The results were also unsatisfactory.

Next, a piece of 0.25-in. molybdenum rod was prepared with various surfaces, as shown in Fig. II'-5. The piece was hydrogen-fired and immersed in acetone; the various surfaces were then rhodium plated at 0.125 amp/m^2 for 40 minutes. On the polished surface, the adherence was very poor, with much peeling and flaking. The smooth machined surface exhibited only slightly better characteristics. The plate on the other two surfaces (the rougher surfaces) appeared quite satisfactory.

A similar test, using 0.75-in. diameter by 0.125-in. molybdenum discs, was performed. The adherence to the smooth surface was poor, but much better on the rougher surfaces.

Test pieces were then prepared from sheet material, cleaned cathodically with dilute H_2SO_4, and anodically with 20% KOH. The resulting plate showed no improvement. From these experimental results, it became increasingly obvious that the cleanliness of the molybdenum surface was not necessarily the only factor affecting the quality of the rhodium plate. Other possible approaches were there-

fore investigated. It was suggested by Battelle Memorial Institute that a substrate plate such as nickel might improve rhodium adherence. Tests based on this principle were then made.

Test pieces were degreased, hydrogen-fired, nickel plated, and then rhodium plated. As the second plate built up, the nickel pulled away from the molybdenum surface. Substituting copper for nickel produced the same poor results.

However, a 0.75-in. molybdenum disc was vapor plated with copper, rhodium plated, and vacuum-fired for 15 minutes. The result was a smooth, mirror-finish, uniform rhodium plate. The vapor deposition of a thin copper plate on the actual generator parts would be exceedingly difficult due to their configuration. Therefore, an investigation of electroplating with copper directly on molybdenum was carried out. It was found that copper would adhere to the molybdenum surface better if the plating were followed by a hydrogen- and vacuum-firing at $900 \pm 50°C$. Rhodium plated to an acceptable degree on the copper surface in all thicknesses.

Following rhodium plating, the copper substrate was driven off by heating in vacuum to 1400°C for 15 minutes. Unfortunately, this process also seems to remove some of the rhodium plate; however, a thin rhodium film remains on the molybdenum surface. The most uniform rhodium plate is achieved when the copper substrate is quite thin. (A current density of 0.2 amp/m^2 for 2 minutes appears to be optimum for copper plating.)

Because of the previously mentioned difficulty of driving off the copper substrate while simultaneously maintaining a uniform rhodium plate on the molybdenum, further experiments, aimed at plating rhodium directly on molybdenum, were carried out.

The following cleaning procedure was recommended by Metals and Controls, a division of Texas Instrument Corp., the supplier of rhodium plating solutions:

(1) Cathodically clean in a saturated solution of tri-sodium phosphate, 180°F, at from 20 to 25 amp/ft^2 for 2 or 3 minutes.

(2) Thoroughly rinse with tap water.

(3) Dip in 50% nitric acid at room temperature for 10 or 12 seconds.

(4) Thoroughly rinse with tap water.

(5) Immerse for 5 minutes in a solution containing 10% chromic acid, 15% hydrocloric acid, 15% sulphuric acid, and 60% distilled water.

(6) Thoroughly rinse in cold water and quickly immerse in the rhodium sulphate plating solution. Plate at a current density between 15 and 20 amp/ft^2 and at a temperature between 110 and 120°F.

This procedure was tried on several test pieces under carefully controlled temperature and current density. Various methods of bath agitation, including ultrasonics, were also used. Several satisfactory pieces were obtained; however, the results were not consistent. The following information was obtained from this procedure:

(1) The test pieces plated well for the first 5 to 8 minutes. A few pieces plated well for longer periods.

(2) The nitric acid dip dulled the surface of the molybdenum, hence the rhodium plating was duller.

(3) When heavier plating was attempted, the pieces sometimes peeled after 5 to 8 minutes of plating.

(4) Vacuum-firing greatly improved the adherence of the rhodium and slightly improved the appearance of the plated pieces. However, the plate often appeared spotty after the firing. It was also noted that a rhodium plate with a tendency to peel, also peeled upon vacuum firing.

When it became evident that this procedure was not completely adequate, a more severe nitric acid etch was tried (one minute). After 8 minutes of rhodium plating, this piece also started to peel. This cleaning method therefore was considered inadequate. It was then decided to try to prepare the molybdenum surface by using a light vapor blast.

Thermo Electron had previously been notified that emissivity tests were to be conducted on rhodium plated molybdenum strips 7.5 in. $\times$ 0.4 in. $\times$ 0.005 in. and that these were to be sent to Pratt & Whitney for determination of spherical emissivity data in the 100 to 2000°K range. In addition, 0.75-in. diameter discs were to be prepared from the same 0.005-in. sheet material, using the same plating procedures. These discs and strips were lightly vapor blasted, rinsed in hot water and immediately immersed in acetone to prevent any oxidation.

An attempt was made to rhodium plate one of the discs by going directly from the acetone into the plating bath, using carefully controlled bath temperature and current density. The plate peeled badly after several minutes of plating. The same procedure was tried with bath agitation; however, the results were no better.

One of the discs was immersed in the previously prepared chromic-sulfuric-hydrochloric acid cleaning solution for 5 minutes, rinsed in cold running tap water, and rhodium plated for 15 minutes. The results were a bright, uniform rhodium plate with very good adherence. With the use of this technique, the strips were plated equally well. It was also observed that there was no apparent limit on the thickness of plate that could be deposited with or without bath agitation. The resulting plate could be polished to a high luster with a cloth buffing wheel and fine aluminum oxide and/or diamond paste. Also, it was discovered that immersion in acetone immediately after vapor blasting is not necessary if a dip in the chromic acid cleaning solution precedes plating. It remains now to try this procedure on the interior surfaces of a molybdenum block with two intersecting cylindrical holes.

B. Heat Balance

1. Generator Performance Characteristics

The calculation of the performance characteristics was made by a process of iteration. It introduced the calculation of the heat requirements made to generate the direct electrical output under the most efficient conditions and compared it with the actual heat available. This comparison indicated the electrical output obtainable with the available heat. The results of the calculations are shown in Table II-1. The

electrical output power obtained is 128 watts; therefore, based on a net heat of 647 watts received by the generator, the generator efficiency is 19.8%. The diode efficiency is 20.8%.

The calculations were based on a prediction of electrical characteristics of the thermionic diodes and on detailed calculations of the heat losses associated with the particular generator design. These heat loss calculations will be presented in later paragraphs of this section.

At present, the state of the art of thermionics is not sufficiently advanced to allow an accurate prediction, for a particular diode configuration, of either the electrical characteristics or the value of some of the thermal losses such as radiation, cesium conduction, and electron cooling. Thermo Electron's prediction of a power density of 14 w/cm^2 (the requirement of the present design) is based on experimental results obtained from a previous converter which operated at a power density of 11.6 w/cm^2, and which utilized a lower emitter temperature ( ) and a larger interelectrode spacing.

The prediction of direct radiation in a cesium converter is subject to error because emission and absorption of electromagnetic radiation by a hot surface can be affected by cesium coverage. This effect has not been considered in these calculations. To date, no satisfactory measurements of cesium conduction at small interelectrode spacings have been performed. As the process of conduction in partially ionized cesium is very intricate, theoretical predictions are subject to considerable error. For the purpose of these calculations, it has been assumed that the maximum possible value of cesium conduction is that corresponding to the upper bound, in the absence of ionization as predicted by kinetic theory.

The magnitude of the electron cooling term involved in the calculation of ideal diode losses is also relatively unknown. A single model of the flow of electrons gives an easily evaluated expression; however, close examination of the transport properties undergone by emitted electrons reveals that substantial departures from the simple model are possible.

Despite the uncertainty of the evaluation of these losses, Thermo Electron believes that the calculations to follow are conservative. This belief is substantiated by application of the same loss theories to previous cesium converters, where the actual measured efficiency was higher than the predicted figure by more than 2%.

Calculations were also made to determine the performance characteristics of the SET generators for various possible conditions. Two calculations of particular interest are

(1) the calculation of generator heat losses and performance based on a diode designed to meet full objective specifications, and

(2) the calculation of generator heat losses and performance based on diode data obtained on unit IIIa and less optimistic values of the heat transfer constants.

Figure II-6 shows the various possible heat transfer paths within the SET generator. Tables II-2 through II-5 show the calculations based on the above conditions.

In the following paragraphs of this section, a complete heat transfer analysis of the SET generator is presented. The calculations were repeated for several diodes and design characteristics. Because of the lack of consistently good data on the emissivities of some surfaces at elevated temperatures, the following calculations were carried out for two extreme limits on the value of the emissivities (an optimistic and a pessimistic limit) as well as for the anticipated values (the most probable). Where sufficient data were available, only the correct value was used.

The results of the calculations for the final design of diode IIIb are shown in the flow diagram (Fig. II -6) and Tables II-3 through II-5. The values given are based on the information available as of September 1, 1961.

2. Over-all Heat Balance Nomenclature

Every component of the generator is given a letter symbol. The heat flow between two such components is denoted by three indices; two letter indices to show the two components and a number index to indicate the mode of heat transfer:

A   flux control

H   cavity

F   front cone

D   cube block

E   emitter

C   collector

S   spacer

R   radiator

O   outside free space

1   heat transfer by radiation

2   heat transfer by conduction

3   heat transfer by electron cooling

Angle brackets ($\langle \rangle$) are used herein to denote the average value of a quantity.

3. Heat Flow Details

The various heat paths, the appropriate cross sections and assumptions are given in detail in the following sub sections:

a. $\langle Q \rangle_{AF1}$, Radiation Heat Flux Impinging on Front Cone

Radiation that does not enter the cavity impinges on the front cone. This value was computed from concentrator efficiency charts given by EOS for the point of operation at 160 million miles from the sun. For maximum misalignment allowed, the value is

$$\langle Q \rangle_{AF1} = 32 \text{ watts.}$$

b. $(\langle Q \rangle_{AF1})_{refl}$

The reflectivity ρ of the front cone (polished rhodium plating) for solar radiation is about 0.77. Thus, part of the impinging radiation would not be absorbed:

$$(\langle Q \rangle_{AF1})_{refl} = \rho \langle Q \rangle_{AF1} = 25 \text{ watts}.$$

c. $\langle Q \rangle_{HF1}$, Radiation from Cavity to Inside Lip of Front Cone (Rhodium Plated)

See Fig. II-7. Area exposed to radiation = 1.22 cm^2.

$$A = \frac{\pi}{4} (0.7^2 - 0.5^2) 2.54^2 = 1.22 \text{ cm}^2.$$

Surface emissivity (insufficient data):*

$$\epsilon = 0.08 \text{ (opt)}$$
$$= 0.13$$
$$= 0.20 \text{ (pess)}.$$

Radiation between blackbody of cavity to surface:

$$\langle Q \rangle_{HF1} = A \epsilon \sigma (T_H^4 - T_F^4),$$

$$T_H = 2000° K \quad \text{and} \quad T_F = 1000° K.$$

$$\langle Q \rangle_{HF1} = 8 \text{ watts (opt)}$$
$$= 14 \text{ watts}$$
$$= 21 \text{ watts (pess)}.$$

d. $\langle Q \rangle_{HD1}$, Radiation From Cavity to Block Cube

The radiation from the thermal cavity to the diode support block is of two categories:

$\langle Q \rangle'_{HD1}$, radiation to exposed triangles,

$\langle Q \rangle''_{HD1}$, radiation between emitter.

Exposed triangles area (four triangles).

$$\text{Area} = 4 \times \frac{1}{2} (1.40 \times 0.30) = 0.84 \text{ cm}^2$$

---

*Where three valves are given for a heat transfer coefficient, the first (opt) represents the optimistic value; the third (pess) represents the pessimestic value, and the second (not marked) represents the most probable value.

For $\epsilon = 0.8$, $\langle Q \rangle'_{HD1} =$ 5. 7 watts (opt).

For $\epsilon = 0.13$, $\langle Q \rangle'_{HD1} =$ 9. 3 watts.

For $\epsilon = 0.20$, $\langle Q \rangle'_{HD1} =$ 14. 2 watts (pess).

<u>Area between emitters (eight openings) depends on the design space</u>
<u>between emitters.</u> For the three design values,

| space, in. | 0.002 (opt) | 0.005 | 0.009 (pess) |
| area, cm^2 | 0.049 | 0.122 | 0.220. |

Radiation from cavity and emitter sides will impinge on the diode support block. Of this, part will be absorbed and part will be reflected to emitter (see Fig. II-8). For a block emissivity between 0.08 and 0.20 and an emitter emissivity of 0.23, the equivalent heat flow will be radiation from blackbody to surface of apparent emissivity of

$$\epsilon_{app} = 0.4 \text{ (opt)}$$
$$= 0.6$$
$$= 0.8 \text{ (pess)}.$$

Therefore,

		(opt)		(pess)
space, in.		0.002	0.005	0.009
$\langle Q \rangle''_{HD1}$, watts	$\epsilon_{app} = 0.4$	1.7	4.1	7.5 (opt)
$\langle Q \rangle''_{HD1}$, watts	$= 0.6$	2.5	6.2	11.3
$\langle Q \rangle''_{HD1}$, watts	$= 0.8$	3.3	8.3	15.0 (pess)

For spaces of 0.005 in. and 0.009 in., the total heat flow

$$\langle Q \rangle_{HD1} = 14.0 \text{ (opt and 0.005 in.)}$$
$$= 24.0 \text{ (average and 0.009 in.)}$$
$$= 29.0 \text{ (pess and 0.009 in.)}.$$

e. $\langle Q \rangle_{EC}$, Heat Flow Between Emitter and Collector

The heat flow between the emitter and collector can be divided into three parts. These are:

(1) radiation, Q_{EC1},

(2) conduction through cesium, Q_{EC2}, and

(3) electron cooling, Q_{EC3}.

The emitter surface temperature will be lower than the cavity temperature due to conduction resistance.

$$\Delta T = \frac{Q_{cond}}{Ak} \Delta x,$$

$A = 2 \text{ cm}^2 / \text{diode}$,

$k = 0.6 \text{ w cm}^{-1} \text{ }^\circ K^{-1}$,

$\Delta x = 0.5 \text{ cm}$,

$Q = 80 \text{ w/diode (to be checked later)}$,

$\Delta T \approx 30^\circ K$,

$(T_E)_{surf} = 1970 \text{ }^\circ K.$

$\langle Q \rangle_{EC1}$, Radiation loss from emitter to collector. The heat loss from emitter to collector may be calculated as follows:

$$Q_{EC1} = A(\epsilon_E^{-1} + \epsilon_C^{-1} - 1)^{-1} \sigma (T_E^4 - T_C^4),$$

$T_E = 1000^\circ K$

(variation of T_C will have only a small effect on the heat flow),

$\epsilon_E = 0.232 \text{ (at } 1970^\circ K),$

$\epsilon_C = 0.14 \text{ (opt) at } 1440^\circ K$

$\qquad = 0.18 \text{ (at } 1400 \text{ }^\circ K)$

$\qquad = 0.22 \text{ (pess) at } 1400^\circ K,$

Area $= 2 \text{ cm}^2 /\text{diode}$,

$\langle Q \rangle_{EC1} = 5 Q_{EC1} = 76 \text{ watts (opt)}$

$\qquad\qquad\qquad = 90 \text{ watts}$

$\qquad\qquad\qquad = 101 \text{ watts (pess)}.$

$\langle Q \rangle_{EC2}$, Cesium conduction. From experimental data obtained at Thermo Electron, the conduction losses at the operating temperature of the diode are found to be 3.5 watts/cm^2.

$$\langle Q \rangle_{EC2} = 35 \text{ watts.}$$

$\langle Q \rangle_{EC3}$, Electron cooling losses. This quantity includes the energy loss of electrons between emitter and collector over and above the useful power.

From measurements at Thermo Electron, it is found that

$$q_3 = 1.67 \text{ w/amp.}$$

Therefore,

$$\langle Q \rangle_{EC3} = 8.35I,$$

where I is the current of a diode.

e. Other Emitter Losses

Other emitter losses may be grouped into one of two categories: losses from the sides of the emitter holder to the cube block, $\langle Q \rangle_{ED1}$; and losses by conduction through the spacer, $\langle Q \rangle_{ES2}$ (see Fig. II-9).

The spacer is arbitrarily divided into two regions:

(1) where good contact with emitter exists (temperature may be assumed equal to emitter temperature) and

(2) thin cross section (with variable temperature).

$\langle Q \rangle_{ED1}$, Emitter block loss. The heat losses from the emitter to the diode support block are:

$$Q_{ED1} = A(\epsilon_E^{-1} + \epsilon_D^{-1} - 1)^{-1} \sigma(T_E^4 - T_D^4),$$

$$\text{Area} = 1.54 \text{ cm}^2,$$

$$\langle T \rangle_E = 1985°K,$$

$$T_D = 1000°K,$$

$$\epsilon_E = 0.232 \text{ at } 1985°K,$$

ϵ_D = 0.08 at 1400°K (opt)

= 0.12 at 1400°K

= 0.14 at 1400°K, (pess)

$\langle Q \rangle_{ED1} = 5Q_{ED1}$ = 39 watts (opt)

= 53 watts

= 59 watts (pess).

$\langle Q \rangle_{ES2}$, Heat conducted from emitter to spacer. This quantity can be calculated only by finding the temperature distribution in the spacer, which requires a trial-and-error calculation. The spacer is divided into nine sections, each 1 mm long. A heat flux is assumed and is checked by fitting the boundary conditions. The assumptions involved are:

	(opt)		(pess)
ϵ_S =	0.21'	0.21	0.21
ϵ_C =	0.12	0.14	0.14
ϵ_D =	0.055	0.08	0.12

Refer now to Fig. II-10.

$$Q_{out} = Q_{in} - \Delta Q_{SC1} - \Delta Q_{SD1},$$

$$\Delta T = \frac{Q_{in} + Q_{out}}{2} \frac{\Delta X}{A_S k},$$

$$\Delta Q_{SC1} = \Delta A_{SC1} (\epsilon_S^{-1} + \epsilon_C^{-1})^{-1} \sigma (T_S^4 - T_C^4),$$

$$\Delta Q_{SD1} \quad \Delta A_{SD1} (\epsilon_S^{-1} + \epsilon_D^{-1})^{-1} \sigma (T_S^4 - T_D^4),$$

$$A_S = \pi \times 1.64 \times 0.00508 = 0.026 \text{ cm}^2 \text{ (spacer thickness, 2 mils)},$$

$$\Delta A_{SC1} = \Delta A_{SD1} = \pi \times 1.64 \times 0.1 = 0.515 \text{ cm}^2,$$

$$T_D = T_C \approx 1000°K.$$

With the above data, the heat quantities are found to be:*

$$\langle Q \rangle_{ES2} = 133 \qquad\qquad 140 \qquad\qquad 147$$

$$\langle Q \rangle_{SC1} = 75 \qquad\qquad 48 \qquad\qquad 47$$

$$\langle Q \rangle_{SD1} = 24 \qquad\qquad 31 \qquad\qquad 41$$

$$\langle Q \rangle_{SR2} = \underset{\text{(opt)}}{66} \qquad\qquad 61 \qquad\qquad \underset{\text{(pess)}}{59}$$

4. Steady-state Temperatures

The steady-state temperature distribution depends on the power input and boundary conditions. The power output is controlled to maintain a cavity temperature of 2000°K. The outside surface of the generator sees itself and free space.

The steady-state temperatures of the following components are of interest:

(1) front cone,

(2) cube block,

(3) radiator, and

(4) cesium reservoir.

Although each of the above components is not at a uniform temperature, it will be assumed that the average temperature prevails throughout the component.

a. Front Cone

Refer to Fig. II-11. The net heat input into the front cone is

$$Q_{in} = Q_{AF1} - (Q_{AF1})_{refl} + Q_{HF1} = 15 \text{ watts (opt)}$$

$$= 21 \text{ watts}$$

$$= 28 \text{ watts (pess).}$$

This same amount must be dissipated through the front surface.

If the heat radiated from the polished surface is neglected, it is found that

$$\langle Q \rangle_{FO1} = A_{rough} \, \epsilon \sigma T_F^4,$$

$$\epsilon = 0.7,$$

---

*All quantities are in watts

$$A_{rough} = \frac{1}{4}\pi \times (5^2 - 4^2) = \frac{9}{4}\pi = 7.07 \text{ cm}^2,$$

$$T_F^4 = \frac{\langle Q \rangle_{FOl}}{A\epsilon\sigma},$$

Hence,

Q_{FOl}, watts	15	21	28
T, °K	860	930	1000

In this analysis, no heat interaction between the cube block and the front cone was taken into account although one exists until a temperature equality between the two components is established. The rough area is an easily changed design value and any desired temperature can be maintained.

b. Cube Block

The heat input to the cube block is

$$\langle Q \rangle_{DOl} = 75 \text{ watts (opt)}$$

$$= 108 \text{ watts}$$

$$= 129 \text{ watts. (pess)}$$

Most of this must be radiated to free space, although some of it can be conducted through the support ring.

The amount radiated to free space is

$$(A_D)_{exposed} F \epsilon_D T_D^4, \text{ where}$$

$$(A_D)_{exposed} = (3.8 \times 3.8 + \frac{3.8}{3.0} \times 4) - 5 \times \frac{\pi}{4} 2.65^2$$

$$= 33.4 \text{ cm}^2,$$

$$\epsilon_D = 0.7.$$

F is the view factor of the cube in free space. It is difficult to calculate the actual value of A. Therefore, with the aid of Fig. II-12, the following calculations can be made:

$$\partial_2 = \left(\frac{4}{\pi}\right)^{1/2} \times 3.8 = 4.2 \text{ cm}$$

$\partial_1 = 2.6$ cm.

NACA TN 2836 gives the view factor for some shapes:

$F_{31} = 0.222$,

$F_{32} = 0.358$,

$F_{30} = 1 - F_{31} - F_{32} = 1 - 0.222 - 0.358 = 0.420.$

Effective area $= (A_D)_{exposed} F_{30} = 14.0$ cm^2

Therefore,

Q, watts	56	75	108	129
T, °K	1000	1080	1180	1230

To maintain the cube block temperature at or below 1000°K, it will be necessary to utilize the support ring to conduct away the excess heat.

c.   Radiator

The heat input $\langle Q \rangle_{RO1}$ is approximately 410 watts (for all cases).

$$\langle Q \rangle_{RO1} = 5 \Sigma (AF\epsilon) \sigma T_R^4,$$

Figure II-13 shows the heat flow at the radiator.

$F_{13} = 0.325.$

Actually, only about 60% of the area below (3) is blocked; thus,

$F_{10} = 1 - 0.6 \times 0.325 = 0.805$,

$F_{20} = 1$,

$A_1 = 2\pi r_1 \ell = 2\pi \times 2.4 \times 2.6 = 3.92$ cm^2,

$A_2 = \pi(r^2 - r_{Cs}^2) = \pi(2.4^2 - 1.3^2) = 12.8$ cm^2,

$\epsilon_1 = 0.70$,

$(\epsilon_2)_{eff} = 0.80$,

$Q = 5 \times 32.3\sigma T_R^4 = 161.5\sigma T_R^4,$

$$Q = 410,$$
$$\langle T \rangle_R = 820^\circ K.$$

If surface emissivity is made 0.6, the average temperature will be
$$\langle T \rangle_R = 850^\circ K.$$

For a detailed analysis of the cesium resevoir temperature control and heat flux calculations refer to Section IV. The calculations and analysis of the start-up procedure are also included in that section.

C.   Mechanical Design

1.   General

As stated in Section II. A, the SET generator is basically cubical. Five diodes form five sides of the cube, while on the sixth side is the entrance of the cavity, through which the thermal energy enters the cavity. A detailed description and analysis of each of the component parts of the generator are included in the following sections of this report. For the most part, only general concepts of the design and mechanical configuration will be discussed in this section.

2.   Weight Breakdown

The weights of the various components of the SET generator are shown in Table II-6 . For calculation of diode weight, the diode was separated into its two component parts, the emitter and collector. Considering the density of tungsten to be 19.3 gm/cm^3, and the density of tantalum to be 16.6 gm/cm^3, the emitter weight was calculated to be 18.17 gm/diode. The weight of the collector, consisting of tungsten (19.3 gm/cm^3), molybdenum (10.2 gm/cm^3), and nickel (8.9 gm/cm^3), was found to be 36.06 gm/diode.

The weight of the niobium-ceramic support associated with each diode was calculated, using ρ = 8.6 gm/cm^3 for niobium and ρ = 4 gm/cm^3 for the ceramic parts. The total weight per diode for these parts was found to be 20.15 gm.

The weight of the copper radiating fin was calculated by dividing the radiator into segments, then adding the weight of each segment. Using a density of 8.93 gm/cm^3 for copper, the radiator weight per diode may be calculated as 78.73 gm.

The copper interconnecting leads were considered as strips with a cross section 1 X 0.55 cm, and 3.18 cm in length. The total weight of the six leads was found to be 93.50 gm.

The cesium reservoir, consisting of a nickel tube 0.125 in. in diameter and a nickel heating block which surrounds the tube, was calculated to weigh 5.46 gm/diode, using the density of nickel given above.

The molybdenum support structure, designed to include the conical front face and the cubical emitter support block, calculated with ρ = 10.2 gm/cm^3, weighed 626 gm.

3. Allowance for Thermal Expansion

Calculations were made to determine the change in the critical clearances within the SET generator as the diodes were warmed from room temperature to operating temperatures. To maintain the desired clearances at operating temperature, minor dimensional changes were required. The most critical point is that between the 45° faces of the adjacent emitter cavity faces. The maximum space between these at room temperature should not exceed 0.0141 in. so that the desired spacing of 0.009 in. can be maintained at operating temperature.

Since the front cone of the diode support structure is removable, these tolerances can be checked during the assembly procedure (see Section X) with a 0.014-in. feeler gauge. By careful inspection of all other dimensions of the diodes and the supporting block relative to the diode seat, and by checking the interdiode clearance, all other critical tolerances should be achieved.

Thermal expansion also creates a problem in the electron-bombardment heater testing of the SET generator, and with similar test apparatus designed by EOS. To facilitate testing with the electron-bombardment heater, the front cone

and the support structure are separate pieces, which can be assembled after initial testing of the generator has been completed. These two pieces must therefore by thermally independent of each other; that is, the front cone and the supporting block must each be capable of dissipating the maximum amount of heat that could be absorbed by each without either exceeding a temperature of 1000°K. Calculations (see Sections II. B. 4. a and b) have shown that the front cone has sufficient emissive area to meet this requirement; however, the diode support block required additional radiating area during testing. This additional area is provided by a thermal connection of the block to the anodized aluminum generator support ring, thus ensuring diode support block temperatures of less than 1000°K. To provide for the differential thermal expansion between the molybdenum block and the aluminum support ring, as well as to provide good thermal contact, the mounting brakets are designed to permit a sliding action at the interface. Copper bypass straps, brazed to the brackets on the diode support block, are connected to the aluminum support ring to ensure adequate and uniform heat transfer. The design of the SET generator is quite intricate, and requires the proper temperature distribution throughout the generator for proper operation.

III. SET DIODE

A. Basic Design

1. General

The configuration of the diodes for the SET generator must be such that when mounted on the diode support structure, the diodes form the cavity walls. Since the SET generator is to produce 133 watts of electrical power when 758 watts of thermal radiation enters the 0.5 in. diameter cavity entrance, each of the five diodes must produce 26.6 watts of output power, with a thermal input power of 128 watts. A cavity temperature of 2000°K had been selected as the operating temperature for the SET generator.

To achieve the necessary diode efficiency, the desired power output must be achieved at power densities in the neighborhood of 14 w/cm^2 and with diode output voltages of one volt or greater. Achievement of the desired diode performance is a function of emitter material, interelectrode spacing, and the optimization of the collector temperature and cesium pressure. In addition, diode efficiency depends on diode heat losses, such as those through the emitter support.

2. Diode Configuration

The basic configuration selected for the SET diode is shown in Fig. III-1. The emitter (1) is supported by a thin-walled tantalum sleeve (2), which is brazed to the center niobium ring of the diode leadthrough (5). The collector is brazed to the bottom niobium ring, which is mechnically fastened to the emitter ring through a ceramic ring forming the diode leadthrough (5). The radiator (7) and the tubulation to the cesium reservoir (8 and 9) are brazed directly to the base of the collector. The diode is supported by means of a niobium ring (6) from the diode support structure of the diode leadthrough, through another ceramic ring which acts as an electrical insulator between the diode and support structure.

3. Selection of Emitter Diameter

The most important design parameter of the diode is the emitter diameter. Its selection establishes the output power of the diode, the heat flux through the

diode, the size of the other diode parts, and the size of the cavity itself.

The diode efficiency depends on emitter diameter, as shown in Fig. III-2. The curve in Fig. III-2 is for a constant output power of 27 watts. Therefore, the power density decreases for increasing emitter diameter.

For the purpose of finding the optimum design point, it was assumed that optimum thermionic generator performance would correspond to the design point optimizing the efficiency of the thermionic diodes. The optimization of diode efficiency was then conducted as follows:

(1) Based on the experimental I-V curves obtained from a diode that produced 11.6 w/cm^2 at a spacing of 2.5 ± 0.5 mils, an emitter temperature of $1920°K$, and a cesium temperature of $603°K$ and, based on correlation procedures evolved at Thermo Electron for the prediction of I-V curves, the I-V curve to be obtained at a spacing of 1.77 mils, an emitter temperature of $2000°K$, and a cesium temperature of $600°K$ was calculated. The equation giving the I-V characteristic found is

$$V_o = 1.200 + 0.207 \ln \frac{24.8 - J_o}{J_o}.$$

(2) Assuming that a total electrical power output of 135 watts (27 watts per diode) had to be produced, it was possible to obtain, for each point of the predicted I-V curve, the required emitter area and, hence, the required emitter diameter.

(3) Assuming losses as follows:

electron cooling $Q_e = (2.11 + V_o) I_o A_E$ watts,

direct radiation $Q_r = 9.45 A_E$ watts,

cesium conduction $Q_{Cs} = 6.82 A_E$ watts,

conduction in spacer $Q_c = 4.98 D_E$ watts,

additional internal radiation loss $Q_{r1} = 1.61 D_E$ watts,

external radiation loss $Q_{r2} = 6.58 D_E$ watts,

III-2

where A_E is the emitter area in square centimeters and D_E is the emitter diameter in centimeters; and assuming a voltage drop in the leads of

$$\Delta V = 0.010 + 0.00469 J_o D_E \text{ volts,}$$

it was possible to obtain a predicted efficiency for each possible emitter diameter. The results of this calculation are plotted in Fig. III-2.

(4) From Fig. III-2, the value

$$D_E = 1.560 \text{ cm} \qquad (A_E = 1.91 \text{ cm}^2)$$

was selected as the emitter diameter.

4. Diode Leadthrough

Another critical design parameter is the diameter of the diode leadthrough. It is critical not only from the standpoint of diode performance, but also from the standpoint of design flexibility in overcoming the mechanical problems of the ceramic-to-metal joints in the diode leadthrough. The limitation of design freedom arises from the amount of space available for the leadthrough once the front cone angle was established as 62.5°. This is shown in Fig. III-3, where it can be seen that the closer the leadthrough is to the center of the cavity, the smaller its diameter must be in order not to interfere with the front cone angle. This restraint created two problems. It will be shown below how the interelectrode spacing is dependent on the location of the leadthrough. The second problem was that associated with the four metal-to-ceramic seals. There was little room for modifications in the leadthrough configuration to adjust the relative stiffness of the various connecting members. In section III.B, a description of how the latter problem was overcome is presented.

5. Interelectrode Spacing

The least possible spacing is achieved when the electrodes are in contact at the time of brazing (at approximately 1050°C). Upon cooling the diode, an interference fit would result at the interface of the emitter and collector. This would produce a rather high compressive stress at the interface and a balancing tensile stress in the spacer ring and diode support structure. This would result

in an undesirable situation since cold-welding at the emitter-collector interface might occur by diffusion during cool-down to room temperature. The condition for achieving the smallest interelectrode spacing at operating temperature, but at the same time obtaining a practical design in terms of fabricability, is to design the diode so that the electrode surfaces just come into contact when the diode is cooled to room temperature. This also offers the most support for the diode when high dynamic loads are applied by the diode environment, such as during launch.

The first design of the diode was examined to determine the extent of the problem in controlling spacing.

Upon cooling to room temperature from the brazing temperature of 1050°C, point A in Fig. III-4 was found to move down by $0.660 \times 0.0064 = 4.22$ mils.* The tantalum spacer contributes to the downward motion of point B by $0.410 \times 0.0073 = 3$ mils, and the niobium support ring contributes to the downward motion of point B by $0.250 \times 0.0085 = 2.12$ mils. This results in an interference fit of $(3 + 2.12) - 4.22 = 0.9$ mil.

It was felt that the situation could be alleviated by replacing a portion of the molybdenum with a material that has a higher coefficient of thermal expansion than tantalum and niobium but that would not hinder the flow of heat from the collector. Nickel is such a material. Its coefficient of thermal expansion is 16×10^{-6} °C^{-1} over the temperature range of interest. In addition, the thermal conductivity of nickel is comparable to that of molybdenum.

6. Selection of Material

The materials to be used for the various parts of the diode are indicated in Fig. III-6.

a.   Emitter

Tantalum was selected as the emitter material for the SET program because

---

*For thermal expansion data, see Fig. III-5.

good results had been achieved previously with tantalum emitters. Tantalum has good high-temperature properties, can be easily machined to the dimensions and shapes required, and (as will be shown in section III. A. 9. a) its evaporation rate is satisfactory for this program. A tantalum surface can be ground and lapped flat to within acceptable limits and can withstand the corrosive attack of a cesium atmosphere. The emissivity of tantalum at the operating temperature of the emitter is reported as 0.228.* Other material properties for tantalum at the operating temperature of the emitter are readily available. A tantalum emitter can be most easily used with the tantalum spacer.

b. Collector

Molybdenum was originally chosen as the collector material. Its material properties are better known than those of the other refractory metals. Molybdenum is easily machined to the desired shape; the required surface flatness can be achieved; it can be more readily outgassed than some of the other refractory metals; and it is compatible with the other diode materials. The thermal conductivity of molybdenum at the operating temperature of the collector is higher than that of any other refractory metal. When the conductivity per unit volume due to the lower density of the material is considered, the advantages of this material are even more obvious. Therefore, the temperature drop to the radiator can be minimized. Molybdenum resists cesium corrosion satisfactorily. The emissivity of molybdenum at the operating temperature of the collector is 0.14. Thermo Electron has had considerable experience in the brazing of other metals to molybdenum.

c. Spacer

Tantalum has been chosen as the spacer material because it could be easily machined into the required thin-walled cylinder, and because of its relatively low thermal conductivity. In addition, its coefficient of thermal expansion is comparable to that of molybdenum, and only slightly higher than that of tungsten.

---

*Kohl, p. 334.

This property facilitates stable 1-to 1.5-mil spacings at operating temperature.

The spacer also serves as the electrical lead from the emitter. The resistivity of tantalum, although slightly higher than that of tungsten and molybdenum, is acceptable.

Tantalum spacers have been successfully used on other thermionic generators at Thermo Electron.

d. Brazes

The brazes used in the thermionic generator for the SET program are those developed by Thermo Electron for similar applications.

The brazes for the SET diode are listed in Table III-1, along with the location of the braze and the melting point of the braze.

e. Other Diode Materials

The radiator for the SET diode is made of copper with a Rokide coating on the exterior surface. The copper minimizes the temperature drop along the radiator, and the Rokide coating provides a highly emissive surface to dissipate rejected heat. This oxide layer increases the surface emissivity to 0.90.*

The cesium reservoir and the tubulation to the diode are made of nickel. Nickel resists cesium corrosion, can be easily machined, and it is readily available at moderate prices. Nickel tubing can be obtained in a variety of sizes as an off-the-shelf item. Nickel can be brazed to other metals quite readily.

The exhaust tubulation for outgassing and cesium-charging consists of a thick-walled copper tube. Copper resists cesium corrosion at reservoir temperatures and, most importantly, copper tubulation can be reliably crimped off.

The diode leadthrough consists of two high-density alumina rings and three niobium rings. The coefficients of thermal expansion of these two materials are quite similar, and both resist cesium corrosion satisfactorily

---

*Rokide coating data sheet, Norton Company, Worcester 6, Massachusetts

at their operating temperature.

7. Temperature Distribution in Diode

To achieve the operating temperatures of the diode, finite temperature drops will be incurred across the emitter and collector. The values of thermal conductivity shown in Fig. III - 7 for tantalum and molybdenum were used to compute the temperatures listed in the following four subsections. The computations were based on

$$Q_{cavity} = 650 \text{ watts},$$

$$T_{cavity} = 2000°K,$$

$$Q_{diode} = 130 \text{ watts}.$$

a. Emitter Temperature Drop

$$\Delta T = \frac{Q\ell}{kA},$$

$$k_{Ta} = 0.635 \text{ w cm}^{-1} \text{ °C}^{-1},$$

$$\ell_{Ta} = 0.120 \text{ in.} = 0.305 \text{ cm},$$

$$A_E = 1.91 \text{ cm},$$

$$\Delta T_E = \frac{130 \times 0.305}{1.91 \times 0.635}$$

$$= 32.7 \text{ °C}.$$

The emitter temperature, then, is

$$T_E = 2000 - 32.7$$

$$= 1967.3°K.$$

b. Collector Temperature Drop

$$Q = (\text{total heat}) - (\text{power output}) - (\text{spacer heat})$$

$$= 130 - 26.6 - 18.4$$

$$= 85 \text{ watts},$$

ℓ = 1.85 cm,

k = 1.27 w cm^{-1} C^{-1}

A = 1.91 cm^2,

$$\Delta T = \frac{85 \times 1.85}{1.27 \times 1.91}$$

= 64.8 °C.

This results in the following temperatures:

cavity	2000°K,
emitter	1967.3°K,
collector	950°K,
radiator(base)	885°K.

c. Spacer Temperature Drop

A heat transfer analysis was conducted for tantalum spacer wall thicknesses of 3, 2, and 1.5 mils. The procedure for the heat transfer analysis is as follows.

The tantalum spacer was divided into 20 equal segments, and the losses were calculated for each segment. For each segment, the quantity of heat supplied was that which was conducted into the segment. The heat loss was the sum of the radiation loss from the inside of the spacer, the radiation loss from the outside of the spacer, the cesium conduction on the inside of the spacer, and the heat conducted into the next segment.

An analysis of the temperature distribution down the emitter gives the temperature of the spacer at the point of separation from the emitter. Using this in conjunction with the assumption that Q watts is conducted into the first segment, one can calculate a temperature difference between the point of connection of the spacer and the emitter and an average temperature for the first segment. One can calculate the losses of the first segment by substituting the proper temperatures and emissivities shown in Fig. III -8 into the following formulas:

$$Q = kA \frac{\Delta T}{\ell},$$

which gives conduction into the segment as well as the temperature between III-8

segments,

$$Q = \sigma A (T_1^4 - T_2^4) (\epsilon_1^{-1} + \epsilon_2^{-1} - 1)^{-1},$$

which gives radiation losses from both the inside and the outside of the spacer,

$$Q = \alpha A \left(\frac{T_1}{1000} - \frac{T_2}{1000} \right),$$

which gives the cesium conduction loss. By subtracting these losses from the original Q watts, one now knows the quantity of heat entering the second segment. The same procedure is repeated for each segment of the spacer.

If the temperature of the final segment is not the same as the temperature of the collector, the procedure is repeated, using a new value for the assumed Q.

Using this process, the assumed Q's for a 1.5-, a 2-, and a 3-mil spacer wall thickness, each at a temperature of 2000°K at the top of the spacer and a temperature of 1000°K at the base of the spacer, were found to be 17, 22, and 41 watts, respectively. The temperature distribution along the 1.5-mil spacer is shown in Fig. III-9. The results of this analysis show clearly the advantage of going to a 1.5-mil wall thickness.

d. Radiator Temperature Drop

The rejected heat to be radiated by each diode is approximately 105 watts. Approximate calculations were made to determine the temperature distribution down the radiating fin as well as the radiating capabilities of the fin. Calculations were based on the assumptions that the temperature distribution down the fin is 10°K cm^{-1}* and that the temperature of the fin at the point nearest the diode is 885°K. This temperature is based on an estimated collector temperature of 950°K and a calculated temperature drop of 65°K across the collector.

---

* $\Delta T / \ell = Q/Ak = 105/(3.7 \times 6) = 4.73°K$ cm^{-1}.

Based on these criteria, the following temperature distribution is obtained if the outside surface of the fin is divided into ten segments of equal length and the temperature of each segment is considered constant (Fig. III-10).

From this distribution, the heat radiated from the fin is readily obtained. Calculations of the amount of heat radiated only from the outside surface of the fin show that each diode will dissipate 120 watts. Since each diode radiator must dissipate 105 watts, it is evident that the radiator design is conservative. When the heat radiated from the inner radiator surface is included, the fin is capable of radiating nearly 1.7 times the amount of heat necessary. By reducing the radiator to the minimum size, ** the temperatures distributed along the fin would be reduced from those shown by

$$\frac{1}{1.7} = \left(\frac{T_a}{T_b}\right)^4 ,$$

where T_b is the temperature of any segment for the present design, and T_a is the temperature of the corresponding segment for the new design;

$$T_a = 1.7^{-1/4} T_b .$$

Figure III-11 shows the various temperatures in the diode.

8.   Calculation of Diode Efficiency

The following efficiency calculation is based on the assumption that the diode produces 13.9 w/cm^2 at the design point. Actual diode efficiency will be discussed further in Section III. C.

a.   Basis of Calculation

The values assumed for clearances in diode structure indicated in Fig. III-8 are:

** It will be shown in Section III. C that the radiator size has been reduced considerably.

d_0 = 0.005 in. = 0.0125 cm,

d_1 = 0.003 in. = 0.0075 cm,

d_2 = 0.021 in. = 0.0530 cm,

d_3 = 0.003 in. = 0.0075 cm,

t = 0.0015 in. = .0038 cm

Values of D = 0.620 in. = 1.575 cm.

Diode emitter area $= \dfrac{(1.75 - 0.015)^2 \pi}{4} = 1.91 \text{ cm}^2$

b. Diode Output

J_0 = 13 amp/cm^2;

$V_0 = 1.200 + 0.207 \ln \dfrac{24.8 - J_0}{J_0}$

$= 1.200 - 0.207 \times 0.095$

$= 1.18$ volts.

$\Delta V = RI$;

$R = \rho \dfrac{\ell}{S}$

ℓ = 0.92 cm;

$\rho = 62.5 \times 10^{-6}$ ohm-cm;

$S = \pi Dt$

$= \pi \times (1.575 + 0.002) \times 0.0038$

$= 0.0188$ cm^2.

$R = \dfrac{62.5 \times 10^{-6} \times 0.92}{0.0188}$

$= 0.306 \times 10^{-2}$ ohm.

$I = 1.91 \times 13$

$= 24.8$ amp;

$\Delta V = 0.076$ volt.

$V = 1.180 - 0.076 = 1.104$ volts.

Estimated potential drop in leads of 3%, or 0.033 volts:

Output voltage $V_o = 1.104 - 0.033 = 1.071$,

Diode power $= 24.8 \times 1.071 = 26.60$ watts.

c.   Losses

Direct radiation loss from emitter to collector

$$(Q_R)_1 = A \frac{90.86 - 5.68}{\underbrace{0.232^{-1}}_{Ta_{2000°K}} + \underbrace{0.141^{-1}}_{Mo_{1370°K}*} - 1} = A \frac{85.18}{4.31 + 7.09 - 1} = 8.20A;$$

$8.20 \times 1.91 = 15.67$ watts.

Electron cooling.

$Q_e = (Q_c + V_o + 2kT_e)I.$

$T_e = 2400°K;$

$Q_c = 1.670;$

$V_o = 1.180.$

$Q_e = (1.670 + 1.180 + 0.413) \times 24.8 = 3.263 \times 24.8 = 80.92$ watts.

Cesium conduction loss. 9.1 w/cm^2 at $T_E = 2000°K$, $T_C = 1000°K$, and $T_{Cs} = 600°K$ is the upper bound.

$9.1 \times 0.75 = 6.82$ w/cm^2.

$Q_{Cs} = 13.0$ watts.

Conduction down tantalum spacer. Assuming the heat transfer conditions of Fig. III-8, Q_{spacer} at point A is

$$Q_{spacer} = \frac{16.61 + 17.42}{2} = 17.01 \text{ watts.}$$

---

* $\sqrt{T_1 T_2} = \sqrt{1967 \times 950} = 1369°K.$

Additional internal radiator loss, assuming apparent emissivity of cavity 1 of Fig. III-8,

$$\epsilon_1 = 0.664,$$

$$T_1 = 2000°K,$$

and that of the cavity 2,

$$\epsilon_2 = 0.63,$$

$$T_2 = 1500°K,$$

it is found that

$$Q_A = \frac{90.86 - 28.75}{0.654^{-1} \times 0.63^{-1}}$$

$$= \frac{62.11 A_a}{1.53 \times 1.59 - 1}$$

$$= 29.3 A_a.$$

$$A_a = (1.575 - 0.0075) \eta \times 0.0075$$

$$= 0.0369 \text{ cm}^2.$$

$$Q_A = 1.08 \text{ watts.}$$

External radiation from spacer wall above point A; length of spacer wall = 0.090 in. = 0.229 cm. = 5 sections.

$$q_1 = 1.042$$

$$q_2 = 0.908$$

$$q_3 = 0.787$$

$$q_4 = 0.679$$

$$q_5 = 0.578$$

$$\overline{\Sigma q = 3.994 \approx 4.0 \text{ watts} = (Q_R)_2.}$$

External radiation from emitter lateral wall to wall of cubical cavity.

$$Area = 0.090 \times 2.54 \times \pi \times 0.660 \times 2.54$$

$$= 1.20 + 0.1565 \, D_c^2$$

$$= 0.1565 \, D^2$$

$$= 0.441 \, cm^2,$$

where

$$D = 0.660 \times 2.54$$

$$= 1.680 \, cm.$$

$$Area = 1.20 + 0.44$$

$$= 1.64 \, cm^2$$

$$(Q_R)_3 = 1.64 \left[\frac{85.18}{0.232^{-1} + 0.08^{-1}} \right]$$

$$= \frac{139.7}{15.91}$$

$$= 8.77 \, watts.$$

d.   Diode Efficiency

$$\eta = \frac{P_o}{\Sigma Q}$$

$$= \frac{26.60}{15.67 + 81.0 + 13.0 + 17.01 + 1.08 + 4.0}$$

$$= \frac{26.60}{131.8}$$

$$= 20.2 \, \%.$$

9.   Factors Affecting Life Characteristics

The factors affecting the life of the diode are

(1)   evaporation rates of the diode materials at the operating temperature, especially of the emitter,

(2)   loss of cesium,

(3)   thermal creep of parts, causing electrical short circuits, and

(4)   outgassing of diode parts.

In addition to an adequate design to prevent any of these conditions from adversely affecting the life of the diode, extreme care must be taken in the fabrication, assembly, and processing of the diode to guarantee that the life designed into each diode can be obtained.

a.   Evaporation Rate of Tantalum

The evaporation rate of tantalum operating at 2000°K in a vacuum environment was calculated as follows:

$$\text{evaporation rate } Ta_{2000°K} = 1.60 \times 10^{-12} \text{ gm cm}^{-2} \text{ sec}^{-1}, *$$

$$Ta_{1900°K} = 1.60 \times 10^{-13} \text{ gm cm}^{-2} \text{ sec}^{-1},$$

$$Ta_{2100°K} = 1.60 \times 10^{-11} \text{ gm cm}^{-2} \text{ sec}^{-1};$$

$$\rho = 17.1 \text{ gm/cm}^3 \ (100\% \text{ theoretical for single crystal}).$$

Therefore,

$$\text{evaporation} = \frac{1.60}{17.1} \times 10^{-12}$$

$$= 9.31 \times 10^{-14} \text{ cm/sec}$$

$$= 9.31 \times 10^{-6} \text{ Å/sec}.$$

Lattice constant (bcc) $= 3.30$ Å . †

Therefore,

$$\text{evaporation} = 2.82 \times 10^{-6} \text{ atomic layers/sec}.$$

In one year $(3.16 \times 10^{+7} \text{ sec.})$.

$$\text{evaporation} = 3.16 \times 10^{+7} \times 2.82 \times 10^{-6}$$

$$= 89 \text{ atomic layers/yr.}$$

The evaporation rates of other diode materials are shown in Table III-2, along with the basis for the calculations.

---

*Kohl, p.525, p.338

† Kohl, p.334.

b. Loss of Cesium

The loss of cesium in the diode will terminate the useful life of the SET diode. There are essentially four ways in which the cesium can be lost; these are by

(1) a small leak due to flaws in fabricated parts (specifically, the tantalum spacer, the ceramic-to-metal seals, and the copper crimp-off),

(2) leaks that develop as a result of a time-temperature effect (specifically, these are due to crystal growth of the tantalum spacer, diffusion of foreign or braze materials into critical areas, or thermal transient effects due to warm-up or cool-down),

(3) chemical reaction of cesium with diode materials, and

(4) a penetration due to collision with a high-velocity particle.

The first of these can be controlled to a satisfactory degree by quality control during construction and by careful examination of the diode during outgassing. Quality control of the tantalum spacer is particularly critical since the slightest flaw is very likely to cause a failure. Future diode fabrication will include x-ray analysis of the thin-walled tantalum spacers to determine accurately the uniformity of spacer thickness or to reveal any localized flaws or tool marks. Only the best spacers will be used for diode fabrication.

It will be shown in Section III. B how the diffusion of nickel braze material caused the embrittlement and subsequent failure of tantalum spacers. Caution must be exercised in the selection of any material that will come into contact with the high-temperature portions of the diode.

Diode tests, to be described in Section III. C, indicate that the diode can withstand considerable thermal cycling. Therefore, transient thermal stresses in the diode design do not appear to be too critical.

Extended diode life tests will show whether crystal growth of the high-temperature components of the diode will adversely affect its life.

III-16

47

Cesium is an active substance and it may react slowly with some of the diode materials used. Corrosion tests have been helpful in determining which materials are violently attacked. They have not satisfactorily determined the rate of corrosion of those substances that are slowly attacked. The interpretation of the tests conducted to date is complicated and will not be elaborated on here. It is presently believed that the cesium reaction with the materials used in the SET diode is of a rate sufficiently low to enable several thousand hours of operation. This will have to be verified, however, by actual diode life tests.

The possibility of a penetration caused by a meteoritic impact is extremely remote because of the small cross section of the diode, the protection afforded by the diode by the remaining components of the generator (particularly the radiator), and the rugged design of the diode. It is true that the penetration of one diode of the SET generator would cause an open circuit in the series connection and that all power would then be lost from the entire generator. However, the probability of a penetration is so low that this factor is not considered to be alarming.

c.   Thermal Creep of Parts

Thermal creep of critical parts could cause failure of the SET diode due to electrical shorting of the emitter and collector. The diode part most susceptible to creep is the thin-walled tantalum spacer, which operates at high temperature. Very little creep data exists for materials operating at 2000°K. However, several interesting qualitative observations can be made. Creep is a function of the loads applied, the temperature of the part under observation, and the time over which the loads are applied. Fortunately, in the SET system, the diode will be in the "cool condition" during periods of high load and, during periods of high temperature operation, the loads will be minimal. Therefore, creep should not present any particularly difficult problems. Diode life tests conducted to date have not shown any ill effects due to creep.

III-17

48

d. Outgassing of Parts

The evolution of gas within the diode as a result of the outgassing of diode parts can cause a considerable degradation of diode performance with time. This results in the contamination of the electrode surfaces and an increase in plasma losses due to the presence of the partial pressure of these extraneous gases. It will be shown in Section III. C how this actually caused an initial degradation of the performance of the IV series of diodes. The solution to this problem is the thorough outgassing of all the diode parts prior to cesium charging and crimp-off.

B. Progression of the Mechanical Design

1. Design of the SET Diode

Once the basic design of the diode was established, fabrication commenced. The purpose of the first series of diodes was to verify and to establish some of the design features. This was necessary since there were many unknown quantities, such as the allowable stress in the metal-to-ceramic boundary layers of the diode leadthrough, which prevented a complete analysis of all aspects of the diode design. The only basis for design was prior experience, and a thorough test program. Diode fabrication also depends heavily on the techniques of assembly; diode design features are often changed to utilize proven techniques.

The first series of diodes, Ia and Ib, were essentially of the design shown in Fig. III-1. Leaks developed at the diode leadthrough when attempts were made to outgas the diode. To overcome this problem, the design was modified to reduce the wall thickness of the three niobium rings of the diode leadthrough.

While this change was in progress, data were generated at Thermo Electron which indicated that a tungsten emitter was capable of greater power density than a tantalum emitter. Since the goal of the SET program was to achieve 14 w/cm^2, a rather stringent requirement, it was decided to incorporate a tungsten emitter in one of the diodes of the II series.

Also, during this period, the study of diode efficiency versus emitter diameter was completed. The results of this study are discussed in Section III. A. (Figure III-2 presents the important results.) Based on the results of this study, the emitter area was reduced from 2.55 to 1.91 cm^2.

An evaluation of diode materials indicated that a tungsten-tantalum alloy (90% Ta-10% W) might prove superior to tantalum as a spacer material. The alloy has a slightly lower thermal conductivity and lower coefficient of thermal expansion than tantalum. (Figures III-12 and 13 show the comparison of Ta and Ta-10% W.) This would result in lower heat losses (hence higher efficiency) and a smaller interelectrode spacing.

Tantalloy is also stronger and more resilient that tantalum, which greatly facilitates the fabrication and handling of a delicate part with a 1.5-mil wall thickness. It was decided to use a Tantalloy spacer on the II series of SET diodes. This resulted in a reduction of the interelectrode spacing from 1.9 to 1.61 mils. It can be seen that the design of the II series of diodes was a significant departure from that of the I series.

Difficulties were encountered in the assembly of diode IIa, and it never materialized. The thin tungsten emitter warped due to the differential thermal expansion of the heavy (0.040-in.) Tantalloy substrate. This was corrected by reducing the thickness of the Tantalloy to 0.010-in.

Diode IIb was successfully completed, outgassed, and charged with cesium on July 14, 1961, the day before the date set for the freeze of the diode design. Figure III-14 shows diode IIb during testing. At an emitter temperature of 2000°K, diode IIb produced 24.5 watts at approximately one volt, just 7.9% below the goal of the SET program.* The cesium reservoir had been overcharged with cesium, so that there was essentially very little control of the cesium pressure. Therefore, it was not possible to determine what was the optimum cesium pressure. The diode was cooled down, exposed to air for seven hours, and cycled to the starting temperature. The data from diode IIb were extremely encouraging. Figure III-15 shows an exploded view of a SET diode. Figure III-16 shows the diode assembly area at Thermo Electron. After 20 hours of operation, a crack developed in the Tantalloy spacer due to a failure at a grain boundary. The results of the analysis of diode IIb are shown in Table III-3, an excerpt from the entry in the data book. Because of the failure observed on the Ta-10% W spacer, a similar spacer assembly was tested. The results of this test are shown in Table III-4.

Diode IIc, which was identical to diode IIb except that it incorporated a tantalum

---

*Details of the progression of diode performance will be discussed in Section III. C.

emitter, was not assembled since a similar failure was bound to occur.* The diode design was modified to incorporate a tantalum spacer.

Diodes IIa and IIb were examined after failure; it was observed that the nickel disc, used for adjustment of the interelectrode spacing and inserted in the collector assembly, had not adhered to the molybdenum. There were obvious signs of failure in the braze due to shear stresses caused by differential thermal expansion. The nickel disc was eliminated from the design and a tantalum collector was substituted. This changed the interelectrode spacing from 1.61 to 2.09 mils at the design temperatures. The nickel evacuation tube was changed to copper because of the leakage in nickel crimp-off of diode IIb.

Diode IIIa was fabricated and placed on test on July 25, 1961. This diode operated for approximately 100 hours†; it failed due to a leak that developed in the tantalum spacer. The location of the failure was such that it appeared that the top of the tantalum spacer (between the tungsten emitter and the tungsten cap) was now too thin. It appeared that a thickness between 0.040-and 0.010-in. would provide the solution to the problem. It was decided to try a 0.025-in. thick tantalum spacer cap.

The question of diode operation in the inverted position was considered at this point. The principal problem appeared to be that of retaining liquid cesium in the reservoir during inverted operation. This problem was overcome by redesigning the cesium reservoir so that it would retain a considerable amount of liquid cesium regardless of diode orientation. Fig. III-17 shows a cross section of the III series of diodes with the revised reservoir.

The proper evaluation of the tantalum spacer problem was delayed at this point by a series of diode assembly problems. The changes in the design of the diode

---

*At the time, it was felt that the failure was due to the characteristically weaker grain boundaries of the alloy. This is uncertain at present because of the subsequent effects observed with the nickel braze on tantalum spacers, which produced similar failures.

†Exact test time was between 97.5 and 108 hours.

affected the assembly procedures required to obtain a sound diode. This became evident as the remainder of the III series of diodes was fabricated. The features and problems of these diodes are briefly summarized below and in Table III-5.

2. Summary of Diode Series III and IV

a. Diode IIIb

Features.

(1) Molybdenum-faced tantalum collector (expected to reduce optimum cesium pressure).

(2) High-purity tantalum spacer.

(3) 0.060-in.-thick tungsten emitter brazed to tantalum spacer (0.025-in. thick on top).

Results.

(1) The diode appeared to be leak-tight on brazing, although difficulty with the final subassembly braze (part 10 to part 29, Fig. III-19), tantalum to niobium, was encountered. Several rebrazes were required before a leak-tight braze was obtained.

(2) After three hours of outgassing, a leak in the thin section of the tantalum spacer (3) developed. Microscopic examination revealed four small holes in an extremely thin (about 0.0005-in.) section of the spacer, probably due to eccentric machining of the inner and outer diameters of the spacer. This thin section was strong enough to withstand a vacuum but not strong enough to withstand the cyclic high-temperature heating during outgassing. This failure could not be repaired.

b. Diode IIIc

Features

Diode IIIc was similar to diode IIIb. Uniform wall thickness of the tantalum spacer was assured by close measurement.

Results.

(1) Difficulties were again encountered with the final subassembly braze, part 10 to part 29. Rebrazing was required.

(2) A leak developed in the final braze of the cesium tubulation. Before this leak was repaired, the diode structure was used to verify the reasons for failure of diode IIIe (to be described below) by cycling the emitter to operating temperature 10 times. The same failure as observed in diode IIIe resulted. (See diode IIIe, below.)

c. Diode IIId

Features.

It was hoped that the difficulty with the final subassembly braze experienced in the brazing of the two preceding diodes could be eliminated by introducing a filler wire of nickel into the braze joint.

Results.

The final subassembly joint (part 10 to part 29) leaked, requiring a rebraze. During rebraze, the nickel-cesium tube (12) alloyed with the original copper braze to the tantalum (29) to such an extent that a hole in the joint was formed by erosion. On repair of this joint, small-order leaks developed in the metal-to-ceramic seal.

d. Diode IIIe

Features.

This diode was similar to the four preceding diodes as follows:

(1) Molybdenum-faced tantalum collector.

(2) Tungsten emitter brazed to tantalum spacer.

(3) Tungsten top piece brazed to tantalum spacer.

After further analysis of the probable reasons for difficulty with the final subassembly braze which required rebrazing, it was decided to double the amount of braze material used to effect the joint.

Results.

(1) Final subassembly braze was leak-tight. Increasing the amount of braze material quantity used seemed to cure the poor braze experience at this joint.

(2) The unit was outgassed for 17 hours at temperatures between 1450 and 1650°C. At the end of the outgassing period, small longitudinal cracks emanating

from the top of the spacer caused leakage. The failure was attributed to the stresses induced in the tantalum spacer by differential thermal expansion in the tungsten and the tantalum. This was verified by a special test on diode IIIc.

e.   Diode IIIf

The final subassembly of diode IIIf was not made since the initial subassemblies were the same as in the preceding tube and therefore known to be unsatisfactory.

A major design decision was made to substitute tantalum for tungsten as the emitter and cavity face material. Diode series IV was based on this approach.

f.   Diode IVa

Features.

Tantalum was substituted in this diode for the tungsten emitter and top piece in an attempt to verify the previous conclusion that a thick tungsten disc brazed to tantalum is incompatible and eventually causes cracks in the tantalum sleeve.

Results.

The ceramic seal assembly failed, due to displacement of the jig during braze. The failure could not be repaired.

g.   Diode IVb

Features.

This diode was similar to diode IVa, having an all tantalum emitter (part 4), and cap (part 2) brazed to the tantalum spacer.

Results.

(1) The diode was constructed with no difficulties in brazing.

(2) The diode was outgassed for a period of 12 hours.

(3) The diode ran for 165 hours with an output of approximately 14 watts.

(4) A leak developed in the tantalum spacer, possibly due to carburization of diffusion-pump oil vapor or the presence of nickel on the thin-walled spacer (due to nickel evaporation and diffusion from the emitter braze area) or distortion of the spacer under cycling to the extent that heavy bulging of the spacer caused

the thin tantalum wall to tear away from the emitter cap.

h.   Diode IVc

Features.

(1) A one-piece tantalum spacer construction with no nickel braze at the high temperature portion of the spacer.

(2) Molybdenum-faced collector.

(3) Spacer thickness of 0.0035-in.

Results.

(1) No brazing difficulties were encountered with this diode.

(2) The diode was test-run for 10 hours; further testing was postponed. Its power output was approximately 14 watts at 2000°K.

i.   Diode IVd

In an endeavor to restore power output to levels experienced on the first diodes made on the SET program, a tungsten emitter and tungsten collector diode were planned.

Thin tungsten facings, 0.005-in. thick, which would crack and stress-relieve themselves, seemed to be a good possibility.

A tungsten disc was nickel-brazed to the tantalum at 1650°C for 20 minutes. After brazing, the tungsten was ground flat and polished smooth. Reheating to 1800°C cracked the thin tungsten into 20 or 30 small areas. The excess nickel was evaporated at this high temperature, but the bond of tungsten to tantalum remained good. Regrinding, repolishing, and refiring at 1800°C produced little change in the tungsten surface profile.

Features.

(1) A thin tungsten emitter brazed to a tantalum backing disc.

(2) A thin tungsten facing on tantalum collector.

(3) A tantalum spacer, ground on outside diameter.

Results.

(1) All brazes were leak-tight.

(2) The diodes remained leak-tight after outgassing for six hours.

(3) On testing, a circumferential crack developed in the tantalum spacer in the vicinity of the tantalum emitter-to-spacer braze joint. Spasmodic shorting in this diode was prevalent on testing. This was believed due to movement in the cracked tungsten emitter face.

3.   Evaluation

A series of tests was run to establish the most probable cause of failure of diode IVb.

Three tantalum spacers of the type used on diode IVb were brazed to copper supports. The spacers were then placed in an oil-diffusion pump vacuum system and electron-bombarded at a temperature of 2000°K, as they would be during diode operation (see Fig. III-20).

The following Table III-6, summarizes the tests and the results.

	Hours of Operation	Results
1st spacer plain sleeve 0.010-in. top	4 (cycled periodically)	No bulge; Ta melted by excessive localized electron bombardment during cycling
2nd spacer	6.3 (cycled 20 times; 5 minutes on, 5 minutes off; then continuous operation)	No bulge
3rd spacer plain sleeve	2.2 (cycled 20 times; 5 minutes on, 5 off)	No bulge after cycling;
0.025-in. top, but with tantalum emitter face and top piece brazed in place	5.3 (continuous operation)	bulge beginning after 7.5 hours

The top section and a portion of the sleeve from diode IVb was sectioned and metallographically examined. An exterior crust on the top section was evident; the hard crust was formed by oil vapor within the pumping system. Considerable quantities of the nickel used for brazing had accumulated at the grain boundaries.

The tentative conclusions drawn from these tests are

(1) that thermal cycling (2000 to 600°K) does not necessarily produce a bulge, and

(2) that migration of minute traces of braze alloy, coupled with possible oil contamination from the pumping system, does produce a brittle bulge, which ultimately leads to failure.

Because of the mechanical difficulties encountered with the diode, the program was re-evaluated at this point. As a result of this re-evaluation, it was decided to concentrate all the remaining effort of the SET generator program on the solution of the mechanical and life problems associated with the diode. The short-range diode program resulting from this re-evaluation was to span seven weeks; the work to be accomplished is discussed in the following paragraphs.

Four diodes were to be fabricated, using a tantalum emitter and collector. The spacer-emitter was to be a one-piece assembly. The four diodes were to be identical (the state of the art permitting). These diodes were also to incorporate collector and cesium reservoir heaters to ensure operation at the optimum point, and to show duplication of performance. These four diodes were designated Va, Vb, Vc, and Vd.

All four diodes were to be tested for 50 hours with a minimum of thermal cycles. At least one of the diodes was to be operated continuously until failure or until the end of the program, at a constant emitter temperature. Two of the four diodes were to be tested with controlled thermal cycling. I-V curves for all diodes were to be taken at one emitter temperature over a wide range of collector temperatures and cesium pressures. The efficiency was to be determined for several output voltages, while other parameters were to be maintained near optimum conditions.

4. Short-range Diode Program

Revision of the diode design received immediate attention when the short-range diode program began. The following revisions were made.

a. Diode Design Revision

A single-piece tantalum emitter sleeve (spacer) (part 3) was substituted for

parts 2, 3, and 4, as shown in Fig. III-19. This was done to eliminate brazes in the high-temperature areas of the emitter as a safeguard against metallic evaporation and diffusion into the thin-walled tantalum spacer.

The collector (parts 29 and 30) was changed from all tantalum to molybdenum faced with tantalum. Since molybdenum is somewhat easier to outgas than tantalum, it will evolve less gas during tube operation. Outgassing is one of the probable reasons for degradation of diode performance during the first few hours of operation, as noted in the work on diodes IVb and IVc. (This will be discussed in more detail in Section III. C.)

The radiator (part 18) has been shortened to decrease the radiating area, thus permitting higher collector operating temperatures.

In an effort to improve manufacturing reliability of the diode assembly, the following work was done.

An emitter-spacer (part 3) was brazed to the center insulator support (part 9). Difficulty in obtaining a leak-tight braze was encountered on the initial subassembly of these parts. Diodes built prior to September 1961 utilized niobium insulator supports made from niobium stock from a different supplier. Whether this difference in stock contributed materially to its ability to be brazed to tantalum has not been firmly established. The manufacturer's analysis of the two batches is shown in Tables III-7 and III-8. It is difficult to draw any concise conclusions from the analysis, however, since the impurity levels were significantly different.

Special fixtures for outgassing the tantalum spacer (part 3) and the molybdenum collector (part 29) were made and used in processing these parts. The fixtures consist of molybdenum pedestals with protruding small-diameter tungsten rods which support the part being outgassed. These fixtures provide a minimum contact area between the part and the pedestal and eliminate the possibility of oven or bucket contamination. Figure III-21 shows one of these fixtures.

External cesium reservoir. To permit testing over the full range of temperatures on the cesium reservoir, the cesium heater had to be removed from inside the calorimeter and an electrical heater added. Figure III-22 shows the calorimeter chamber with the reservoir and heater protruding from the calorimeter. This was accomplished by allowing three inches of the copper tubulation to remain after the final pinch-off of the portion containing the liquid cesium. The nickel tubulation was then bent approximately 30° to allow the copper pinch-off tube to extend through a hole drilled into the base of the calorimeter pedestal. The three calorimeter test pedestals were modified to allow the tubulation to protrude in this manner.

Cesium tubulation heater. A clamp-on tubulation heater was designed and constructed to locate the heating wire on the protruding tubulation and also to act as a heat reservoir. Three of these clamp-on tubulation heaters were made. The heater is shown in Fig. III-23. Approximately four turns of 0.020-in. diameter molybdenum wire, insulated with Al_2O_3 beads, were wrapped around the diode tubulation protruding from the calorimeter. The wire and beads were contained by a split copper oven which would act as a stabilizing heat reservoir. The oven was clamped on the tubulation by two turns of tightened copper wire, one turn of which held the thermocouple bead firmly in place against the oven.

Collector heater. To test the effect of various collector temperatures on output power, a means of heating the collector was provided. The heater consisted of four turns of 0.030-in. diameter molybdenum wire placed within a spiral groove on the outside diameter of a ceramic tube. The ceramic heater was located by a molybdenum ring, on which it rested. This molybdenum ring, in turn, located the position of the diode with respect to the heater, and also located on the original insulating ceramic within the calorimeter. The heater leads were insulated with aluminum oxide tubing. An ac power supply provided power to the heater.

Special precautions were taken during outgassing and testing to minimize exposure of the tantalum spacer and emitter structure to oil vapor from the vacuum diffusion pumps. One high-capacity Vac Ion pump has been made available to ensure a

good, clean vacuum environment in which to operate at least one diode.

b. Diode Fabrication

All four diodes were made as follows:

Emitter: all tantalum,

Collector: molybdenum with a 0.020-in. tantalum face,

Spacer: Tantalum, 0.0030 ± 0.0001-in. in wall thickness.

The dates of completion were: Va, September 25, 1961; Vb, September 29, 1961; Vc, October 2, 1961; and Vd, October 9, 1961.

c. Outgassing

In addition to the emphasis on longer outgassing of parts prior to assembly, the outgassing of the completed diodes was extended for a longer period of time. The general outgassing procedure was as follows. The set-up was as described in Fig. III-24.

(1) The diode radiator was covered with a molybdenum shield to reduce radiation and secure higher temperatures within the diode as an aid to proper outgassing.

(2) The diode emitter was heated slowly over a 1- to 2-hour period to a temperature of 1550 ± 50°C, and kept at that temperature for approximately 12 hours or more. The VacIon pump by-pass valve was left open, connecting the diode to the diffusion pump vacuum system during this period of outgassing.

(3) After this initial period, testing for outgassing completion was accomplished by closing the by-pass valve to the diffusion pump system and noting the change in pressure on the VacIon pump system. If gas were being evolved at a faster rate than the VacIon pump could handle while remaining at the previous system pressure, the diode was deemed insufficiently outgassed and the by-pass valve was opened and further outgassing performed.

(4) When no appreciable change in pressure occurred with the by-pass valve closed, the diode was considered sufficiently outgassed and the VacIon pump was

III-30

65

allowed to complete the outgassing. After two or more hours of VacIon outgassing, the tube was cooled and pinched off. Table III-9 shows the total outgassing periods for the four diodes.

d.   Cesium Charging

To prevent oxidation of the copper exhaust tube and other exterior tube parts, cesium charging for all four diodes was done within an evacuated chamber. Table III-10 shows the period of cesium charging. (See Fig. III-24). The four diodes were charged with cesium and tested.

e.   Results of Short-range Diode Program

The minimum requirements of the short-range diode program were more than met. At the conclusion of the program, the diode design was reproducible, capable of being reliably produced, not particularly sensitive to thermal cycling, and capable of continuous operation for several hundred hours.

III-C.   PROGRESSION OF DIODE PERFORMANCE

Diode II b was the first SET diode to produce power. This diode employed a tungsten emitter and a molybdenum collector. At the design emitter temperature of 2000°K, the diode produced 24.5 watts at approximately one volt. (See Fig. III-26 for the I-V curve.) The goal of the SET program is to obtain 26.6 watts per diode; diode II-b came within 7.9% of that goal. At 2030°K, the diode produced 29.4 watts at 1.05 volts, exceeding the goal of the program. The diode performance was also reproducible, as shown in Fig. III-26.

The cesium reservoir had been overcharged with cesium, so that there was essentially no control of cesium pressure. Therefore, it was not possible to determine if the optimum cesium pressure had been obtained. The design inter-electrode spacing was 1.61 mils. The data for diode II-b can be found in Volume II of this report, along with the data sheets for all other diodes tested on the SET program.

Diode III-a, employing a tungsten emitter, a tantalum collector, and an interelectrode spacing of 2.09 mils, produced 18.6 watts at 1700°C (1973°K) at 1 volt. Families of I-V curves were taken at emitter temperatures of 1700°C and 1660°C (see Figs. III-27 and III-28). From Fig. III-27, it can be seen that at 1 volt, the power density could be obtained with the cesium reservoir between 366 and 386°C, a spread of 20°. In diode III-a, it was not possible to vary the cesium pressure and the collector temperature independently. Therefore, it was not possible to obtain both the optimum cesium temperature and the optimum collector temperature simultaneously.

The performance of diode III-a was lower than that of diode II-b by approximately 25%. The two features that were different between the diodes and that could cause differences in electrical performance were the interelectrode spacing and the collector material. Which of the two contributed most to the reduction in power density is not known, and an attempt to draw any more definite conclusions at this point would be mere conjecture. The power output of diode III-a over its

100 hours of testing was relatively constant.

Diode IV-b differed considerably from both diode II-b and III-a, in that it employed a tantalum emitter and a molybdenum collector. The diode initially produced 18.2 watts at 1 volt with an emitter temperature of approximately 2000° K. However, the power output dropped to approximately 14 watts at 1 volt after 10 to 12 hours of operation (an effect not observed on previous diodes). Also, the output dropped some 25% below that of diode III-a, or 43% below that of diode II-b.

The conclusion drawn concerning the initial drop in power is that it was due to inadequate outgassing of the diode. Hence, when the diode was operated, parts continued to outgas, and this contributed significantly to the total gas pressure within the diode. This caused increased losses due to collisions in the interelectrode space, and hence decreased power density. The initial power output was almost equal to that of diode III-a. The two diodes had approximately the same spacing (2.09 mils), but different emitter and collector materials. It should be pointed out that the optimum cesium temperature was approximately 25° C higher in the case of diode IV-b, which had a tantalum emitter. This indicates that a higher cesium pressure is required for a tantalum emitter than for a tungsten emitter at the same temperature if sufficient coverage of the emitter for effective reduction of the work function of the emitter and maximum emission are to be obtained. This is as one would expect from the theoretical relationship between coverage and bare-metal work function. Also, with the higher cesium pressure, one would expect greater plasma losses, and hence lower power density. However, even with the higher cesium pressure, the initial power density of diode IV-b was comparable with that of diode III-a. There is a possibility that the substitution of a molybdenum collector for the tantalum collector had some compensating effect on the performance decrease due to higher cesium pressure.

Diode IV-c was essentially of the same design as diode IV-b, at least from the standpoint of the factors that affect the electrical characteristics of the diode.

The performance of diode IV-c reproduced the performance of diode IV-b within approximately 6 to 8%. It also exhibited an initial drop in output power. One of the unexplained differences between the performances of diodes IV-b and IV-c was the fact that the cesium reservoir temperature of diode IV-c was lower than that of IV-b by as much as 60°C.

The design of diodes V-a, V-b, V-c, and V-d are identical. All employ tantalum electrodes (both emitter and collector), and the design interelectrode spacing is 2.3 mils, greater than for any of the previous SET diodes. These diodes also incorporated separate collector and cesium reservoir heaters to permit the independent optimization of the collector and cesium temperatures. The power outputs of the four diodes simulated one another quite well, producing approximately 12 watts at one volt. There was no appreciable decrease in output power with time.*

It can be concluded that the progression of diode performance indicates that spacing and emitter material are important variables. The present state of the art in construction of reproducible diodes with a life expectancy of several hundred hours has been evolved for diodes with a tantalum emitter and a designed interelectrode spacing of about 2.3 mils. It seems, from the progression of diode performance described, that changing the emitter material to tungsten and reducing the design interelectrode spacing to about 1.6 mils would result in a great improvement of the diode performance characteristics, possibly sufficient to attain the SET performance goals. The investigation of other emitter materials would provide a further area of performance improvement. It must be pointed out, however, that these conclusions are based on a limited number of tests, some of them incomplete because of the short life of the diode tested. In several cases only one diode was tested to find the performance characteristics of a particular diode configuration. It is therefore quite possible that factors, observed and unobserved, other than spacing and

---

*Each of these aspects of the performance of the series V diodes is discussed individually in Section III.E.

electrode materials, influenced the diode performance in these tests. Further work on diodes should be directed at clarifying the extent to which diode performance depends on electrode materials and spacing.

III-D. TEST PROCEDURES

Before describing the detailed test data obtained from the series V diodes, it is appropriate that the methods and equipment used for testing be described.

1. Test Plan

The plan for the complete testing of the series V diodes, in compliance with the applicable portions of the Statement of Work, is described below.

The four diodes in this series (Va, Vb, Vc, and Vd) were initially subjected to 50 hours of testing without thermal cycling. Two of the four diodes (Vc and Vd) were then tested to evaluate the effect of thermal cycling. The results of these tests are presented in Section III-C. Diodes Va and Vb were subjected to life testing without thermal cycling. The results of this study are presented in Section III-E.

In addition to thermal cycling and life testing, the following evaluations were also made.

(1) A search for optimum output power was made by maintaining the input power constant while independently varying the collector and cesium bath temperatures.

(2) I-V curves were taken to determine the I-V characteristics resulting from variation in the output voltages between 0.5 and 1.2 volts.

(3) Efficiencies were determined at 1.07 and 0.8 volts.

(4) The cesium temperature was varied $\pm 8°C$ and $\pm 20°C$ from the optimum point; at each new cesium temperature, a search was made for the corresponding optimum collector temperature. The I-V characteristics for these conditions were measured while varying the voltage from 0.5 to 1.2 volts.

It was also necessary to make an accurate determination of the emitter temperature during operation. This temperature is a direct function of electron-bombardment current. Power supplies used in diode tests provide an inherently fluctuating output, which induces a corresponding fluctuation in the emitter temperature. A certain smoothing of this fluctuation can be made

by continually monitoring and adjusting the output of the power supply; even so, since the output can be read only to the nearest 2 ma, some fluctuation necessarily remains.

Table III-11 shows the variations in temperature measurement that appear reasonable for personnel trained in making pyrometer readings. In the 350-ma range (at approximately 1700°C), a change of 20 ma in the electron-bombardment current reflects itself in a change of approximately 40°C in the emitter temperature for the given configuration. Assuming linearity near the operational range, normal deviations in the emitter temperature during operation, with the current manually adjusted before the reading, would be approximately ± 4°C.

2. Equipment Used

The equipment used to test the diodes in series V was divided into three separate test set-ups. Each diode remained with its initial test set-up regardless of the type of test it was undergoing. Diode Va was tested on set-up number 1. Diode Vb was tested on set-up number 3 until it failed; this unit was then used to test diode Vd. Diode Vc was tested on set-up number 2.

Each of these test set-ups consisted of the following equipment:

(1) a vacuum system,

(2) a Thermo Electron electron-bombardment unit,

(3) an optical pyrometer,

(4) two output meters (dc voltage and current),

(5) two collector heater meters (ac voltage and current),

(6) a test rack,

(7) a diode test device,

(8) a potentiometer, and

(9) a Variac

A complete description of each set-up is given in Table III-12. A schematic of the test set-up is shown in Fig. III-28A.

3. Calibration of Equipment

To maintain a high degree of accuracy in the measurements made on the series V diodes, standard test equipment was used for all the tests. The accuracy of the various meters was checked. Table III-13 shows the meter variation from the standard for the three meters used, and the correction factor to be applied to the meter readings. It can readily be seen from this table that the power output calculations may be considered to be valid within 0.1 to 4.0%, depending on the set-up used. The accuracy of meter scale readings varies from reading to reading; the values indicated are also shown in Table III-14.

III-E. SUMMARY OF PERFORMANCE OF SERIES V DIODES

1. Life Testing

Figures III-29 through III-32 are time-history charts (graphical representations of output power versus hours of operation) for the V series of diodes. Various factors affecting diode performance are noted on these charts, explaining some otherwise anomalous behavior. When this test was initiated (October 3, 1961), the diodes were allowed to run untended for certain periods of time (one night, and weekends). At various points during this continuous operation, curves of various types were taken, and necessary adjustments were made in the test set-ups. Commencing on October 13, 1961, diode testing was placed under continuous surveillance, with a data point recorded each hour. This produced a slightly different type of curve.

At the end date of the contract, three of the four diodes of the V series were still in operating condition, with no signs of a decrease in power. Further life testing is required before any conclusive statements can be made regarding the life of the SET diode.

2. Effects of Collector and Cesium Reservoir Temperatures

The diode heat transfer characteristics are such that the diode radiator temperature is relatively insensitive to changes in cesium reservoir temperature. The cesium reservoir temperature, however, is greatly affected by changes in the diode radiator temperature. Because of these coupling characteristics between the diode radiator and the cesium reservoir temperatures, the search for optimum collector and cesium reservoir temperatures is best carried out by choosing a fixed diode radiator temperature. Scanning the cesium reservoir temperature range while maintaining output fixed at 1.07 volts allows the corresponding optimum cesium temperature to be obtained. Fig. III-33 shows typical results obtained for diode Vd.

This graph is of great interest as it shows a plateau of cesium temperatures over which there is no variation in power output. It can be seen that as the collector temperature is increased from 544 to 620° C the width of the plateau indicating constant power output increases substantially. The data on the higher collector temperature of 642°C are incomplete because lower cesium reservoir temperatures could not be obtained for such high radiator temperatures.

The cesium temperature was varied from 330 to 410°C. The optimum cesium temperature was found to be between 370 and 375°C, the location of which was not affected by collector temperature.

One might observe that the width of the cesium reservoir temperature plateau is greater than the anticipated requirements for the cesium reservoir temperature control. This would indicate that the control requirements could be relaxed considerably. However, as better performance is achieved, and diode performance approaches the specifications for the SET generator, the optimum cesium temperature curve is expected to be sharper. Therefore, the control requirements should not be relaxed, at least until more data are obtained at higher power densities.

Collector temperatures of 642°C and higher produced higher output power. However, operation at these relatively high seal temperatures was not con- sidered practical, at least until further seal testing is carried out.

The effect of collector temperature on output power is shown in Fig. III-34 for two different output voltages. Each curve is for a relatively constant cesium temp- erature. It is apparent from the figure that the collector temperature has not reached its optimum value. However, the curves have begun to flatten out considerably at a collector temperature of 640°C. The effects at lower diode voltage are more pro- nounced, as shown in Fig. III-34.

Figure III-35 is a section of the recorder chart showing variations in diode output as a function of changes in cesium heater input, collector heater input, and diode emitter heating current (electron-accelerating current). Note that

although the electron-accelerating current was manually adjusted every 5 or 10 minutes at 400 ma, current fluctuations did occur as indicated on the chart. A résumé of the variations in temperature, current, and voltage occuring over a one-hour period appears in Table III-15. Because of these variations, the output power readings could vary by approximately 0.50 watt, or 5%. By referring again to Fig. III-35, the direct correspondence between emitter heating power (11) and diode power output (9)(7) can be seen; for every slight change in (11) there is a similar change in (9) and (7).

Figure III-36 shows a section of the chart where the cesium temperature was varied. As the cesium temperature (5) was varied above and below the optimum point, the power output is reduced.

Figure III-37 shows a single heating and cooling cycle taken during the thermal cycling of diode Vc. Note that different components of the diode heat and cool at different rates.

It may be said in conclusion that cesium temperature measurements are not uniform from diode to diode; they may differ by as much as 10 to 20°C among diodes. (Note: Some of this variation is due to the location of the thermocouple head and its surrounding geometry). An examination of the I-V characteristics indicates that a cesium temperature between 330 and 370°C is approximately optimum for these diodes. Power output was found to be relatively insensitive to small changes in collector temperature. Optimum collector temperatures appear to be near 640°C. I-V curves are presented in Figs. III-38 through III-40 for diodes Va, Vc, and Vd, respectively, operating at the optimum cesium reservoir temperature. (A few points for diode IVb are included. Similar curves are presented for those diodes operating at a cesium temperature approximating ± 8°C and ± 20°C from the optimum. No data are presented for diode Vb, which failed prematurely due to machining imperfections in the tantalum spacer. It can be seen by comparison that the optimum cesium temperature is slightly different for each diode at 1.07 volts. This is believed to be due to the fact

that performance at the constant 1.07-volt output is only a weak function of cesium temperature. This point is better illustrated in Fig. III-41, where the power output versus voltage is shown for diode Vc, for five cesium temperatures.

Figure III-42 shows the I-V characteristics of diodes Va, Vc, and Vd, at approximately the same cesium temperature (365 ± 4°C). As diode Vb is not operated at 365°C, the I-V curve at 330°C is shown so that the operation of Vb can be compared with that of the other three. It can be seen that their output is quite similar in the vicinity of 1.07 volts, but divergence is evident at lower voltages.

3. Diode Reproducibility

The four diodes which comprise series V have shown themselves to be reproducible. Parts for four diodes were started; four sound diodes were completed. They were fabricated in the same manner and have proven to be physically and electrically reproducible.* For example, during outgassing, the first three diodes in this series "unshorted" at approximately the same emitter temperature (1000°C). This was determined by taking resistance measurements during the initial warm-up period of the outgassing phase. It should also be pointed out that the curves of the I-V characteristics for the diodes are almost identical in the region of interest (from 0.9 to 1.1 volt) for approximately similar conditions of cesium pressure and collector temperature. The power output measured while the diodes were being life tested (with the voltage held at a constant 1.0- to 1.1-volt level) attained a level of 11.0 ± 1 watt. This characteristic was evident for all four diodes.

It may be said, therefore, that the four series V diodes have proved that a number of diodes producing approximately the same results can be fabricated. Testing to date has proven these diodes to possess a high degree

---

*Two SET-type diodes were simultaneously fabricated by another group at Thermo Electron under a company-sponsored program. Those diodes also had very similar characteristics, even though fabricated by a group not thoroughly familiar with the design.

of similarity when their I-V characteristics and power output are considered.

4. Series Operation

Diode Va was operated in series with two other diodes of the SET configuration. The characteristics of series operation were found to be identical with the predicted characteristics that is, the sum of the individual readings. The composite I-V characteristic of the three diodes operating in series is shown in Fig. III-43. The I-V curve is based on the common current through all three diodes and the voltage across the three diodes in series. A point indicating the summation of individual voltages at approximately a common current is also given on this plot. This point was found by adding the individual diode voltages while operating individually with approximately the same current. The correlation is quite satisfactory.

5. Diode Efficiency

The efficiency of the series V diodes was measured by using the calorimeter portion of the diode test devices. The accuracy of the calorimeters is discussed in detail in Section V. As noted in that section, there are certain variable terms that cannot be accurately determined at any one particular time. Therefore, the efficiencies reported herein must be considered more as approximations than as accurately measured values. Note that, initially, the calorimeter would indicate a value of efficiency that was high by approximately one point and, as the diode was operated, the measured efficiency beame progressively lower until finally the indicated value could be too low by as much as five points.

The measured efficiencies of diodes Va, Vc, and Vd are shown in Figs. III-44 through III-46, respectively. These measurements were made over a period of a few hours. Therefore, the values should be accurate relative to one another, if not absolutely. Note also the efficiency is highest for the 0.8-volt curves on all three diodes.

IV. CESIUM RESERVOIR TEMPERATURE CONTROL

A. General

An important generator component is the cesium reservoir because diode operation is highly dependent on the presence of cesium ions to eliminate the space charge present between the emitter and collector in a diode of the SET type. To achieve the desired cesium pressure, the temperature of the cesium reservoir must be maintained at a prescribed level in the neighborhood of 600°K, varying within close limits if constant power is to be maintained. The cesium reservoir is located in close proximity to the diode radiator, whose operating temperature is approximately 850°K. It is obvious therefore that the reservoir must be provided with sufficient area for heat dissipation, while also being shielded from the radiator. A simple and reliable device to control the heat fluxes is required for the reservoir to be maintained at constant temperature, even while the radiator temperature varies.

B. Possible Approaches

Two possible approaches to the problem of cesium reservoir temperature control have been studied, an electrical and a thermal control system. In the original design concept, the most attractive system appeared to be that of an electrically heated system employing a thermostatic control. This approach to the control device seemed the most advantageous not only because of its relative simplicity, but because, based on existing technology, it appeared to be the approach most easily accomplished within the time alloted for the development of the SET generator.

Essentially, the basis of this first approach was that the electrical power for the cesium reservoir heater would be supplied by the diodes. This was practical since only a fraction of a watt would be required, which was small compared with the 26.6-watt diode output. However, a major design problem soon developed. It was found that the heat from the collector was not sufficient to heat the reservoir during start-up, thereby causing a start-up problem.

Since the concept of an electrical heater could be used only when the diode was producing power, it became obvious that a supplementary method was needed to facilitate the start-up process. Analysis indicated that a fully thermal control system would obviate this start-up problem, and would also be practical during operation.

1. Design of Cesium Reservoir with Electrical Heater

a. Original Design

The basis for the design of the electrically heated reservoir is essentially that the reservoir must have sufficient area to dissipate the heat absorbed by conduction down the support tube at an equilibrium temperature slightly less than the optimum operating temperature. A small additional quantity of heat would be added by means of an electrical heater on the reservoir to raise its temperature to the optimum cesium temperature. A bimetallic switch would control the quantity of heat provided by the electrical heater to ensure operation within a few degrees of the optimum temperature (see Fig. IV-1).

The details of the cesium reservoir are shown in Fig. IV-2. It consists of a cylindrical nickel block approximately 0.5 in. long and 0.350 in. in diameter. A hole is drilled longitudinally through the cylinder of sufficient diameter to accommodate a 0.125-in. tube out both the top and bottom. The tube out the top connects to the rear of the collector, which has been bored to provide a path for the cesium to reach the interelectrode space. The nickel tubing to the collector, which serves as a structural support for the cesium reservoir, contains a fine-mesh screen or porous plug to prevent liquid cesium from entering the diode while the generator is in a zero g-field. However, the screen would allow equal cesium pressure on both sides. The lower tube is provided for pumping out and cesium-charging the diode. After the diode is evacuated and charged with cesium, this tube is crimped off to provide a vacuum-tight seal.

The cesium reservoir has two other components, as shown in Fig. IV-2. The first of these is a bimetallic (W-Ta) strip mounted on a nickel plate for

sensing the temperature of the cesium reservoir. This is calibrated for 600 ± 2°K.

The reservoir is so designed that under all operating conditions the equilibrium temperature is less than the desired 600°K. The second component is an electrical resistance heater in a four-hole alumina-ceramic cylinder. The heater, electrically connected across the diode through the bimetallic switch, provides the additional power for accurate control of the reservoir temperature.

b. Subsequent Modifications

The question of operation in the inverted or horizontal position was examined, and it was felt that the porous plug would not be sufficient to prevent the liquid cesium from entering the diode during inverted or horizontal operation while subject to earth's gravity.

To eliminate this problem, the reservoir was modified as shown in Fig. IV-3. The re-entrant effect permits orientation in any direction and yet provides a reservoir for the liquid cesium. Should a small quantity of liquid cesium enter the tube during the process of inverting the diode, it would be at a higher temperature than the liquid cesium in the reservoir, and would therefore be distilled back to the reservoir.

For the design to be effective, the level line of the liquid cesium originally distilled into the reservoir, in any position, should be below the entrance tube to the reservoir.

The porous plug is required only for zero gravity operation, and since the program is not near operation in zero gravity, the porous plug has not been designed or tested. This will be accomplished in a later phase of the program.

2. Design of Cesium Reservoir with Thermal Control

The thermal control system operates from the reject heat of the diode radiator. Thermal radiation shields are activated by means of bimetallic strips, which are calibrated with the cesium reservoir temperature. Movement of the shields alters the view factor between the radiator and the reservoir, which in turn alters the

energy absorbed by the cesium reservoir. This, in turn, causes an equivalent change in the reservoir temperature. The cross section of the radiator, reservoir, and control shields is shown in Fig. IV-4.

The cesium tube reservoir (R) is brazed to part (A), which has a conical outside surface and into which the cesium tube is connected. (This assembly can be passed through the opening in the radiator for assembly purposes.) Part (B) has an inside conical surface to fit that of part (A). This part can be mounted on part (A) after complete assembly of the diode. The bottom surfaces of both parts (A) and (B) are plated with silver (or gold) and are well polished to achieve a low emissivity ($0.03 \leq \epsilon \leq 0.05$). All other surfaces are prepared by grooving and coating with chromium oxide to achieve a high emissivity ($\epsilon \approx 0.8$).

Three bimetallic strips (C) are attached to part (B) and activate a shield (S) vertically. (It is also possible to divide the shield into three independent sections, each being activated by one bimetallic strip.) The movement of the shield will expose a variable side area of part (B) to radiation from the radiator. The lower the cesium temperature, the larger the area exposed, allowing higher heat flux into the cesium reservoir.

C. The Start-up Problem

When the emitter of a cold diode is brought to operating temperature, a flow of heat to the diode radiator is established in the amount

$$Q_R^{\cdot} = A_E (q_r + q_c), \qquad \text{(IV-1)}$$

where $Q_R^{\cdot}$ is the heat flow to the diode radiator, A_E is the emitter area, q_r represents the internal radiation losses per unit emitter area, and q_c represents the conduction loss from the emitter to the diode radiator occurring through the emitter spacer. There is no heat transfer by electron cooling or cesium conduction. Since both q_r and q_c are very strong functions of emitter temperature, $Q_R^{\cdot}$ may be regarded as a constant during warm-up at fixed emitter temperature. This flow of heat $Q_R^{\cdot}$ to the diode radiator will cause an increase in radiator temperature as long as it is not offset by the heat radiated by the radiator. The increase in

radiator temperature is, in turn, followed by an increase in cesium reservoir temperature. If the cesium reservoir temperature reaches about 580°K, Q_R' increases because cesium conduction and electron cooling start to appear at about this temperature. Then, the radiator temperature increases further, and after a short period the diode reaches its design-point temperature distribution.

Whether start-up will be accomplished at all depends on whether the Q_R' given by Eq. (IV-1) will exceed the heat radiated by the diode radiator until T_{Cs} = 580°K. The rate of diode warm-up will, of course, depend on the magnitude of the excess of Q_R' over the radiated heat and on the increase in Q_R' occurring at cesium temperatures exceeding 580°K. This is a complicated process, best analyzed experimentally. The problem to be treated here is that of whether full diode warm-up can be achieved.

Assume a cesium reservoir of small thermal inertia connected thermally to the diode radiator by a conducting path of fixed thermal conductance C.* Then the heat received by the cesium reservoir Q_{Cs} would be

$$Q_{Cs} = K_1 T_{Cs}^4 = C(T_R - T_{Cs}). \qquad \text{(IV-2)}$$

Equation (IV-2) gives the relationship between corresponding values of T_R and T_{Cs}. For a diode designed to reach a T_R of 870°K and a T_{Cs} of 620°K, the radiator temperature when T_{Cs} is 580°K, as given by Eq. (IV-2), is 770°K. To determine whether the Q_R' given by Eq. (IV-1) is sufficient to bring T_R to 770°K, one must consider the radiator design. The radiator is designed to radiate.

$$Q_R = A_E(q_r + q_c + q_{Cs} + q_e) - P = Q \text{ in } - P, \qquad \text{(IV-3)}$$

where q_{Cs} and q_e represent the cesium conduction and electron cooling losses per unit emitter area, respectively, and P is the diode output power.

*C = k(A/ℓ).

Equation (IV-3) may be written in terms of diode efficiency as follows:

$$Q_R = P\left(\frac{1}{\eta} - 1\right) \tag{IV-4}$$

and

$$Q_R = K_2 T_R^4. \tag{IV-5}$$

Combination with Eq. (IV-1) yields

$$\frac{Q_R'}{Q_R} = \left(\frac{T_R'}{T_R}\right)^4, \tag{IV-6}$$

where T_R' is the temperature to which the diode radiator is brought by Q_R', which should exceed 770°K to enable completion of diode warm-up. The solution of Eq. (IV-6) is

$$T_R' = T_R\left[\frac{A_E(q_r + q_c)}{P\frac{1}{\eta} - 1}\right]^{1/4}. \tag{IV-7}$$

Typical values for the SET diode would be

$$A_E = (q_r + q_c) = 40 \text{ watts},$$

$$P = 25 \text{ watts},$$

$$\eta = 20\%.$$

Using these values in Equation (IV-7) yields

$$T_R' = 870\left(\frac{40}{100}\right)^{1/4}$$

$$= 690 °K < 770 °K, \tag{IV-8}$$

and it is therefore seen that the cesium resevoir system considered would not be capable of reaching 580 °K and hence diode warm up would stop before reaching the design point.

To circumvent this, a possibility is to make the thermal conductance, C, Equation (IV-2) variable: high at low reservoir temperature and low at high reservoir temperatures. This can be achieved by having bimetallic-controlled

shield that expose the cesium reservoir to varying amounts of radiation from the diode radiator. A complete analysis of such a system has not been made, but it should yield a solution because the start-up conditions are almost achieved [690°K versus 770°K in Eq. (IV-8)], with a fully static system. An abbreviated analysis of such a system is presented in Section IV. E. 4.

D.   Analysis of the System

The cesium reservoir receives approximately 1.45 watts by conduction from the diode radiator. The reservoir and its attachment tube are assumed to be well shielded from the diode radiator, so that no other heat is received by radiation from the radiator. For the reservoir temperature to be 600°K, it must be capable of radiating at least the 1.45 watts received at 600°K. This means that additional increments of heat of 1/8, 1/4, 1/2, and 1 watt will result in corresponding increases in temperature* of 12, 24, 47, and 84°K, respectively. It appeared possible, therefore, to achieve a ±6°K control of reservoir temperature by using an electrical heater rated at 1/8 watt. To actuate this heater, it was decided to use a precalibrated thermostat control that would close or open the connection of the electrical heater to the output of the diode at the desired temperature level. The thermostat would, of course, have to be mounted on the cesium reservoir in such a way that it would always be in good thermal contact with the reservoir and remain relatively insensitive to temperature changes, other than those of the cesium reservoir. For the thermostat to respond to changes in temperature as small as 1°C, assuming that a 1-mil bimetallic movement would suffice to close the electrical contact controlled by the thermostat, the bimetallic constant would have to be as large as 1 mil/°C.

From elementary strength of materials, it can be shown that a bimetallic made of bonded equal thickness of metals with dissimilar coefficients of thermal expansion will have the following operating characteristics:

---

*Calculated assuming that the heat dissipated by the cesium reservoir increases as the fourth power of its temperature.

$$\sigma = E (a_1 - a_2) \Delta T$$

$$\delta = (a_1 - a_2) \Delta T \frac{L^2}{t}$$

where σ is the maximum bending stress in bimetallic, E is the common value of Young's modulus for both metals, $(a_1 - a_2)$ is the difference in linear thermal expansion coefficients, ΔT is the temperature change from stress-free condition, δ is the deflection, and L and t are the length and thickness of the bimetallic strip. The formulas may be combined into:

$$\frac{\delta}{\Delta T} = \frac{\sigma_{max}}{E \, \Delta T_{max}} \frac{L^2}{t}$$

which, for a range of temperatures of ΔT_{max} = 300° C, E = 30×10^6 psi, and σ_{max} = 10,000 psi, yields, for $\frac{\delta}{\Delta T}$ = 1 mil / °C,

$$\frac{L^2}{t} = 1100,$$

where L and t are in inches.

For t = 6 mils, L would than have to be 2.5 in. long. Such a bimetallic length can be placed conveniently around the cesium reservoir in the form of a spiral coil with an outside diameter of 9/16 in. (see Fig. IV-5).

To power an 1/8 watt electrical heater, the coil should be capable of conducting a current of about 1/8 amp with a power loss of about 1/80 watt. This means that the series resistance of the bimetallic coil should be less than

$$R = \rho \frac{\ell}{s} < 0.08 ,$$

assuming $\rho = 30 \times 10^{-6}$ ohm cm,

$$s > 2.5 \times 10^{-4} \, cm^2 \text{ cross-sectional area,}$$

which, for a 6-mil-thick bimetallic, amounts to a minimum width of 6 mils, a requirement quite easily met.

E.   Analysis of the Thermal Control System

1.   Nomenclature*

q_0 radiation from cesium-bath enclosure

q_1 conduction through cesium tube

q_2 radiation to cesium tube

q_3 radiation to bottom of (A) and (B)

q_4 radiation to exposed side of (B)

q_5 radiation to shield (S) (net radiation)

q_6 direct solar radiation (only for back diode)

2.   Heat Transfer

$$q_0 = A \epsilon \sigma T_{Cs}^4,$$

where

$$A = \frac{1}{4} \pi 2.5^2$$
$$= 4.9 \text{ cm}^2,$$
$$\epsilon = 0.8.$$

Hence,

$$q_0 = 3.92 \sigma T_{Cs}^4.$$

For q_1,

$$q_1 = Ak \frac{\Delta T}{\Delta x}.$$
$$D_o = 0.125 \text{ in.},$$
$$t = 0.010 \text{ in.},$$
$$A = 0.0233 \text{ cm}^2,$$

---

* Refers to Fig. IV-6.

$$\Delta T = (T_{rad})_{base} - T_{Cs} \, ,$$

$$\ell = 1 \text{ in.} = 2.54 \text{ cm}$$

$$k = 0.6 \text{ w/cm}^2 \text{ (Ni)};$$

$$q_1 = 0.0055 \, \Delta T = 0.55 \frac{\Delta T}{100}$$

$$= 0.55 \frac{(T_{rad})_{base} - T_{Cs}}{100}$$

For q_2,

$$q_2 = A \epsilon \sigma (\langle T_{rad} \rangle^4 - \langle T_{tube} \rangle^4).$$

$$A = \pi \times 0.125 \times 1 \times 2.54^2 = 2.53 \text{ cm}^2,$$

$$\epsilon = 0.07 \text{ (polished Ni)};$$

$$q_2 = 0.177 (\sigma \langle T_{rad} \rangle^4 - \sigma \langle T_{tube} \rangle^4).$$

For q_3,

$$q_3 = A \epsilon \sigma (\langle T_{rad} \rangle^4 - \langle T_{Cs} \rangle^4).$$

$$A = \frac{1}{4} \cdot (\pi \, 2.5^2) = 4.9 \text{ cm}^2,$$

$$0.03 \leq \epsilon \leq 0.05;$$

$$q_3 = 0.245 (\sigma \langle T_{rad} \rangle^4 - \sigma T_{Cs}^4).$$

For q_4,

$$q_4 = A_{exposed} \, \epsilon (\sigma T_{rad}^4 - \sigma T_{Cs}^4) .$$

$$A_{exposed} = \pi \times 2.5 \times \ell_{exposed} = 7.85 \, \ell_{exposed},$$

$$\epsilon = 0.80;$$

$$q_4 = 7.85 \times \ell \times 0.80 (\sigma T_{rad}^4 - \sigma T_{Cs}^4)$$

$$= 6.28 \, \ell (\sigma T_{rad}^4 - \sigma T_{Cs}^4).$$

For q_5,

$$q_5 = AF_{sh, rad} \, \epsilon\sigma \, (T^4_{rad} - T^4_{sh}) - AF_{sh, 0} \, \epsilon\sigma \, T^4_{sh}$$

$$A = \pi \times 2.8 \times \ell = 8.8 \text{ cm}^2,$$

$$F_{sh, rad} = 0.5,$$

$$F_{sh, 0} = 0.5,$$

$$T_{sh} = T_{Cs},$$

$$\epsilon = 0.03$$

$$q_5 = 0.132 \, (\sigma T^4_{rad} - 2 \, \sigma T^4_{sh}).$$

For q_6,

$$q_6 = C \times A.$$

$$A = \frac{1}{4} \, \pi \times 2.8^2 = 6.15 \text{ cm}^2,$$

$$C - (\text{Solar constant}) = 0.138 \text{ w/cm}^2 \text{ near earth}$$
$$= 0.058 \text{ w/cm}^2 \text{ near Mars};$$

$$q_6 = 0.680 \text{ w/cm}^2 \text{ near earth}$$

$$= 0.286 \text{ w/cm}^2 \text{ near Mars.}$$

3.   Steady-state Temperature of the Cesium Reservoir as a Function of the Radiator Temperature

For a steady-state cesium temperature of 625 °K,

$$\sigma T^4_{Cs} = 0.865,$$

$$q_0 = 3.39 \text{ watts}$$

T_R	700	725	750
q_1	0.550	0.688	0.825
q_2	0.062	0.083	0.105
q_3	0.123	0.174	0.228
q_4*	1.945	2.760	3.618
q_5	-0.036	-0.021	0.006
Σq_{in}	2.64	3.68	4.78
$\Sigma q_{in} - q_0$	-0.75	0.29	1.39

Thus for $T_R = 719°K$,

$$\Sigma q_{in} = q_0.$$

For a steady-state cesium temperature 600°K,

$$\sigma T_{Cs}^4 = 0.735,$$
$$q_0 = 2.88$$

T_R	675	700	725
q_1	0.550	0.688	0.825
q_2	0.050	0.064	0.083
q_3	0.110	0.154	0.206
q_4	1.750	2.490	3.265*
q_5	-0.038	-0.014	0.013
Σq_{in}	2.42	3.38	4.39
$\Sigma q_{in} - q_0$	-0.46	0.50	1.51

*For exposed length of 6.2 mm.

4. Start-up Conditions

To evaluate the start-up problem associated with the thermal control system, calculations were made to determine the amount of heat necessary for start-up and operation.

During start-up, no (or little) current passes through the diode because the cesium pressure is too low. Thus the total heat transferred to the radiator is less than that of normal operation (even though the emitter temperature reaches 2000 °K). The only heat fluxes are those due to radiation and conduction, and there are no electron cooling losses.

The steady-state temperature under these conditions will be lower than the design temperature by the ratio

$$\frac{T_{start}}{T_{design}} = \left(\frac{Q_{RO1\ start}}{Q_{RO1\ design}} \right)^{1/4}$$

For optimistic operation,

$$\frac{Q_{RO1\ start}}{Q_{RO1\ design}} = \frac{220}{429} = 0.513,$$

$$\frac{T_{start}}{T_{design}} = 0.846,$$

$$T_{start} = 0.846 \times 875 = 720\ °K.$$

For pessimistic operation,

$$\frac{T_{start}}{T_{design}} = \frac{243}{393} = 0.619,$$

$$T_{start} = 0.887 \times 875 = 774\ °K.$$

Thus, under all possible operating conditions, the steady-state temperature of the cesium reservoir will not be below 625°K. This allows sufficient cesium pressure to start the current.

VI. ELECTRON-BOMBARDMENT HEATER

A. General

An electron-bombardment heater was chosen for the SET generator because of its ability to deliver high power inputs at high temperature. Also, this type of heater can be accurately controlled. Electrons are emitted by a hot surface and then accelerated by an applied voltage toward the rear faces of the five emitters of the diodes. To achieve uniform heating, the electron-emitting surface must be equidistant from all the diode faces, and the same amount of area must be exposed to each diode.

B. Requirements

An electron-bombardment heater designed to simulate the heat supplied to the cavity by the solar concentrator was required to test the SET generators (see Fig. VI-1). It was therefore necessary that this heater meet a number of very basic requirements. It must have a power output sufficient to raise the SET generators to their operating temperature of 2000°K. An estimated power input of 650 watts is necessary to meet this requirement. Uniform heating of all five diodes in the SET generator must be attained. Finally, this heater must be of such physical configuration and dimension that it can be used with the SET generator.

A number of other lesser requirements also entered into the design and fabrication of the electron-bombardment heater. The unit was to be equipped with a calorimetric device (see part 5, Fig. VI-2) to measure the amount of heat reabsorbed by the electron-bombardment heater. The design of the unit was such that when the heater is used in conjunction with a SET generator, the input power P_{in} (filament power and electron-bombardment power) minus calorimeter power P_{cal} equals the power P actually absorbed by the SET generator.

Another consideration which had to be taken into account in the design of the electron-bombardment heater was that when the diodes are cold, the accelerating potential must be applied across each emitter separately, or else a shunt must be provided across each diode.

C.   Design Calculations

The primary electron-bombardment element, a tantalum block (part 3, Fig. VI-2) delivers approximately 700 watts to the diodes. At electromotive forces of below 330 volts, the space charge begins to limit the current.

The tantalum surface temperature necessary to supply sufficient emission to heat the emitters, given a voltage of 300 volts and a power input of 700 watts, may be derived from the following equations:

$$IV = 700 \text{ watts}, \tag{VI-1}$$

$$I = \frac{700}{300} = 2.33 \text{ amp}, \tag{VI-2}$$

$$J = \frac{2.33}{4.92}, \tag{VI-3}$$

$$J = A_R T^2 e^{-b/t}, \tag{VI-4}$$

$$\log \frac{J}{A_R} = 2 \log T - \frac{b}{T}, \tag{VI-5}$$

$$\log \frac{475}{52} = \log 9.12 \times 10^{-3}$$

$$= 2 \log T - \frac{48600}{T} + 4.69. \tag{VI-6}$$

Then

$$T_{Ta} = 2180 °K. \tag{VI-7}$$

Assuming that the tantalum radiates to low-temperature blackbody surroundings in the upper portion of the cavity, its equilibrium temperature at the base may be calculated:

$$Q_1 = Q_c = Q_2, \tag{VI-8}$$

$$Q_2 = \epsilon \sigma A_2 T_2^4, \tag{VI-9}$$

$$Q_c = k \frac{A_c}{\ell_c} (T_{Ta} - T_2), \tag{VI-10}$$

$$\epsilon \sigma A_2 T_2^4 = k \frac{A_c}{\ell_c} (T_{Ta} - T_2), \tag{VI-11}$$

$$T_2^4 = \frac{k A_c}{\sigma \ell_c A_2} (T_{Ta} - T_2)$$

$$= \frac{0.69 \times \pi \times 0.2 \times 0.005 \times 10^{12}}{0.25 \times 5.67 \times 0.5 \times 2.54 \times \pi \times 1.56} (2200 - T_2)$$

$$= 1.59 \times 10^9, \tag{VI-12}$$

$$T_2 = 1140°K. \tag{VI-13}$$

The following heat losses were also calculated: conduction down the support, radiation to the diodes, electron cooling, radiation up the supports, and total heat loss. The heat loss by conduction down the support is

$$Q_{cond} = k \frac{A_{Ta}}{\ell} \Delta T$$

$$= k \frac{2\pi R d}{2\ell} \Delta T$$

$$= 0.69 \frac{0.400}{0.500} \pi \frac{0.005}{2} 2.54 \times 1060$$

$$= 1.12 \times 10$$

$$= 11.2 \text{ watts.} \tag{VI-14}$$

The heat loss by radiation

$$Q_{rad} = \epsilon_{Ta} \; \sigma A_{Ta} (T^4_{Ta} - T^4)$$

$$= 0.25 \times 5.67 \times 10^{-12} \times 4.92 \times (2.2^4 - 2.0^4) \times 10^{12}$$

$$= 6.91 \times 7.4$$

$$= 51.2 \text{ watts} \qquad\qquad (VI-15)$$

The electron cooling loss is

$$Q_{ec} = \frac{IV}{V} \; \phi_{Ta}$$

$$= \frac{700}{300} \; 4.1$$

$$= 8.7 \text{ watts.} \qquad\qquad (VI-16)$$

The heat loss by radiation back up the support may be determined by

$$(Q_{rad})_2 = \epsilon \; \sigma A_{Ta} \; T^4_{Ta}$$

$$= 0.35 \times 5.67 \times 10^{-12} \times \pi \times 0.27^2 \times 6.45 \times 2200^4$$

$$= 1.91 \times 2.2^4$$

$$= 63.0 \text{ watts} \qquad\qquad (VI-17)$$

The total heat loss from the tantalum is the sum of these losses:

$$Q_T = 134.1 \text{ watts} \qquad\qquad (VI-18)$$

Since about 50 watts is transmitted by radiation to the diodes, the necessary electrical heat input is decreased to 650 watts. The temperature of the tantalum block needed to achieve this power remains relatively unchanged, however, at about $2175^\circ K$.

To maintain the tantalum block at a temperature of $2175^\circ K$, the tungsten filament (part 16, Fig. VI-2) should supply about 150 watts. The necessary filament

temperature may thus be derived from an accelerating voltage of 500 volts:

$$T_W = \log \frac{J}{A_R}$$

$$= \log \frac{1.85}{72}$$

$$= 2.58 \times 10^{-2}$$

$$= 2 \log T - \frac{32430}{T} + 3.66$$

$$= 2770° K. \tag{VI-19}$$

The conduction heat loss through the tungsten filament leads is

$$q = kA \frac{\delta T}{\delta x}$$

$$= 1.26 \times 5.06 \times 10^{-4} \times 7.55 \times 10^{3}$$

$$= 4.8 \text{ watts}, \tag{VI-20}$$

$$Q_{fil} = 2 \times 4.8$$

$$= 9.6 \text{ watts.} \tag{VI-21}$$

For this case, consider a 0.010-in. tungsten wire at 2300° K:

$$I = 5.4 \text{ amp} \quad \text{(from Kohl)}, \tag{VI-22}$$

$$\rho = 4 \times 10^{-5} \text{ ohm/cm}, \tag{VI-23}$$

$$\epsilon = 0.15, \tag{VI-24}$$

$$L = 0.203 \text{ cm}, \tag{VI-25}$$

$$T_{max} = 2300° K, \tag{VI-26}$$

$$T = 300° K, \tag{VI-27}$$

$$T_E = 2000° K. \tag{VI-28}$$

The total heat into the gun structure is therefore the sum of Eqs. (VI-14), (VI-17), and (VI-21):

$$Q_T = Q_{cond} + (Q_{rad})_2 + Q_{fil} = 83.8 \text{ watts.} \qquad \text{(VI-29)}$$

For a rise of 50°C in the water which cools the heater, a water velocity of 0.962 ft/sec is required in a 65-mil tube, 7.7 ft long.

D. Description of Design

As stated previously, uniform heating of all five diodes by the electron-bombardment heater is essential to the operation of the SET generator. A cylindrical heating element (part 3, Fig. VI-2), cut from a single piece of tantalum, was used as the electron-bombardment emitter. This primary emitter was, in turn, heated by electron bombardment from a secondary tungsten filament (16), which was supplied with power by external leads (11).

The area of the tantalum block emitter (3) is identically viewed by the four side emitters, and the distance from the block to each emitter is identical. The bombardment current received by each should, therefore, be equal. The bottom diode, however, views a different area of the emitting element; therefore, the distance between the emitting element of the heater and the diode element must be adjusted to equalize the heat input to all five diodes. This adjustment will be accomplished experimentally after the final assembly of the heater by moving the primary emitting element (3) and inserting metal washers between the insulator support (15) of the primary emitter and the emitter itself. A fine correction can also be achieved by varying the accelerating voltage. Operation of the electron-bombardment heater in the space-charge region allows another correction in the power distribution among the diodes through variation of the accelerating voltage.

The electron-bombardment element is completely surrounded by a chamber (2) equipped with a water-cooling coil (5). Any heat supplied to the heater and not transferred to the generator will be absorbed by the cooling water. Thus, the heat absorbed by the generator may be determined as the difference between the total electrical input to the electron-bombardment heater and the measured heat

93

rejected to the water. The calorimeter to measure the heat reabsorbed is an integral part of the electron-bombardment heater. This permits a direct measurement of the efficiency of each generator

The circuit diagram for the electron-bombardment unit is shown in Fig. VI-3.

V. DIODE TEST DEVICE

A. Requirement

One of the contract requirements for the SET program was to measure calorimetrically the efficiency of the diodes fabricated during the program. This was to be accomplished by measuring the rejected heat from the diode and computing the efficiency as

$$\eta = \frac{\text{electrical power output}}{(\text{reject heat}) + (\text{electrical power output})}.$$

In addition to accurate measurement of the heat rejected from the diode during operation, the diode test device was to be a complete set-up for testing the SET diode. This included an electron-bombardment heater, a vacuum enclosure, and a base plate with sufficient leadthroughs for power output leads, thermocouple leads, etc.

B. Description of Design

The diode test device consists of a diode enclosure, a calorimeter to measure the rejected heat from the diode, a water-cooled base plate which serves as both a heat sink and a means of locating the necessary electrical leadthroughs, an electron-bombardment heater with an electrostatic shield, and a Vycor vacuum enclosure. A cross section of the diode test device is shown in Fig. V-1. The diode test device, with the equipment necessary to conduct diode evaluation tests, is shown in Fig. V-5.

1. Calorimeter

The calorimeter consists of an OFHC copper housing, which encloses the diode under test. The heat rejected from the diode is radiated to the black (chromium-oxide-coated) interior of the housing and passes through a 1-in.- diameter copper post to the water-cooled base. Temperature measurements at the top and bottom of the post are made with Pt | Pt-10% Rh thermocouples brazed into small-diameter stainless steel tubes, which are in turn soldered to the post. The copper exterior of the calorimeter and the post are polished to minimize radiation.

V-1

95

The various constants for the calorimeter are:

distance between thermocouples: l = 10.85 cm,

diameter of post: D = 2.54 cm,

K_{Cu} = 3.80 (see Table V-1).

From these constants, the Q of the calorimeter per degree centigrade may be established:

$$Q = k \frac{A}{l} \Delta T ,$$

$$A = \frac{\pi D^2}{4} = \frac{\pi (2.54)^2}{4}$$

$$= 5.065.$$

Therefore,

$$Q = k \frac{A}{l} \Delta T$$

$$= 3.80 \frac{5.065}{10.85} \Delta T ,$$

$$Q_{cal} = 1.774 \Delta T.$$

2. Other Components

The diode to be tested is placed inside the copper housing in such a way that it is supported on the lip of the radiator by an insulating ceramic ring. This ensures that the maximum heat transfer from the radiator to the housing is by radiation. The collector lead is grounded to the copper housing, and the emitter lead is connected to a leadthrough in the base plate by means of a heavy copper strap. A copper cap is placed over the housing and bolted in place. The cap has a hole in its center through which the tantalum spacer and emitter of the diode protrude. The walls of the hole through the copper cap act as radiation shields for the tantalum spacer, simulating the rhodium plated walls of the diode support structure of the SET generator.

To prevent electron-bombardment heating of the calorimeter, an electrostatic shield is placed around the emitter (see Fig. V-2). The shield is made of molybdenum,

the outer surfaces of which are Rokide-coated to increase their emissivity (0.9). The shield was made quite large so that it would have sufficient area to dissipate any stray heat absorbed, at a relatively low equilibrium temperature. The shield has 30.40 cm^2 of Rokide-coated area which, at the average design temperature of the top of the calorimeter, is capable of dissipating

$$Q = A\epsilon\sigma(T^4)$$

$$= 30.4 \times 0.9 \times 5.67 \times 10^{-12} \times 372^4$$

$$= 2.76 \text{ watts.}$$

The electrostatic shield is supported by a ceramic ring to minimize heat transfer between the calorimeter and the shield, and to electrically insulate it from the housing, which is at the collector potential. This would allow the potential of the shield to assume its own potential, and hence draw a minimum current by electron-bombardment.

C. Design Accuracy of Measurement

The calorimeter is in a vacuum enclosure; there is no convection heat loss. The radiation from the exterior of the housing and the copper rod amounts to less than 1.6 watts. The calculations supporting this loss follow.

1. Housing Radiation

a. Upper Portion

$$Q = A\epsilon\sigma T^4,$$

$$T = \frac{100 + 90}{2} + 273$$

$$= 368°K,$$

$$A = \pi D \ell$$

$$= \pi \times 3 \times 5.55 \times 2.54$$

$$= 132 \text{ cm}^2,$$

$$\epsilon = 0.05,$$

$$\sigma T^4 = 1.043 \times 10^{-1},$$

$Q = A\epsilon\sigma T^4$

$\quad = 132 \times 5.67 \times 0.05 \times 368^4$

$\quad = 132 \times 5 \times 1.043 \times 10^{-3}$

$\quad = 0.690$ watt.

b. Lower Portion

$Q = A\epsilon\sigma T^4,$

$T = 87 + 273$

$\quad = 360°K,$

$A = \pi D\ell$

$\quad = 2.25 \times \pi \times 1.0 \times 6.45$

$\quad = 45.5 \text{ cm}^2,$

$\sigma T^4 = 9.538 \times 10^{-2},$

$Q = A\epsilon\sigma T^4$

$\quad = 45.5 \times 0.05 \times 5.67 \times 360^4$

$\quad = 0.215$ watt.

c. Cap

$Q = A\epsilon\sigma T^4,$

$T = 100 + 273$

$\quad = 373°K,$

$A = \pi D\ell$

$\quad = \pi \times 3 \times 0.87 \times 6.45$

$\quad = 52.80 \text{ cm}^2,$

$\sigma T^4 = 1.101 \times 10^{-1},$

$Q = A\epsilon\sigma T^4$

$\quad = 52.8 \times 5 \times 10^{-2} \times 1.101 \times 10^{-1}$

$\quad = 0.290$ watt.

2. Radiation from Rod

$$Q = A\epsilon\sigma T^4,$$

$$\ell = 5.125 \text{ in.},$$

$$A = \pi D\ell$$

$$= \pi \times 1.0 \times 6.45 \times 5.125$$

$$= 103.8 \text{ cm}^2,$$

$$T = \frac{84 + 20}{2}$$

$$= 52 + 273$$

$$= 325°K,$$

$$\sigma T^4 = 6.345 \times 10^{-2},$$

$$Q = A\epsilon\sigma T^4$$

$$= 103.8 \times 5 \times 6.345 \times 10^{-4}$$

$$= 0.328 \text{ watt.}$$

3. Total Radiation Losses

$$\Sigma Q_i = \Sigma Q_{rad}$$

$$= 0.290 + 0.215 + 0.690 + 0.328$$

$$= 1.523 \text{ watts.}$$

4. Conduction Losses

The conduction down the copper strap from the emitter lead amounts to a maximum of 11.5 watts, depending on the degree of thermal contact of this lead with the emitter lead. This is arrived at as follows:

Q_1 = heat conducted through diode emitter lead,

Q_2 = heat conducted down copper strap;

$$Q_1 = kA_1 \frac{\Delta T_1}{\ell_1},$$

$$Q_2 = kA_2 \frac{\Delta T_2}{\ell_2},$$

$$\Delta T_1 + \Delta T_2 = 700°C,$$

$$Q_1 = Q_2,$$

where

$$A_1 = 0.193 \text{ cm}^2,$$

$$A_2 = 0.302 \text{ cm}^2,$$

$$\ell_1 = 3.18 \text{ cm},$$

$$\ell_2 = 20.3 \text{ cm}.$$

Then,

$$A_1 \frac{\Delta T_1}{\ell_1} = A_2 \frac{\Delta T_2}{\ell_2},$$

$$\Delta T_1 = \frac{\ell_1 A_2}{A_1 \ell_2} \Delta T_2$$

$$= 700 - \Delta T_2,$$

$$700 = \frac{\ell_1 A_2}{A_1 \ell_2} \Delta T_2 + \Delta T_2$$

$$= \Delta T_2 \left(\frac{\ell_1 A_2}{A_1 \ell_2} + 1 \right)$$

$$= \Delta T_2 \frac{3.18 \times 0.302}{0.193 \times 20.3} + 1,$$

$$\Delta T_2 = 203°K,$$

$$\Delta T_1 = 700 - 203$$

$$= 497°K,$$

$$Q = kA \frac{\Delta T}{\ell}$$

$$= 3.8 \times 0.302 \frac{203}{20.3}$$

= 11.5 watts.

Radiation from the pyrometer reading hole is not heat that would otherwise flow through the diode, and therefore it is not a serious source of error.

The radiation from the opening for the emitter lead is less than 2.25 watts. The basis for this loss is the radiation from the hole in the calorimeter to the emitter output lead:

$$Q = \sigma A f T^4,$$

where

$$T = 950\,°K,$$
$$\sigma T^4 = 4.634,$$
$$f = 0.3,*$$
$$A = 1.61\ cm^2.$$

Then,

$$Q = \sigma A f T^4$$
$$= 0.3 \times 4.634 \times 1.61$$
$$= 2.24\ watts.$$

Therefore, the maximum total extraneous heat losses amount to 15.3 watts. The total rejected heat from the diode is approximately 105 watts, so that the total extraneous heat losses represent 14.6% of the rejected heat. Therefore, the calorimeter would tend to read high by 2.6 efficiency points, at full SET diode output. It should be pointed out that this is the maximum error on the high side, and that for lower diode efficiency, it would read more accurately than at the SET specification.

D. Modifications to the Diode Test Device Heater

During tests using the diode test devices, shorting of the tungsten filament due to vibration of the vacuum system caused unnecessary thermal cycling and delay

---

*View factor for a plane point source and a right circular cylinder. ATI 187828 (NACA-TN-2836), p. 25, configuration p. 8.

in testing. Since the testing of diodes Va, Vb, Vc, and Vd included periods with a minimum number of thermal cycles, it was found necessary to modify the filament and filament support structure of the electron-bombardment heater. A long-life filament with a rigid support was designed and fabricated.

The long-life filament assembly consists of an insulator support piece (part 1, Fig. V-3), which has two insulators (part 2) brazed into it. These insulators hold the filament blocks (3 and 4). The tungsten filament (5) is held in the blocks by headless-socket set screws; a molybdenum shield (6) surrounds the filament; these parts are shown in Fig. V-4. The insulator support plate is fastened to the top of the vacuum plating. Three threaded-stud copper leads run from the insulators in the top vacuum plate to the filament insulators.

A filament-annealing fixture was designed and constructed to permit precise forming of the tungsten filament and proper stress relief after forming. This fixture is shown in Fig. V-5.

The revised filament assembly features

(1) convenient adjustment of filament-to-target spacing,

(2) 0.030-in. diameter tungsten wire with an estimated life of 3,500 hours in a vacuum of 10^{-5} mm Hg or better at an operating temperature of 2550°K (see calculations below for the design of the filament),

(3) a rigid structure which is not so sensitive to vibration as the previous filament assembly, and

(4) extra holes for filament replacement in case of breakage. (Figure V-6 shows the assembly.)

The rate of evaporation of tungsten at 2550°K is 5.4×10^{-9} gm cm^{-2} sec^{-1}.*
The decrease in thickness corresponding to this evaporation rate is

$$\frac{5.4 \times 10^{-9}}{19.3} = 2.8 \times 10^{-10} \text{ cm/sec.}$$

The life of a filament is generally defined as the time required to effect a 10% decrease in filament diameter due to filament evaporation.† For a 0.030-in. diameter

_____

*Kohl, p. 275.
†Kohl, p. 273.

filament, this represents a surface evaporation of

$$\frac{0.030}{2} \times 2.54 \times 0.10 = 3.8 \times 10^{-3} \text{ cm.}$$

The time and, according to the preceding, the life of such a filament are then

$$\frac{3.8 \times 10^{-3}}{2.8 \times 10^{-10}} = 1.35 \times 10^{7} \text{ sec}$$

$$= 3760 \text{ hours.}$$

E. Actual Calorimetric Measurements of Efficiency

Efficiency measurements on diode Va, using the calorimetric devices in which the diode was tested, yielded values of efficiency of 10.9% and 13.1% at output voltages of 1.07 and 0.8 volt, respectively.*

Where similar tests were performed on diodes Vc and Vd, however, the efficiency values obtained were respectively 8.3 and 9.4% for diode Vc and 6.8 and 10.0% for diode Vd. These values were obtained even though all the diodes required an input of approximately 245 watts and yielded the same power output. Detailed investigation of the operating conditions of the calorimeter revealed several sources of substantial error.

A portion of this error is felt to be due to the 9/16-in. hole that was cut in the bottom of the calorimeter to permit the protrusion of the cesium reservoir outside the calorimeter. The decision to cut this hole in the calorimeter was made just prior to the short-range diode program at the end of August, to permit better control of the cesium pressure by adding a heater to the reservoir. A heater was also added to the collector to ensure optimum collector temperature. These heaters are shown in Fig. V-7. The power to the collector heater varied from diode to diode, and varied for different points on the I-V curve. This caused a variable loss. The spread of efficiency measurements is felt to be partly due to this variation.

---

*These can be calculated from data points 8-3 and 9-23. (Data sheets for diode Va; first number is page, second number is the line).

Further examination of the diode calorimeter was carried out in an attempt to explain the spread of the efficiency measurements.

Tungsten evaporated from the filament of the electron-bombardment heater operating at 2550°K and deposited on the copper walls adjacent to the tantalum spacer. This increased the emissivity from 0.08 to 0.82 (minimum), increasing the heat loss from the spacer to the calorimeter to 69 watts. Fig. V-8 shows the amount of deposition on the top of the calorimeter. Part of the 69-watt increase was due to the increase in lateral area of the spacer operating at essentially emitter temperature. This was due to the revision in the spacer design for diodes V.

The tungsten evaporation also coated the inside surface of the ceramic ring, insulating the electrostatic shield from the housing. The film of tungsten was electrically conductive, and this brought the electrostatic shield essentially to the potential of the diode collector. The shield then began to draw an appreciable current from the electron-bombardment heater, and became visibly hot (hotter than 700°C). Under these circumstances, the heat absorbed by the diode calorimeter by conduction through the ceramic ring and tungsten filter could be as high as 29 watts, depending on the degree of thermal contact between the ceramic ring and the surface of the calorimeter.

Adding the effects of these errors, it was found that the apparent heat rejection may be too high, by as much as 83 watts, under the circumstances described above. However, it should also be pointed out that the entire outer surface of the calorimeter became quite discolored and, although it was not possible to measure the emissivity, the emissivity was obviously higher than that of polished copper. Also, the temperature of the calorimeter housing was considerably higher than the design value. Therefore, radiation from the calorimeter could be as high as 12 watts.

The basis of this estimate is the approximate average temperature during operation:

top plate: 350°C,

housing: 200°C,

pedestal: 180°C.

$$Q_{radiated} = \epsilon \sigma T^4 A,$$

where

$\epsilon = 0.1$,

$\sigma = 5.67 \times 10^{-12}$.

Then,

top plate $= 0.1 \times 5.67 \times 10^{-12} \times 623^4 \times 52.8$

$= 4.54$ watts,

housing $= 0.1 \times 5.67 \times 10^{-12} \times 473^4 \times 177.5$

$= 5.05$ watts,

pedestal $= 0.1 \times 5.67 \times 10^{-12} \times 453^4 \times 103.8$

$= 2.47$ watts,

$\Sigma Q_{rad} = 12.06$ watts.

Since the power output of the diodes is about 13 watts and the measured heat rejection is between 130 and 180 watts, the measured values of efficiency are too low by 1 to 6 points. This source of error also accounts for the deviation of measurements, both between different calorimeters and with the same calorimeter as a function of time.

F. Conclusion

The revised diode test device, with its related test equipment, is shown in Fig. V-9. The conclusion drawn here is that the present diode test devices are satisfactory for diode testing; however, calorimeter measurements are unsatisfactory for the measurement of diode efficiency. This is due primarily to the large inherent extraneous heat transfer quantities. This in turn, is due primarily to the evaporation of material from the electron-bombardment filament. These sources of error can

105

be eliminated by constructing a calorimetric device that is specifically directed toward precise measurement of all heat quantities and that reproduces the actual diode environment in a generator configuration rather than one that serves only as a low-cost, quick-test, multipurpose diode test device. The construction of such a precision calorimeter is definitely recommended.

VII.   DIODE SUBLIMATION TEST

A.   Objective

The purpose of the diode sublimation test was to have been to determine the effects of evaporation of emitter materials on the electrical power output of the thermionic diode to be used in the SET generator.   The basis of the following test was that the only factor affecting the life characteristics of the diode is the evaporation of emitter material.   Such an assumption may be dangerous if care is not exercised in evaluating the resulting data, for the assumption that any and all changes in diode output are the result of emitter evaporation may be fallacious. To avoid this pitfall, the complete characteristics of the diode must be evaluated should any significant changes in diode performance occur.   From such an evaluation, an attempt must be made to determine the reason for the change in performance and whether or not it is related to emitter evaporation.   Should a failure or change occur which can be shown to be independent of emitter evaporation, a detailed chemical analysis would not be conducted.

B.   Procedure

1.   General

A diode considered by Thermo Electron engineering personnel to be representative of the diodes to be used in the SET generator was to have been selected for the diode sublimation test.   It was first to be tested to ensure structural reliability, integrity, and electrical performance.   The diode was then to be mounted in a vacuum chamber and brought up to operating temperature ($2000°$K) with an electron-bombardment heater.   The load required to draw maximum power (approximately 0.04 ohm) would then be connected across the diode.   The following parameters were to have been recorded:

(1) power input,

(2) output current (or voltage),

(3) collector temperature,

(4) cesium bath temperature.

2. Testing

Some difficulty was encountered in the initial evacuation of the test chamber (Fig. VII-1) as well as in the maintenance of a sufficiently hard vacuum to permit operation of the electron-bombardment heater. The tubulation from the pump to the base plate of the test device was, therefore, replaced with shorter tubing of larger diameter, which considerably improved the initial evacuation of the device. However, the outgassing rate of the diodes and the test device was so high that the VacIon pump could not maintain the vacuum. This necessitated a very gradual increase in the electron-bombardment power on the first run, but after the operating conditions had once been achieved, the 8-liter/sec VacIon system operated successfully.

(Concurrently, two identical test devices used for other diode evaluation were connected to conventional mechanical diffusion pump systems; no difficulty was encountered in their use. Diodes were tested in each device and the operation of both devices was quite satisfactory.)

Although the diode sublimation test was not started, a general outline of the philosphy upon which the test was based can be made. Daily inspection of the diode under test was to have been made. An abrupt change or gradual drop in output power to less than 85% of original power would have set in motion a complete checking process. The diode was to have been thoroughly examined by running tests to obtain a complete I-V curve for several collector and cesium bath temperatures in the region of the operating point. If the diode could be brought back to full power by minor adjustments in power input to the cesium reservoir or collector heaters, the test would be resumed. If the diode characteristics had changed apprecably, however, testing would be terminated,

the cesium removed, and the diode cut open. The collector would then be removed and its surface inspected to determine if there were any unusual effects due to the evaporation of emitter material. The collector was to have been quantitatively analyzed to determine the amount of emitter material deposited on the collector surface.

If, at the end of the first 1000 hours of testing, the performance of the diode had remained essentially constant, I-V curves would be taken for several cesium bath temperatures in the vicinity of the optimum bath temperature. The test was then to be recurred for another 1000-hour period, following essentially the same procedure as outlined above.

C. Status

All preparations are made for the start of the diode sublimation test except for obtaining a suitable diode. As was shown previously, the test procedures had been determined, written, and approved by EOS. The test setup had been designed and fabricated; the equipment had been assembled and collected. All was in readiness to conduct the test. Subsequent changes in the SET were such that the life testing of many diodes was required. The results of these tests were explained in Chapter III. The information obtained from these extensive diode life tests was far more than could have been obtained from a simple diode sublimation test. Since life testing has superseded sublimation testing, the diode sublimation test will not be conducted.

VIII.   DUMMY CAVITY

A.   Requirements

The objective of the dummy cavity was to determine the uniformity of cavity temperature for the cavity design of the SET generator. As previously stated, all five diodes must be maintained at equal temperatures. The relationship of heat flux and temperature among the four side diodes and the single rear diode was therefore of paramount importance for the proper functioning of the SET generator.

To meet these objectives, a number of general requirements were met. The geometry of the dummy cavity must be identical to that of the proposed generator. Accurate temperature measurement of the various portions of the cavity must be maintained at all times. Of particular interest were the relative temperatures of the rear and side diodes as well as the difference in temperature between one side diode and another. Therefore, it was necessary to incorporate in the cavity a means of accurately measuring diode temperatures. Absolute temperature levels within the dummy cavity must also be known, and it was highly desirable to have, in addition, a device capable of measuring the temperature distribution over the cavity face of a single diode.

It was also considered desirable to incorporate a calorimeter so that the total heat absorbed by the cavity could be measured and compared with the incident energy (the known heat flux at the cavity entrance). A comparison of the amount of heat absorbed by the cavity and the incident flux provided an accurate indication of the effectivness of the cavity design.

In addition to these design factors concerning cavity operation, other factors required that the design be capable of incorporating provisions for mounting the cavity on the EOS-designed equipment, so as to facilitate testing. The dummy cavity was also to serve as a check on the EOS-designed equipment prior to investigation of the actual solar heated unit.

B.   Description of Design

A cross section of the dummy cavity is shown in Fig. VIII-1. The front cone and the inner surfaces of the cavity are identical with those of the SET

generator. In lieu of the SET diodes, tantalum dummy diodes have been substituted. The heat absorbed by these dummy diodes flows down a thin-walled tantalum sleeve to the molybdenum block, which is water-cooled. The temperature of the back side of the diode (emitter cavity face) is measured with two tungsten|tungsten-26% rhenium thermocouples for each dummy diode. This permits comparison of the temperatures of the various diodes and provides direct measurement of the temperature distribution over the face of any one particular diode.

The cooling coil includes inlet and outlet thermocouples and a cooling-water flow meter so that the amount of heat absorbed by the cavity can be measured calorimetrically. The design of the dummy cavity is such that it can be mounted on the supporting ring that was designed and fabricated for the SET generator.

Other details of the dummy cavity design are such as to facilitate the mounting and proper support of the W|W-26% Re thermocouples. The proper mounting and attachment of these thermocouples was the most difficult task in the fabrication of the dummy cavity. For the most part, the design of the cavity was dictated by the mounting and attachment requirements of the W|W-26% Re thermocouples.

C. Tungsten-rhenium Thermocouple Testing

1. Summary

The principal problem encountered in the fabrication and testing of the dummy cavity was the choice of a suitable method of attachment of the W|W-26% Re thermocouple to the dummy diodes to obtain accurate, stable, and reproducible thermocouple readings. When the decision to use the W|W-26% Re thermocouple was made, the local offices of both Minneapolis-Honeywell and Engelhard Industries were consulted on the proper use of this thermocouple. Engineers from both offices suggested methods of attachment, giving the impression that these methods were proven and trouble-free. Attempts to apply these methods to test pieces proved the contrary.* Both EOS and Minneapolis-Honeywell referred Thermo

---

*Details of the methods of attachment are covered in Section VIII. C. 2.

Electron to the Brown Instrument Division of Minneapolis-Honeywell in Philadelphia. The intended use of the W|W-26% Re thermocouple and the methods of attachment that had been unsuccessfully tested to date were explained to engineers from the Sensor Department of Minneapolis-Honeywell. Engineers from that research group recorded the information given them and stated that they would study the problem and recommend a solution. They recommended methods of attachment similar to those previously tested. The ideas were tried again, exercising all due precautions. The result was, as before, an unstable thermocouple.

After detailed discussions at Thermo Electron, a method of attachment evolved that appeared to be quite reasonable. A thermocouple was fabricated, attached to a specimen, and tested. After 15 hours, the thermocouple was still giving a constant output, but it was not in good agreement with the optical pyrometer.

It was then decided to build a test specimen with two thermocouples, using the latest method of attachment. The specimen was fabricated, thermocouples were attached, and the specimen was tested. The result, though better than for any method previously tested, was still not sufficiently accurate or stable to warrant its use in the dummy cavity. EOS suggested several authorities on W|W-26% Re thermocouples, one of whom (Dr. Kuether) proved to be quite helpful.

Using the idea suggested by Dr. Kuether, a test specimen employing four W|W-26% Re thermocouples was fabricated, and thermocouples were attached and tested. The difference among the initial readings of the thermocouples was less than 30°C (see Fig. VIII-2) and, over a period of 80 hours, the variation in the difference between any two thermocouples was approximately 14°C. These results were sufficiently encouraging to permit the use of this method of attachment with the dummy cavity.

The design of the dummy cavity was revised, new dummy diodes and the other revised parts were fabricated, and the dummy cavity was assembled. The dummy cavity, complete with carrying case, flow meter, low-temperature thermocouples, and operating manual, was delivered to EOS on August 3, 1961 (see Fig. VIII-3).

A description of the principal methods of thermocouple attachment and the resulting test data are presented below.

2. Methods of Attachment and Results

a. Wires Wedged with Plug

The two thermocouple wires were wedged in a hole in the specimen with a tantalum plug (see Fig. VIII-4). The readings were about 500°C lower than the actual temperatures as measured with an optical pyrometer.

b. Wires Wedged and Brazed

The thermocouple wires were wedged in a hole in the specimen, and a nickel braze wire was included in the bottom of the hole (see Fig. VIII-5). After brazing at 1500°C, the thermocouple read approximately 200°C below actual temperature and kept dropping steadily thereafter with time.

c. Wires Beaded at the End of Tantalum Insert. Insert Brazed in Specimen

A tantalum insert was made, and the two thermocouple wires were beaded with the thin end of the tantalum cylinder (see Fig. VIII-6). Then the entire assembly was inserted and brazed in the specimen. This thermocouple read correctly for 10 hours; then it started drifting downward at the rate of 42°C/hr. The results of this test are shown in Fig. VIII-7.

d. Wires Beaded in Tantalum Insert. Insert Not Brazed

The same procedure was repeated, but the insert was pricked in the specimen (again see Fig. VIII-6). This method of attachment gave a consistent reading for approximately 15 hours. After 15 hours, the reading began to drift downward at the rate of 25°C/hr.

e. Wires Individually Pricked in Holes

In accordance with the suggestion of Dr. Kuether, of the Minneapolis-Honeywell Research Center, two 0.020-in. wires* were inserted in two individual holes in the specimen and pricked in place (see Fig. VIII-8). A test specimen with four thermocouples was tested and, after 65 hours of operation, the thermocouples did not exhibit any drift. The spread of the four thermocouples was approximately 30° C. The maximum variation in the difference between any two thermocouples was approximately 14° C. The detailed test results are shown in Fig. VIII-2.

D. Test to Determine Heat Loss from Dummy Diode

One dummy diode was tested for heat transfer, as shown in Fig. VIII-9. By measuring the temperature difference between TC_1 and TC_2, the heat flux down the copper rod was calculated and the design of the dummy diode was checked to assure that the heat transfer by radiation and conduction would approach that of the actual diodes. The final thickness of the tantalum spacer was designed to yield a heat transfer through the dummy diodes of from 10 to 15% lower than that through the actual diodes. The detailed test data obtained from this test are plotted in Fig. VIII-10.

---

*The previous methods of attachment had been made with 0.005-in. wire.

IX. JG-P GENERATOR

A. Requirements

The object of the construction of the JG-P dynamic test generator is to determine the ability of the SET generator, and more specifically the SET diode, to withstand the dynamic environment which would exist during the missile launch. Because the diode would be unheated during launch, all tests will be run with the emitter at room temperature. To decrease the costs of the JG-P unit, only one authentic diode will be incorporated in the dynamic test generator. This will be a side diode; the remaining three side diodes and the rear diode will be simulated by stainless steel dummies. For the tests to produce valid information, the simulated diodes will be identical in mass and location of center of mass. The same spring constant will be used in the mounting ring which attaches the diode to the block.

Before incorporation into the JG-P generator, the single authentic diode will first be thoroughly tested. The JG-P generator will then be assembled with the dummy diodes and the authentic diode, and the generator forwarded to EOS for dynamic testing. When the testing is completed, the generator will be returned to Thermo Electron, the diode removed, and retested. The data from the second test will then be compared with that obtained from preliminary testing. The results of this comparison should indicate the ability of the diode to withstand the dynamic environment of a launch.

B. Design

The JG-P generator for dynamic testing will be identical in all aspects of configuration to the final SET generator. For the purpose of dynamic testing, only one SET diode will be used, however. The remaining four diodes were fabricated from 304 stainless steel, maintaining the shape, weight, and center of gravity for the actual SET diode. Each of the dummy diodes will be placed into a molybdenum diode support structure which is identical in all respects to that used in the SET generator.

The same type of tantalum ring will be used to secure the diode to the mounting block. Thus, although the diode materials are not the same as for the SET diode, the spring constant of the mounting ring and configuration of the JG-P generator are identical with those of the SET generator.

To maintain all parameters constant for the JG-P dynamic test generator, it was necessary to make extensive calculations first on the authentic diode to determine its center of gravity and mass, and then on the dummy diodes of both types (side and rear). This was necessary since these two differ slightly, due to the different emitter cavity face of the rear diode. The initial calculations on the authentic diode are quite involved because the inner configuration differs greatly from that of the dummy diodes, which is not so intricate. The presence of many different materials with various densities in the authentic diode also complicates these calculations. The calculations for three diodes (an authentic, a dummy side, and a dummy rear) will be presented in the following section.

Calculations were also made to determine the proper spring constant for the stainless steel supporting ring [corresponding to the niobium ring (part 6, Fig. III-1)] of the authentic diode to determine the proper length and wall thickness, considering the difference in Young's modulus of the two materials.

C. Design Calculations

The basic cross-sectional configuration of each diode was considered as a combination of simple shapes, e. g., cylinders, discs, etc.; from this, the mass and center of gravity of each subsection could be computed by elementary mathematics. The sums of the masses and centers of gravity of the subsections produce the total mass and collective center of gravity. The calculations are somewhat simplified by the fact that the diode design is completely symmetrical so that the y-axis is common to all subsections. No calculation of the y-coordinates is necessary, since $\langle y \rangle = 0$.

The basic equation for the x-coordinate is

$$\langle x \rangle = \frac{\Sigma m_i x_i}{\Sigma m_i},$$

where m_i is the mass of the ith section and x_i is the center of gravity of the ith section.

Calculations based on the proposed configuration of the dummy diode were made in much the same manner as those for the authentic diode. They were much simpler, however, in that the dummy diodes involved the use of a single material and a simpler internal geometry.

To gain a fuller understanding of the method used to calculate the mass and center of gravity of each unit, consider the relatively simple procedure used in calculating these parameters for a dummy side diode. Figures IX-1 and IX-2 show the side diode; superimposed on this drawing are the basic geometrical forms used in the calculations. Again, due to symmetry, the $\langle y \rangle$-coordinate is equal to zero.

First, consider the weight and center of gravity of the authentic diode, for it is on these calculations that the entire JG-P generator development rests. By referring to Table IX-1 and the formula previously given, the coordinates of the authentic side diode are found to be

$$\langle y \rangle = 0,$$
$$\langle x \rangle = 1.248 \text{ in.}$$

For the rear diode they are

$$\langle y \rangle = 0,$$
$$\langle x \rangle = 1.212 \text{ in.}$$

The weight of the actual diode is compared with its calculated weight in Table IX-3. Because of the large number of calculations required due to the complexity of the design and the number of materials used, the complete calculations are not included in this report. Detailed calculations of the dummy diode are given to demonstrate the method used.

The following calculations were made for the dummy diodes, mass m_i, center of gravity x_i, and the product $m_i x_i$. These are shown in Table IX-2. The density of type 304 stainless steel is 0.29 lb./in^3. Part 1 of Fig. IX-3 is a cylinder 0.590 in. X 0.660 in. diam. This part is the same for both the front and the rear diodes. The mass was calculated as follows:

IX-3

$$\frac{\pi}{4} \; 0.66^2 \times 0.59 = 0.229 \text{ in}^3,$$

$$0.29 \times 0.229 = 0.0675 \text{ lb.}$$

The center of gravity of this piece is at 0.630 in.

$$m_i x_i = 0.0425 \text{ lb-in.}$$

Part 2 for the front diode is a cylinder 0.140 in. × 1.020 in. diam., whose mass was calculated as follows:

$$\frac{\pi}{4} \; 1.02^2 \times 0.14 = 0.1143 \text{ in}^3,$$

$$0.29 \times 0.1143 = 0.0331 \text{ lb.}$$

The center of gravity is at 0.990 in.

$$m_i x_i = 0.0330 \text{ lb-in.}$$

For the rear diode, the size of this cylinder is changed somewhat; its mass was found to be 0.0466 lb. The center of gravity is at 0.990 in.

$$m_i x_i = 0.0461 \text{ lb-in.}$$

Part 3 is also a cylinder, having the same mass for both the rear and side diodes. This was calculated to be

$$\frac{\pi}{4} \; 1.3^2 \times 0.25 = 0.331 \text{ in}^3,$$

$$0.331 \times 0.29 = 0.096 \text{ lb.}$$

The center of gravity is at 1.18 in.

$$m_i x_i = 0.113 \text{ lb-in.}$$

Part 4, a cylinder 0.145 in. long, has a mass

$$\frac{\pi}{4} \; 1.50^2 \times 0.145 = 0.2562 \text{ in}^3,$$

$$0.2562 \times 0.29 = 0.0743 \text{ lb.}$$

Its center of gravity is found to be at 1.38 in.

$$m_i x_i = 0.103 \text{ lb-in.}$$

Part 5 was considered to be a trapezoid rotated about the axis of symmetry. Its mass was found to be

$$\frac{h}{2} (a + b) 2\pi R = \frac{0.06}{2} (0.35 + 0.87) 2\pi \times 0.87$$

$$= 0.0877 \text{ in}^3,$$

$$0.0877 \times 0.29 = 0.0254 \text{ lb.}$$

The center of gravity of this piece is at 1.50 in.

$$m_i x_i = 0.038 \text{ lb-in.}$$

Part 6 is treated as a triangle rotated about the axis of symmetry; its mass for both the rear and side diodes is

$$\frac{0.115 \times 0.05}{2} 0.95 \times 2\pi = 0.0172 \text{ in}^3,$$

$$0.0172 \times 0.29 = 0.0050 \text{ lb.}$$

The center of gravity is at 1.60 in.

$$m_i x_i = 0.0080 \text{ lb-in.}$$

The mass of the emitter cavity faces was determined by actually weighing the pieces. These valves are:

        side diode: 0.0023 lb,

        rear diode: 0.0109 lb.

Their center of gravity is at 0.3 in.

        side diode: $m_i x_i = 0.0007$ lb-in.,

        rear diode: $m_i x_i = 0.0033$ lb-in.

The weight of the seventh cylinder is determined by subtracting the total weight of the other six parts and the emitter cavity face from the total weight of the authentic diode. By knowing the weight of this cylinder, its length can be determined.

Thus, for a dummy side diode,

      0.4550 lb (weight of authentic diode)
    -0.3036 lb (weight of subcomponents)
      0.1411 lb (weight of the cylinder).

Therefore, the cylinder length may be calculated:

$$\frac{0.1411}{0.29} = 0.487 \text{ in}^3,$$

$$\frac{\pi}{4} (D_1^2 - D_2^2) x = 0.487,$$

$$\frac{0.481}{0.785 (4 - 3.1)} = 0.690 \text{ in.}$$

The center of gravity is at 1.960 in.

$$m_i x_i = 0.2766 \text{ lb-in.}$$

To check the quality of the fabricated dummy diodes they were weighed, and the resulting weights were compared with the desired weights as determined by the calculated values. See Table IX-2.

The center of gravity for a dummy diode may now be calculated, considering that the $\langle y \rangle$-axis is the axis of symmetry and therefore constant at zero:

$$\langle x \rangle = \frac{\Sigma m_i x_i}{\Sigma m_i}$$

$$= \frac{0.6148}{0.4450}$$

$$= 1.38 \text{ in.}$$

The same consideration is used in the calculation of the center of gravity of the $\langle x \rangle$-axis of the rear diode:

$$\langle y \rangle = 0,$$

$$\langle x \rangle = \frac{\Sigma m_i x_i}{\Sigma m_i}$$

$$= \frac{0.6305}{0.4669}$$

$$= 1.35 \text{ in.}$$

Calculations were also made to determine the stiffness of the niobium ring (part 6, Fig. III-1) on the real diode so that a ring with the same

spring constant could be built for the dummy diode (although different materials were used).

The Young's modulus of elasticity, E, for niobium is given as 12.4×10^6 psi (E_1). For type 304 stainless steel, the figure is 28.0×10^6 psi (E_2). I is the moment of inertia; in this case, inertia is equal to the thickness t. Thus, for niobium,

$$\delta_1 = \frac{PL^3}{3 E_1 I_1}$$

$$\delta_2 = \frac{PL^3}{3 E_2 I_2}$$

for stainless steel.

$$\frac{PL^3}{3 E_1 I_1} = \frac{PL^3}{3 E_2 I_2} \ .$$

Therefore, by cancellation

$$E_1 I_1 = E_2 I_2 \ ,$$

$$E_1 t_1 = E_2 t_2 \ ,$$

$$12.4 \times 10^6 \times 3 \times 10^{-2} = 28 \times 10^6 \times t_2 \ ,$$

$$t_2 = \frac{12.4 \times 3 \times 10^4}{28 \times 10^6}$$

$$= 0.0133 \text{ in.}$$

The wall thickness of the holding ring for the stainless steel dummy diode is therefore found to be 0.0133 in.

D. Status

The dummy diodes for the JG-P generator were designed and fabricated. The generator was not tested, however, because the authentic diode was not built. Final assembly of the generator was not carried out, therefore, in spite of the fact that the dummy diodes were ready for testing.

Due to changes in the collector radiator design to be made on the SET diode, certain changes will have to be made in the size and configuration of the dummy diodes. These changes have not yet been completely evaluated, nor have the contingent recalculation of mass and center of gravity been made.

122

X.   BRAZING FIXTURE FOR SUPPORT STRUCTURE

A.   Requirements

Two approaches to making the sixty nine brazes on the diode support block were possible.   Either a series of brazes, each using a successively lower-melting braze material, could be made, or all the brazes could be made simultaneously.   Because of the large number of brazes required and the difficulty in obtaining a large number of sequentially lower-melting braze materials, the latter alternative was chosen.

This decision having been made, it was then necessary to design and fabricate a braze fixture capable of holding firmly in position during the brazing operation all the parts of the diode support block to be brazed.   The following brazes were required.   (See Fig. X-1.)

(1)   Braze the molybdenum brackets to the molybdenum supporting block (four brazes).

(2)   Braze the tantalum diode mounting rings to the molybdenum block (five brazes).

(3)   Braze the copper thermal bypass strap to the molybdenum bracket (four brazes).

(4)   Braze the copper straps together (56 brazes).   Each copper strap is composed of eight thin sheets of copper which must be brazed together to achieve good thermal contact.   Seven brazes are required for each end of a single strap, or 14 for the whole strap.   Therefore, a total of 56 brazes is required for all four copper straps.

B.   Design

The brazing fixture was designed and fabricated entirely of type 304 stainless steel.

Essentially, the design (see Figs. X-2 and X-3) consists of a disc which has been so machined as to leave a wide pin in the center of the block, surrounded

X-1

123

by a smoothly machined surface with a high lip around it. Two sets of four vertical holes are drilled through the plate: one set is evenly spaced about the section surrounding the central pin. The other set, on the same radii as the inner set, is situated on the outer lip.

Although it is customary to oxidize such a brazing fixture before use to prevent the braze material from sticking to the jig, another method of lubrication was investigated. The central pin, the locating pins, and the area around the bolts holding the copper straps to the lip were painted with magnesium oxide. This process worked very well.

C.   Brazing Operation

The central pin (see Fig. X-1) was so designed that it would support the molybdenum block on the cavity entrance side of the cube. In the brazing procedure an 18% Ni-82% Au braze alloy (PB 130) was placed at the four vertical corners of the block, and the molybdenum brackets (2) were screwed into place with tantalum screws. The partially assembled support block was then placed on the brazing jig, located by the pins, and inserted in the four holes in the base of the fixture plate. Copper straps were then bolted to the top of the brackets (2) and to the lip of the jig at the four lip holes. Braze material was inserted beneath each of the copper straps and between the straps and the brackets before the bolts were tightened. On each side of the support block where the diodes are to be inserted, the braze material and a tantalum ring (7) were inserted. There were five such rings to be mounted, one on each of the four sides and one on top. To ensure a tight braze, a small weight was placed on the top ring to prevent its floating out of place when the braze melted. To hold the tantalum rings for the side diodes in position, pieces of ceramic rod were placed on opposite sides of the block. A wire was passed first through the hole forming the central cavity, then around the ceramic, and then tightened by twisting. Care was taken to prevent excessive tension in the wire from deforming the tantalum ring or breaking the

ceramic beam. A specially made brazing oven (see Fig. X-4), also made of 304 stainless steel, was placed around the brazing fixture and the diode support block. The entire assembly was then vacuum-brazed with an rf coil at 950°C for about one minute. All the 69 brazes exhibited good mechanical characteristics.

D. Status

The brazing fixture was designed, fabricated, and used at Thermo Electron's facilities. It was used to fabricate the diode support structure for the JG-P generator and proved satisfactory in all aspects. No changes in the design are recommended.

XI. THE SET GENERATOR ASSEMBLY FIXTURE

A. Requirements

An assembly fixture was needed to enable the accurate positioning of the diodes on the supporting block. Such a fixture had to be designed so that the emitter cavity faces could be adjusted in the diode support structure after they were in position but prior to crimping firmly in place. Spacing and relative positioning of the five diodes are of primary importance to the operation of the SET generator. The clearance between any two adjacent 45° faces of the emitter cavity cannot exceed 0.014 in. when the generator is cold. The minimum clearance is 0.008 in. to allow for thermal expansion of the emitting surface during operation. The emitter faces which form a 45° angle with the axis of symmetry must be parallel to one another around the cavity (see Fig. XI-1).

B. Design

The assembly fixture (Figs. XI-1 and XI-2) consists essentially of two flat aluminum plates, a base plate (1), and a top plate (9) supported by four stainless steel rods (3). A hole is drilled through the center of the base plate to simulate the cavity opening. An aluminum supporting ring (2), cut from a cylinder in such a way as to provide four supporting legs, is bolted to the base plate. The diode support block stands about 1.5 in. above the face of the base plate. A similar cylinder (10), without the supporting legs, is mounted on the top plate. Four aluminum brackets (4) are mounted at the central edge of each of the four sides. Each of these five brackets (the four side and one top) are designed to accommodate a slide-fit stainless steel rod (7 and 8), whose position is maintained by a set screw (17).

Another portion of the assembly fixture consists of an aluminum cylinder (5) counterbored to accommodate the rear end of the diode. The opposite end of this aluminum piece is also counterbored to hold a spring (11), which fits into the lip of a second aluminum plug (6). This piece is threaded to accommodate the steel rod (7). Proper use of this fixture allows assembly of the JG-P or SET generator in the assembly procedure to be described in the following section.

XI-1

C.   Assembly Procedure

The assembly of the JG-P and SET generators is carried out in the following manner, using the assembly fixture described above.

The jig is assembled by placing the steel rods (3) through the base plate (1) and then adding the top plate (9), the top and bottom supporting rings (2 and 10), and the side brackets (4). The molybdenum generator supporting block is then bolted into place on the bottom supporting ring (2). The plug gauge (Fig. XI-3) is then inserted into the supporting block cavity and screwed into place. The diodes are next inserted in the following manner. The diode is placed into its hole in the emitter support block in such a way that the tantalum ring on the block can be crimped around the niobium flange on the diode. The aluminum cap (5) is placed on the back of the diode, the spring is inserted, and the rod and cap are adjusted in such a way that the diode is held loosely in place. This procedure is carried out for the four side diodes. The diodes are then rotated so that they fit tightly against the plug gauge; the springs are tightened and the entire assembly is held in this position by adjusting the set screws on the side brackets. The plug gauge is then removed, the assembly fixture is turned on its side, and the fifth (rear) diode is inserted in the above manner (see Figs. XI-4 and XI-5). When it is loosely in position, a feeler gauge is used to adjust it so that all four of its 45° surfaces are parallel to the four adjacent faces of the four side diodes. At the same time, use of the gauge affords the opportunity to check the spacing and positioning of the side diodes. As stated previously, the spacing between the emitter cavity surfaces should not be more than 0.014 nor less than 0.008 in. When the diodes are tightly set in position, the diodes are ready to be crimped to the supporting block. A second special tool has been designed to crimp the tantalum ring of the emitter supporting block to the niobium flange of the diode itself (to the stainless steel flange of the dummy diodes). Certain problems in the use of this tool are evident by inspection. For example, crimping the tantalum ring to the diode in the areas near the support block bracket will be extremely difficult.

D. Status

The assembly fixture has been designed and fabricated at Thermo Electron. To date, it has been used only with the dummy diodes of the JG-P generator because the authentic diode has not yet been built. Upon its completion, the unit will be used to complete fabrication of the JG-P generator. Final changes in the design and tools will be made as needed.

XII.   CONCLUSIONS

Phase I of the SET generator program has progressed reasonably well, except for the mechanical problems encountered with the diode. Because of these unexpected mechanical problems (not an uncommon occurrence in programs of the advanced nature of the SET program), the remaining efforts during Phase I were focused solely on these diode problems. The results were more than expected at the outset of the short-range diode program. The diode design can be reproducibly and reliably fabricated, resulting in diodes with an average life of several hundred hours, capable of withstanding a sufficient number of thermal cycles to permit adequate ground testing of a SET generator.

Based on the design of the Phase I diode, a SET generator can now be fabricated and tested. To achieve the original SET specification, diode performance must be improved without endangering the life and reliability already established. Using the results of the generator test incorporating present diode technology and factoring in the results of the advanced diode development, it would be possible to embark on the fabrication of a SET generator, the performance objective of which would be the original SET specifications.

APPENDIX A

OPERATING MANUAL FOR

DUMMY CAVITY

TABLE OF CONTENTS

Operating Manual for Dummy Cavity

I.   INTRODUCTION

This manual describes the proper operating instructions to be followed in the assembly and testing of the dummy cavity.

The dummy cavity was designed and fabricated by Thermo Electron Engineering Corporation in fulfillment of paragraph 4, Article I of Contract No. 11483 with Electro-Optical Systems, Inc. The purpose of the dummy cavity is to provide experimental verification of the cavity design for the SET generators.

This operating manual contains the manufacture's instructions on all standard components used on the dummy cavity (see Sections III, IV & V) in addition to instructions on the over-all operation of the unit (Section II). Section VII contains log sheets for recording the operating history of the unit.

SECTION II

DESCRIPTION OF THE UNIT

II. DESCRIPTION OF THE UNIT

A. Over-all Description

The dummy cavity consists of a thermal cavity surrounded by five dummy diodes to simulate the heat transfer characteristics of the thermionic diodes to be used in SET generators JG-1 and JG-2. The cavity entrance and the internal characteristics of the cavity walls are similar to those of the cavity for JG-1 and JG-2. The dummy cavity is to be tested by EOS in a vacuum chamber, using solar radiation to heat the cavity. The dummy cavity is equipped with a calorimeter to measure the total heat absorbed by the cavity. This measurement is made by measuring the flow rate of the coolant water [using a Fisher & Porter Flow-Meter, Model 10A2735 (see Section IV)] and the temperature rise of the coolant water across the dummy cavity. The inlet and outlet temperatures are measured with copper-constantin thermocouples (see Section V). The temperatures of the diode surfaces forming the cavity walls will be measured with 0.020-in. tungsten, tungsten-26% rhenium thermocouples (see Section III). Eight thermocouples are used. The location of the thermocouples on the diodes, relative to the cavity, is shown in Fig. II-1; also shown are the positions of the leads for the various thermocouples and the coolant water inlet and outlet.

The use of thermocouples to measure temperatures in the neighborhood of 2000°K is still in the research and development stage. Standard methods of attachment have not been developed sufficiently to guarantee accurate and constant results over an extended period of operation. Therefore, in addition to providing the eight W,W-26% Re thermocouples, openings have been provided for temperature measurement of the rear and one side diode by optical pyrometer.

The thermal resistance of each of the dummy diodes is slightly greater than that of the actual diodes to ensure that the operating temperature of the cavity can be achieved with the solar flux available. This means that the total thermal power absorbed by the dummy cavity will be slightly less than that of the actual SET generators.

134

B. Installation Instructions

The dummy cavity can be mounted in accordance with the specifications provided by EOS in drawing No 785-11042.

Sufficient length of thermocouple wire (2 ft) has been provided to permit attachment of the thermocouple leads to suitable leadthroughs in the base plate of the vacuum test chamber. In accordance with the manufacturer's information supplied with the W, W-26% Re thermocouples (p. III-2), copper extension leads can be used when a temperature gradient no longer exists in the thermocouple wire. Therefore, copper wire can be used from the leadthroughs for the W, W-26% Re thermocouples in the base plate to the potentiometer or other recording instrument.

The temperature of the coolant water is within 10 or 20°C of room temperature. Therefore, more care must be exercised in measuring the inlet and outlet coolant water temperature. The copper and constantin wire for these two thermocouples should be continued through the leadthroughs in the base plate, to an ice bath and potentiometer, for accurate temperature measurement.

The flow meter is to be mounted outside the vacuum chamber in accordance with the manufacturer's specifications (see Section IV). Connections to the flow meter, source of coolant water, and sink, are to be by suitable tubing or pipe through the base plate of the vacuum chamber. The type of connection used within the chamber must be capable of maintaining a leak-tight joint under vacuum conditions; preferably using brazed or soldered connections.

C. Operating Instructions

The dummy cavity is to be installed in the test chamber, and the chamber sealed and evacuated. Prior to heating the cavity, the coolant water should be turned on, and a flow of approximately 0.08 to 0.10 gal/min established. The heating of the cavity can then commence. While the cavity is being heated, the temperature of the cavity should be carefully monitored. As the cavity walls approach their operating temperature (2000°K), the flow rate of the

coolant water should be increased until, at operating temperature, the flow rate is approximately 0.16 to 0.18 gal/min. The system should then be allowed to attain steady-state equilibrium prior to proceeding with the test.

Figure II-2 is a plot of the temperature rise of the coolant water versus coolant flow rate (gal/min), parametric in power absorbed. Using this figure, it is possible to read directly the power absorbed by the coolant water if the temperature difference of the copper-constantin thermocouples and the coolant water flow rate are known.

D. Special Precautions

Extreme care should be exercised in handling the W, W-26% Re thermocouple leads. The ends of the thermocouple wire are only crimped in place on the rear face of the dummy diodes. Therefore, care should be exercised in handling the dummy cavity to ensure that the wires are not jerked loose. Also, once the cavity is operated at 2000°K, the tungsten wire will become extremely brittle. Light shock or vibration loads may well fracture the wire once the cavity has been so operated.

If the vacuum test chamber is equipped with a window for taking optical pyrometer readings, care should be exercised when installing the cavity in the chamber to ensure that the side diode with provisions for optical pyrometer readings is aligned with the window in the test chamber.

The coolant water tubing from the base plate to the inlet and outlet connections of the dummy cavity should be brazed or soldered, and then thoroughly leak tested. Even the smallest leak in the coolant water line will make it difficult if not impossible to obtain a good vacuum in the test chamber.

If copper extension leads are used on the W, W-26% Re thermocouples, the temperature of the base plate should be checked to see that it is at the same temperature as the potentiometer. The coolant water outlet line should not pass through the base plate anywhere near the thermocouple leadthroughs.

Figure VI-1.

Ni braze
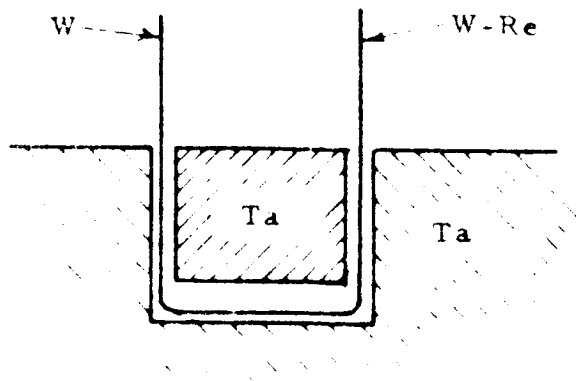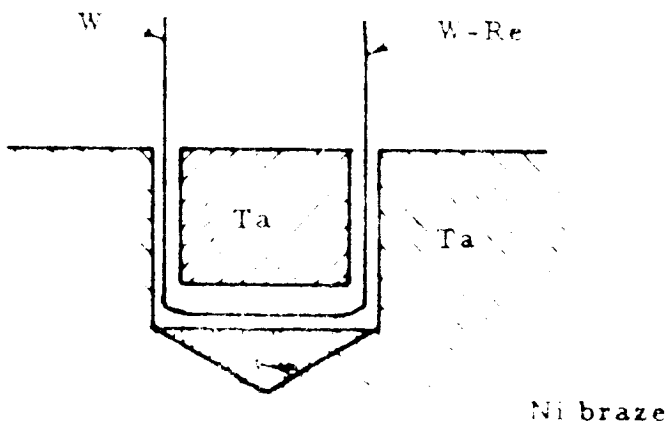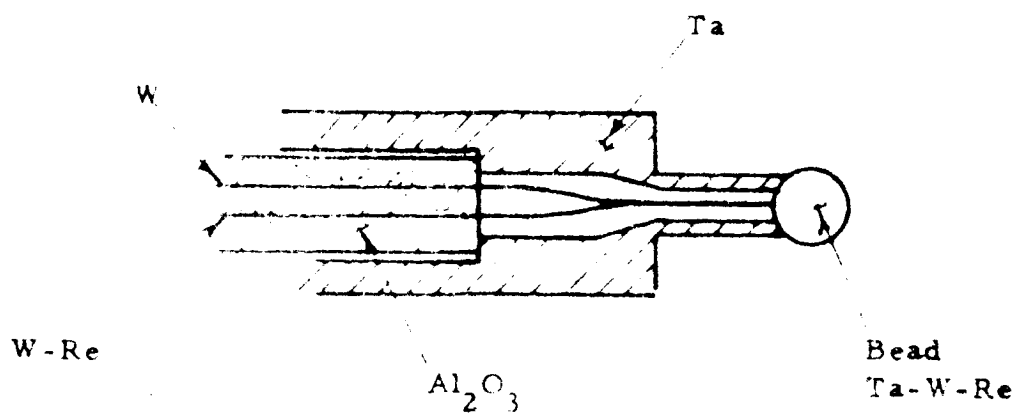
Figure VI-2.

Figure VI-3.
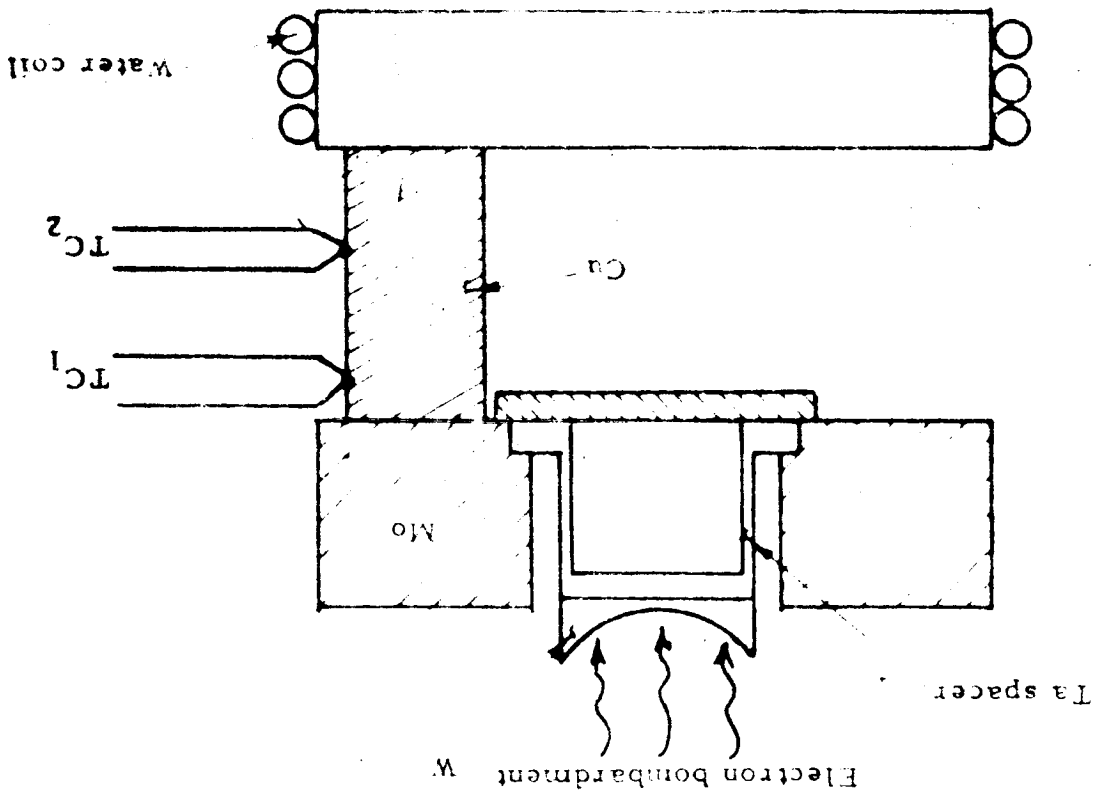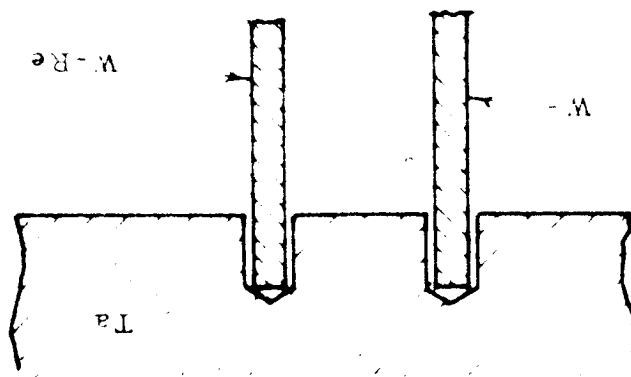
SECTION III

TUNGSTEN, TUNGSTEN-26% RHENIUM THERMOCOUPLES

(Data supplied by Engelhard Industries, Inc, with thermocouple wire.)

TUNGSTEN VS. TUNGSTEN 26% RHENIUM THERMOCOUPLE

In recent years, due to advances in high temperature technology, there has been an increasing need for materials that are suitable for thermo-electric applications at high temperatures.

Engelhard Industries, Inc. manufactures a series of noble metal thermocouple wires, which in selected combinations provide research and industry with the essential means for precise high temperature measurement. In addition to these, Engelhard Industries now offers a thermocouple -- Tungsten vs. Tungsten 26% Rhenium -- made of refractory metals that moves the range of reliable temperature measurement up to $2800^{\circ}C$ ($5072^{\circ}F$).

Uses

The Tungsten vs. Tungsten 26% Rhenium thermocouple is suitable for use in vacuum, hydrogen and inert gases such as nitrogen, argon and helium. It is especially recommended for use in the range from 2000-2800°C ($3632^{\circ}F$-$5072^{\circ}F$). However, its high output also makes it useful for the measurement of temperatures below this range. The high melting point of the elements comprising the thermocouple (Tungsten 3380°C, Rhenium 3167°C) plus a low vapor pressure makes it attractive for use in a vacuum at inter-mediate and high temperature.

- 1 -

140

It should be pointed out that this thermocouple is not suitable for use under oxidizing conditions or in the presence of hydrocarbon vapors which will rapidly attack tungsten at temperatures above 1000°C.

Standard Calibration

A standard calibration chart has been determined and all wires are manufactured and tested to meet this calibration.

The EMF of these couples conforms to the standard calibration curve within a tolerance of ± 1%. The reproducibility of readings obtained on a particular couple is, of course, appreciably closer than this.

Fabrication of Thermocouple

Hot junctions may be formed by inert arc welding. Since the wires may become embrittled in the vicinity of the weld, it is important that the wires are not flexed in this region after the junction is formed. This problem may be overcome by placing a double bored insulator in position prior to forming this junction.

Extension Leads

Plain copper leads are considered satisfactory because the output of the thermocouple at temperatures up to 100°C is relatively low. Because of this, the errors introduced by normal fluctuations in room temperature are small in relation to the accuracy of calibration.

For the most accurate work an ice or isothermal cold junction should be used.

- 2 -

In normal industrial applications no correction need be made for cold junction temperatures between 0 and 10°C; above this temperature the corrections on the attached sheet may be added to the observed output.

Insulators

Double bored insulators of high purity alumina may be used to approximately 1800°C. Above this temperature Beryllium Oxide (M. P. 2570°C or 4650°F) and Thorium oxide (M. P. 3299°C or 5970°F) should be considered.

Material is furnished through agreement with A.E.I. Lamp and Lighting Company Ltd., Leicester, England.

Engelhard Industries, Inc.
Baker Platinum Division
113 Astor Street
Newark 2, New Jersey

Engelhard Industries, Inc.
Industrial Equipment Division
Instruments & Systems Section
850 Passaic Avenue
East Newark, New Jersey

FORM 5224B

TEMPERATURE – E.M.F. – RELATION
FOR
TUNGSTEN Y TUNGSTEN RHENIUM THERMOCOUPLES.

TEMP °C.	1000	1100	1200	1300	1400	1500	1600	1700	1800	1900	2000	2100	2200	2300	2400	2500	2600	2700
0	13.13	15.63	18.25	20.75	23.00	25.13	27.13	29.13	30.88	32.50	34.13	35.50	36.83	38.13	39.25	40.25	41.25	42.25
10	13.38	15.89	18.50	20.97	23.21	25.33	27.33	29.30	31.04	32.66	34.27	35.64	37.00	38.24	39.35	40.35	41.35	42.35
20	13.63	16.15	18.75	21.20	23.43	25.53	27.53	29.48	31.20	32.82	34.40	35.78	37.13	38.35	39.45	40.45	41.45	42.45
30	13.88	16.41	19.00	21.42	23.64	25.73	27.73	29.65	31.37	32.99	34.54	35.91	37.25	38.47	39.55	40.55	41.55	42.55
40	14.13	16.67	19.25	21.65	23.85	25.93	27.93	29.83	31.53	33.15	34.68	36.05	37.38	38.58	39.65	40.65	41.65	42.65
50	14.38	16.93	19.50	21.87	24.06	26.13	28.13	30.00	31.69	33.31	34.81	36.19	37.50	38.69	39.75	40.75	41.75	42.75
60	14.63	17.20	19.75	22.10	24.28	26.33	28.33	30.18	31.85	33.46	34.95	36.33	37.63	38.80	39.85	40.85	41.85	42.85
70	14.88	17.46	20.00	22.32	24.49	26.53	28.53	30.35	32.03	33.62	35.09	36.47	37.75	38.91	39.95	40.95	41.95	42.95
80	15.13	17.72	20.25	22.55	24.70	26.73	28.73	30.53	32.18	33.80	35.23	36.60	37.89	39.02	40.05	41.05	42.05	43.05
90	15.38	17.98	20.50	22.77	24.92	26.93	28.93	30.70	32.34	33.97	35.36	36.74	38.00	39.14	40.15	41.15	42.15	43.15
100	15.63	18.26	20.75	23.00	25.13	27.13	29.13	30.88	32.50	34.13	35.50	36.88	38.13	39.25	40.25	41.25	42.25	43.25

COLD JUNCTION CORRECTION

TEMP °C.	'0	20	30	40	50	60	70	80	90	100
MILLIVOLTS	.02	.04	.06	.09	.13	.16	.20	.25	.29	.33

SEPTEMBER, 1960

August 9, 1961

CORRECTION TABLE FOR W - W 26% Re

Thermocouples used in Dummy Cavity

°F	°C	Minneapolis-Honeywell Certified Data mv	Data from Engelhard Tables in Oper. Manual mv	Difference
1800	982	14.02	-	-
2000	1093	16.42	15.43	-0.99
2200	1205	18.82	18.38	-0.44
2400	1317	21.22	21.13	-0.09
2600	1429	23.37	23.62	+0.25
2800	1539	25.60	25.91	+0.31
3000	1650	27.66	28.13	+0.45
3200	1760	29.67	30.18	+0.51
3400	1871	31.67	32.05	+0.38
3600	1982	33.65	33.85	+0.20
3800	2093	35.43	35.46	+0.03
4000	2204	37.15	36.03	-0.22
4200	2315	38.67	38.30	-0.37

144

SECTION IV

FLOW METER

INSTRUCTION BULLETIN

for

SERIES 10A2700
FLOWRATOR METERS

FIG. 1 MODEL 10A2735, STANDARD
ENCLOSED FLOWRATOR METER

FISCHER & PORTER CO.

Complete Process Instrumentation

TABLE OF CONTENTS

The instructions given herein cover generally the description, installation, operation and maintenance of subject equipment. Should any questions arise which may not be answered specifically by these instructions they should be directed to the Fischer & Porter Co. for further detailed information and technical assistance.

FIG. MODEL 10A2770 SIDE PLATE DESIGN

I. INTRODUCTION

Series 10A2700 Flowrator Meters use the variable area principle to meter fluid flow. Two versions of this series meter are available. The first is the side plate design. This meter consists essentially of a tapered glass metering tube with adapters, float, float stops and fittings and side plates. By the addition of bezels, the standard enclosed meter may be obtained.

The position of the float in the tapered glass metering tube is proportional to the fluid flow rate. Readings are taken from the scale on the metering tube. The scales are graduated to provide one of four readings: diameter ratio (D), percentage, milligram or direct reading. When required a variable calibration handbook or curves will accompany the meter.

II. GENERAL INFORMATION

Series 10A2700 Meters are available with either vertical or horizontal fittings for horizontal piping.

The side plates, end and center plates are all of steel construction which offers resistance to corrosion as well as considerable strength. The side plates are predrilled to facilitate mounting the meter. O-rings and float stops of materials

specified at the time of purchase. When O-rings and float stops are made of FP270 material they are coded with a green marking. Buna-N parts are plain. Should requirements of the fluid being metered demand a change in materials, this may easily be accomplished in the field.

III. INSTALLATION

A. General

The meters are shipped from the factory with the end fitting connections arranged as ordered. However, both end fittings of the 10A2700 Series Meters may be rotated horizontally a full 360. Slowly and carefully rotate the end fittings to the desired position. A nipple threaded into the end fitting may be used as a lever. For flanged end fittings, a nipple and flange bolted to the fitting may be used as a lever.

In general, when a meter is to be used for gas service it should be located as closely as possible to a throttling point but preferably with the valve located at the outlet fitting. Inlet piping size for gas service should be kept to a minimum. For liquid service however, piping should be as large as economically practicable.

Meters must be installed vertically with the outlet (highest scale graduation) at the top. Use of a plumb bob or equivalent device to check vertical alignment is recommended. Except with small meters the float is usually packed separately and must be installed before the meter is placed in operation. Often the float is protected during shipment by a plastic coating or by a strip of tape around the metering edge. Remove the protective covering just before installing the float in the meter. Refer to the maintenance section for instructions on float installation.

B. Surge Chambers and Accumulators

Surge chambers or accumulators are frequently used on flowmeter installations to smooth out pulsations of the metering float where reciprocating pumps or compressors are used on the feed lines to the meter. Surge chambers, when used on liquid service, may have a gas introduced on the upper side of the chamber.

When it is objectionable to have the gas in contact with the liquid, accumulators are used. Accumulators are similar to surge chambers except that they include a rubber bag on the upper side which seals the gas from the liquid. Accumulators usually have a bladder that is precharged with an gas or nitrogen to a pressure approximately 60 per cent of the operating pressure. It is recommended that surge chambers or accumulators be installed for the use of surge chambers or accumulators required on the installation.

END PLUG

INLET END FITTING

"O" RING

"O" RING

OUTLET FLOAT STOP *

METERING TUBE

FLOAT

INLET FLOAT STOP *

FLOAT ASSEMBLY

INLET END FITTING

END PLUG

OUTLET TUBE ADAPTOR PIECE

OUTLET TUBE REST GASKET

SIDE PLATE ASSEMBLY

CUT AWAY, ILLUSTRATING
ASSEMBLY OF SIDE PLATES
AND END FITTING.

INLET TUBE ADAPTOR PIECE

"O" RING

INLET TUBE REST GASKET

"O" RING

SPRING
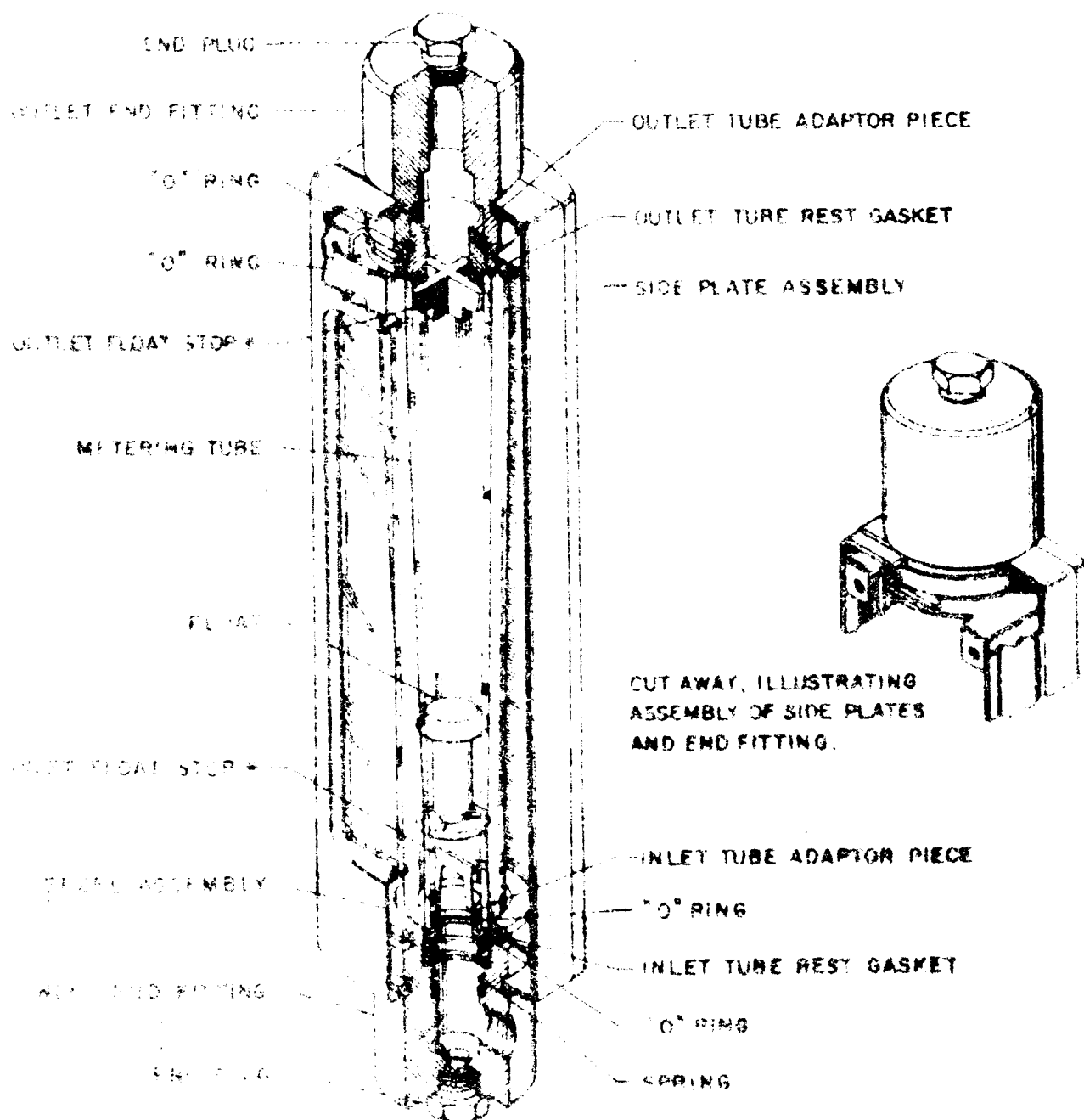
* FLOAT STOPS ILLUSTRATED ARE FOR 3/4" METER   FLOAT STOPS
FOR 1/2" METER INLET ARE AN INTEGRAL PART OF THE TUBE. THE
OUTLET STOP IS INCORPORATED IN THE OUTLET ADAPTOR.
THE 1 1/2" METER IS PROVIDED WITH A PIN TYPE INLET STOP AND A
WIRE INSERT OUTLET STOP

149

INSTALLATION (Continued)

C. Mounting & Piping

1. General

Flowrater meters may be mounted on either side of a panel or installed directly in a pipe line. Each type of installation is discussed below. When panel mounting a flowmeter refer also to pipe mounting installation instructions for important piping information.

2. Pipe Mounting

Flowrater meters of a smaller size will, in general, be adequately supported by the connecting piping. It is recommended that by-pass piping be placed around the meter to allow continuous flow through the pipe line while the meter is being serviced. Figures IV & V show typical installation piping of flowrater meters.
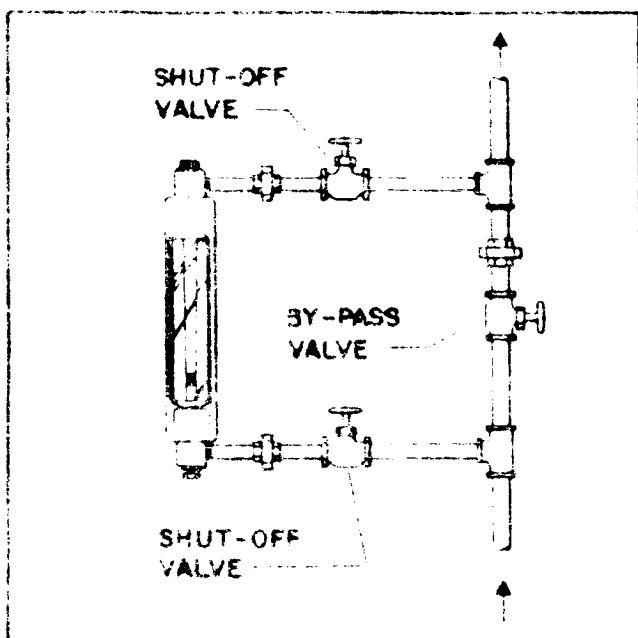
FIG. IV   TYPICAL VERTICAL LINE INSTALLATION
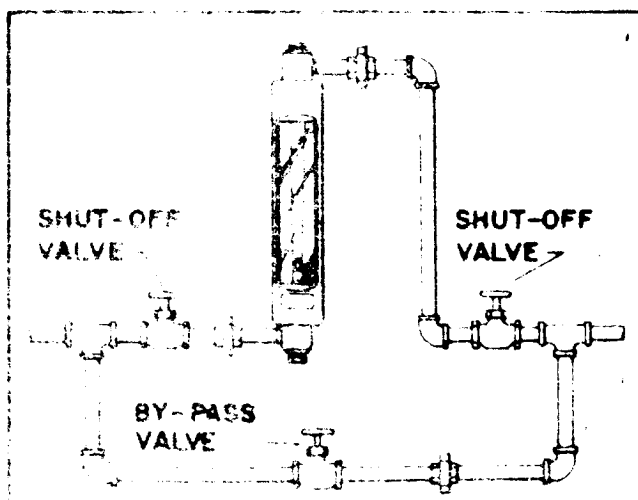
FIG. V   TYPICAL HORIZONTAL LINE INSTALLATION

NOTE THAT MOUNTING PLATE BOSSES MUST FACE PANEL.
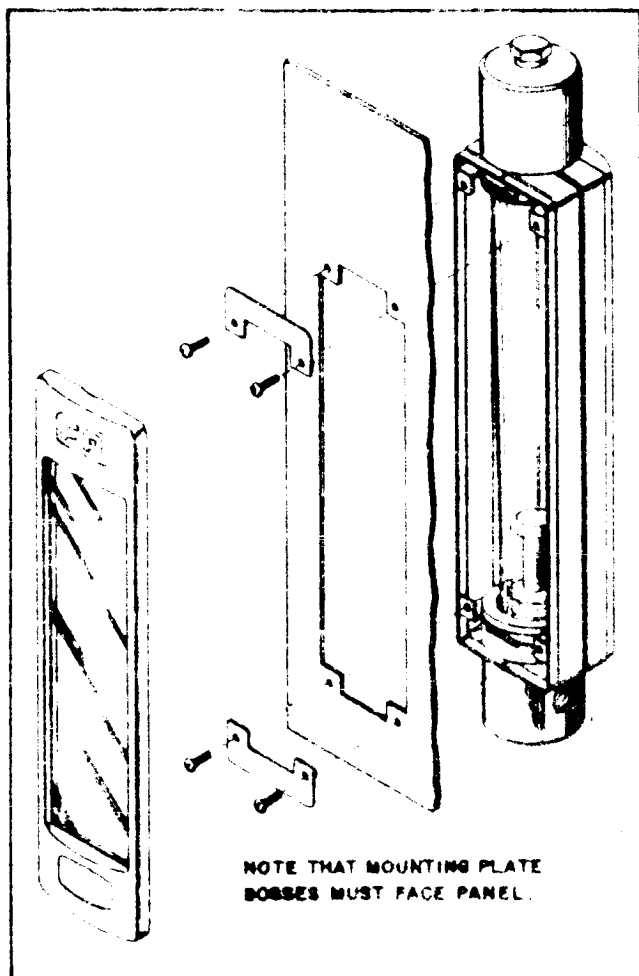
FIG. VI.   PANEL MOUNTING A SERIES 10A2700 FLOWRATOR METER

D. Panel Mounting

1. General

The meter may be mounted on either the front or rear of a panel. Rear panel mounting has the advantage of affording protection for the instrument and piping, and in addition presents a neat appearance.

When the meter is to be panel mounted, secure from Fischer & Porter the necessary hardware which consists of four screws and two panel mounting plates.

2. Installation

Panel thickness, which in general is determined by the total weight carried may be up to 1" in thickness when standard panel mounting parts are used. Precautions sited for pipe line mounting apply here also, that is panels should be rigid, vertical and installed in a location free from severe vibrations. The minimum distance between adjacently mounted instruments is determined by piping requirements and the meter size.

Refer to the certified dimension drawing make the necessary cut-outs and drilling, then refer to Figure VI and proceed as follows:

(1) For meters completely assembled remove the head assembly.

Install the screws through Panel Mounting Plate, into meter. Note that the metal bosses on the mounting plate must rest against the panel.

Snap the bezel assembly over the Panel Mounting Plate.
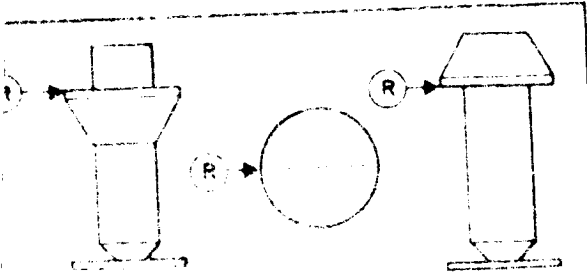
NOTES

1. FLOATS SHOWN IN CORRECT METERING POSITION
2. READING EDGE OF FLOAT IS LABELED (R)

FIG. VII   FLOAT READING EDGES

IV. PLACING THE METER IN OPERATION

Gradually start flow through the meter by opening the outlet rate valve. A gradual start-up reduces flow surges that might damage the float, outlet float stop or tube. All air or vapor must be vented from the meter and pipe line when metering a liquid. Meter readings must be taken from the scale at the graduation which coincides with the reading edge of the float. Figure VII illustrates the reading edges of the various types of floats.

Should float bounce occur in meters being used in gas service, it may be the result of any of the following reasons: Low pressure operation, long range tube and float combinations, heavy floats, operation near tube zero (at very low diameter ratios), or large piping volumes.

If bounce occurs or initiates only at low diameter ratios and the lower portion of the scale is not normally used, the problem may be corrected in the size 1½" meter by using an extra long inlet float stop. This will of course render the lower portion of the scale unusable.

Liquid pulsation is often caused by a pump with a pulsating discharge by pipe vibrations. If these conditions can not be alleviated, a surge chamber is usually the best available solution (refer to paragraph III b) This chamber should be located as closely as possible to the pump or source of vibration.

V. MAINTENANCE

A. Tube & Float Removal, Tube Cleaning and Float Installation

The float is a precision manufactured part; be careful not to nick, drop or otherwise damage it as these will adversely affect accuracy. Never subject the metering tube to unnecessary shock or strain. Care must be taken when removing the metering tube to note locations of float stops at both ends of the tube. When re-assembling meter, stops must be located as they were originally. In order to remove the metering tube and float proceed as follows.

1. Remove bezel assembly from the meter. The bezel assembly is secured in position by spring clips spot welded to the bezel. Removing the bezel assembly is simply a matter of lifting it off the meter.
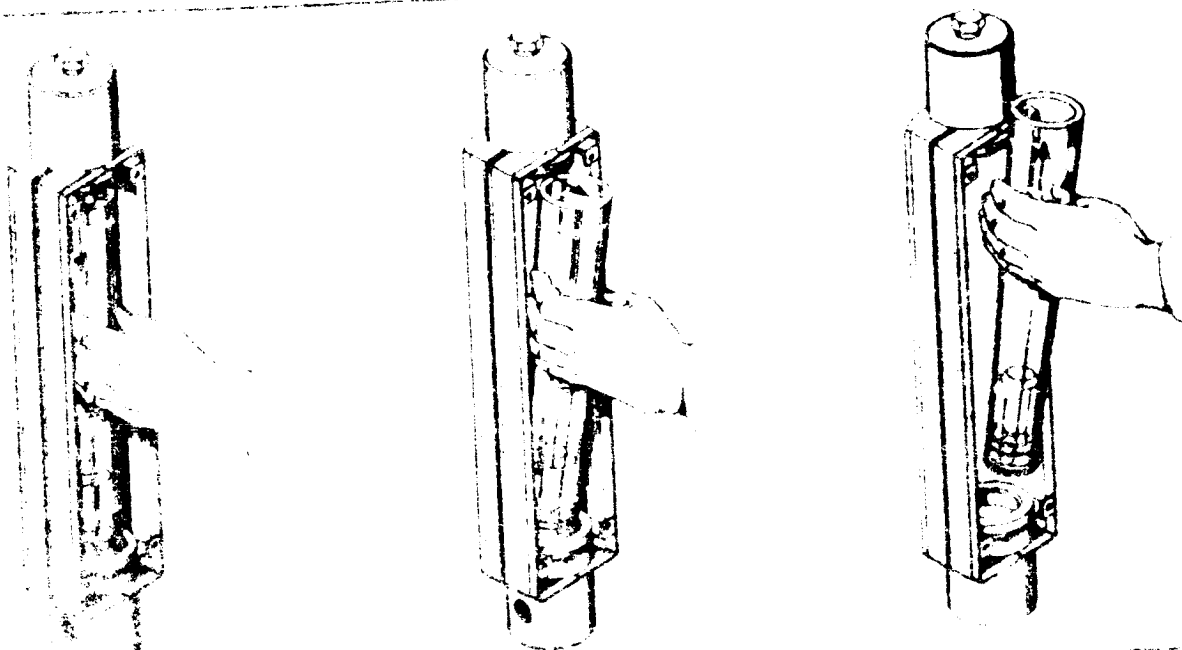
REMOVAL OF METERING TUBE

FIG. 3   EXPLODED VIEW OF SERIES 1CA2700 SERIES METER

The numbered parts list includes:
1. Seal Ring
2. Outlet End Fitting
3. "O" Ring
4. Inlet Tube Adaptor Plate
5. Outlet Float Stop
6. Outlet Tube Rest Corner
7. Metering Tube
8. Inlet Tube Rest Corner
9. Float
10. Inlet Float Stop
11. Inlet Tube Adaptor Plate
12. Spring
13. The End Fitting
14. The Plate
15. Inlet
16. Window
17. Seal

MAINTENANCE (Continued)

A. Disassembly

B. Disassembly

C. Assembly

IN HATBORO AND THROUGHOUT THE WORLD, FISCHER & PORTER
ENGINEERS ARE PREPARED TO ASSIST WITH INSTRUMENTATION SURVEYS
AND TO PROVIDE EFFICIENT SERVICE ON ALL OF OUR PRODUCTS

FP

FISCHER & PORTER COMPANY
HATBORO, PENNSYLVANIA U.S.A.

SECTION V

COPPER-CONSTANTIN THERMOCOUPLES

Table 9. Copper-Constantan Thermocouples

(Electromotive Force in Absolute Millivolts. Temperature in Degrees C (Int. 1948). Reference Junctions at 0° C.)

Millivolts	0.00	0.10	0.20	0.30	0.40	0.50	0.60	0.70	0.80	0.90	1.00	Millivolts
5.00	169.1	174.3	179.7	185.4								5.00
4.00	124.1	128.1	132.5	136.7								4.00
3.00	87.9	91.3	94.8		101.8			112.5	116.2	120.5	124.3	3.00
2.00	55.9	58.9	62.0		68.3	71.		77.9	81.2	84.5	87.6	2.00
1.00	28.9	29.7	32.5		38.2	41.	44.0	46.4	49.9			1.00
0.00	0.0	2.6		7.	10.	13.		18.	21.	24.1	26.	0.00
0.00	0.0	2.6		7.	10.8			17.	20.	22.8		0.00
1.00		27.	30.1					42.1		46.8		1.00
2.00	49.2	51.5	53.8	56.2			63.0		67.6		72.	2.00
3.00	72.1	74.3	76.5	78.7	81.0	83.2		87.5			94.0	3.00
4.00	94.0	96.2	98.3	100.5	102.6							4.00
5.00	115.3	117.4	119.4	121.	123.				131.	133.	135.	5.00
6.00	137.0		139.0	141.0				147.		151.0	153.	6.00
7.00												7.00
8.00		177.1										8.00
9.00				200.0	202.							9.00
10.00									224.8	243.7		10.00
11.00											249.	11.00
12.00											267.	12.00
13.00					276.							13.00
14.00										302.3		14.00
15.00	302.					310.				319.4		15.00
16.00										336.5		16.00
17.00												17.00
18.00	353.0									360.		18.00
19.00	358.									385.		19.00
20.00												20.00
Millivolts	0.00	0.10	0.20	0.30	0.40	0.50	0.60	0.70	0.80	0.90	1.00	Millivolts

Table 10. Copper-Constantan Thermocouples—Con.

Electromotive Force in Absolute Millivolts. Temperatures in Degrees C. (Int. 1948). Reference Junctions at 0° C.

°C	0	1	2	3	4	5	6	7	8	9	10	°C
						Millivolts						
200												200
210												210
220												220
230												230
240												240
250												250
260												260
270												270
280												280
290												290
300												300
310												310
320												320
340												340
350												350
360												360
370												370
380												380
390												390
	0	1	2	3	4	5	6	7	8	9	10	

SECTION VI

TEST RESULTS

VI.   TEST RESULTS

A. Thermocouple Attachment And Stability Investigation

1. Summary

Four different attachment techniques were investigated. None of these methods gave satisfactory results. Finally, after a consultation with Minneapolis-Honeywell's Dr. Kuether, a method of attachment was suggested, which after 60 hours of operation yielded a 30°C spread on the four thermocouples tested.

2. Methods of Attachment and Results

a. Wedged wires with plug

The two thermocouple wires were wedged in a hole in the specimen with a tantalum plug (see Fig. VI-1). The readings were about 500°C lower than the actual temperatures as measured with an optical pyrometer.

b. Wedged and brazed wires

The thermocouple wires were wedged in a hole in the specimen and a nickel braze wire was included in the bottom of the hole (see Fig. VI-2). After brazing at 1500°C, the thermocouple read approximately 200°C below actual temperature and kept dropping steadily with time.

c. Wires beaded at the end of tantalum insert. Insert brazed in specimen

A tantalum insert was made, and the two thermocouple wires were beaded with the thin end of the tantalum cylinder (see Fig. VI-3). Then the whole assembly was inserted and brazed in the specimen. This thermocouple read correctly for 8 hours; then it started drifting downward at the rate of 50°C/hr.

d. Thermocouple wires in tantalum insert beaded. Insert not brazed

Same as in Fig. VI-3, but insert pricked in specimen. This method of attachment gave a consistent reading for approximately 15 hours. Then it started drifting downward at the rate of 25°C/hr.

e. Thermocouple wires individually pricked in holes in specimen

In accordance with the suggestion of Minneapolis-Honeywell, the two wires were inserted in two individual holes in the specimen and pricked in place (see Fig. VI-4). A test specimen with four thermocouples is under test presently; after 65 hours of operation the thermocouples have not exhibited any drift. The spread of the four thermocouples is about 30 °C. The maximum variation in the difference between any two thermocouples was 14 °C.

B. Test to Determine Heat Loss from Dummy Diode

One dummy diode was tested for heat transfer as shown in Fig. VI-5. By measuring the temperature difference between TC_1 and TC_2, the heat flux down the copper rod was calculated and the design of the dummy diode checked, so that the heat transfer by radiation and conduction would approach that of the actual diodes. The final thickness of the tantalum spacer was determined so that the dummy diodes have from 10 to 15% lower heat transfer than the actual diodes.
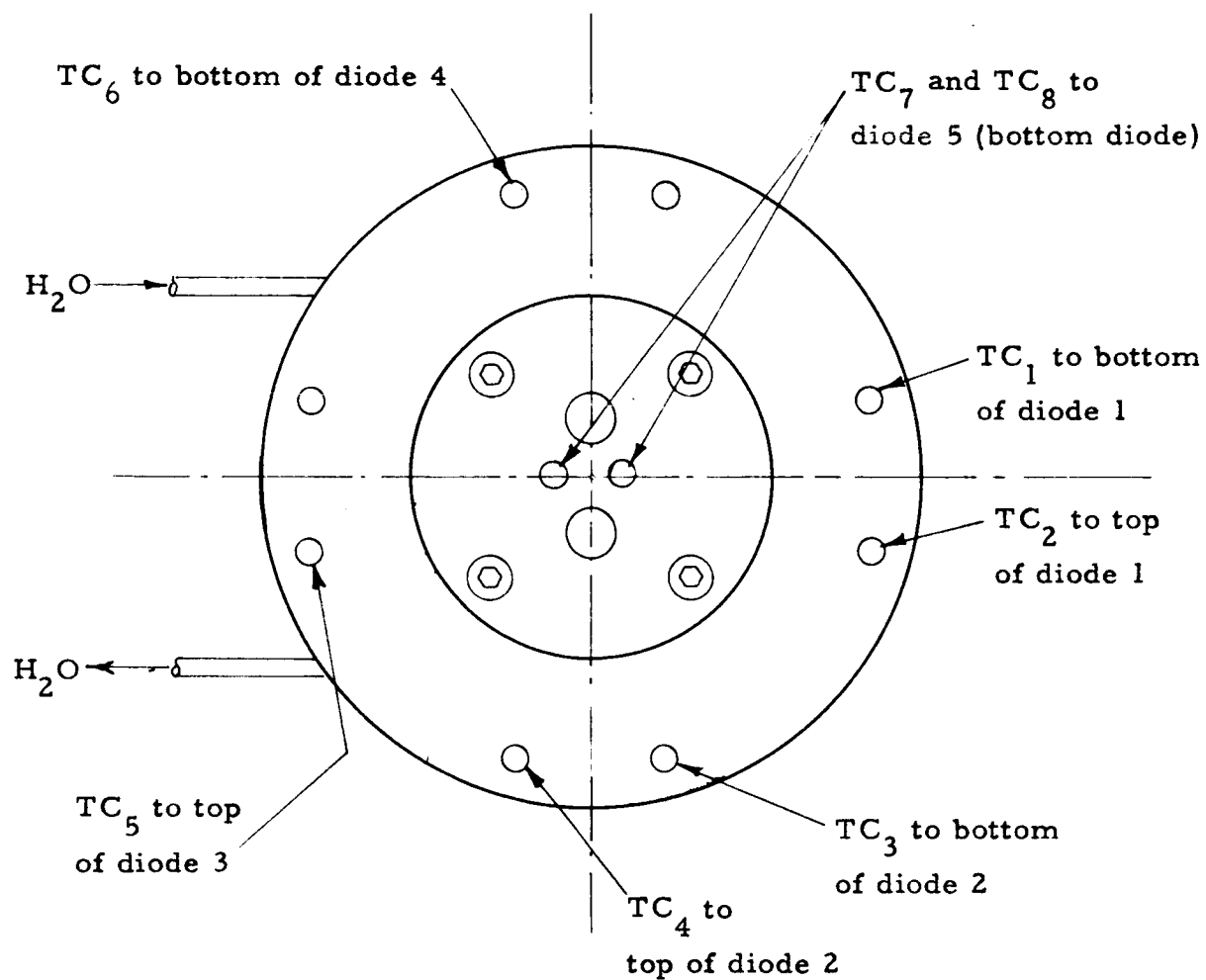
TC$_6$ to bottom of diode 4

TC$_7$ and TC$_8$ to
diode 5 (bottom diode)

H$_2$O

TC$_1$ to bottom
of diode 1

TC$_2$ to top
of diode 1

TC$_5$ to top
of diode 3

H$_2$O

TC$_3$ to bottom
of diode 2

TC$_4$ to
top of diode 2

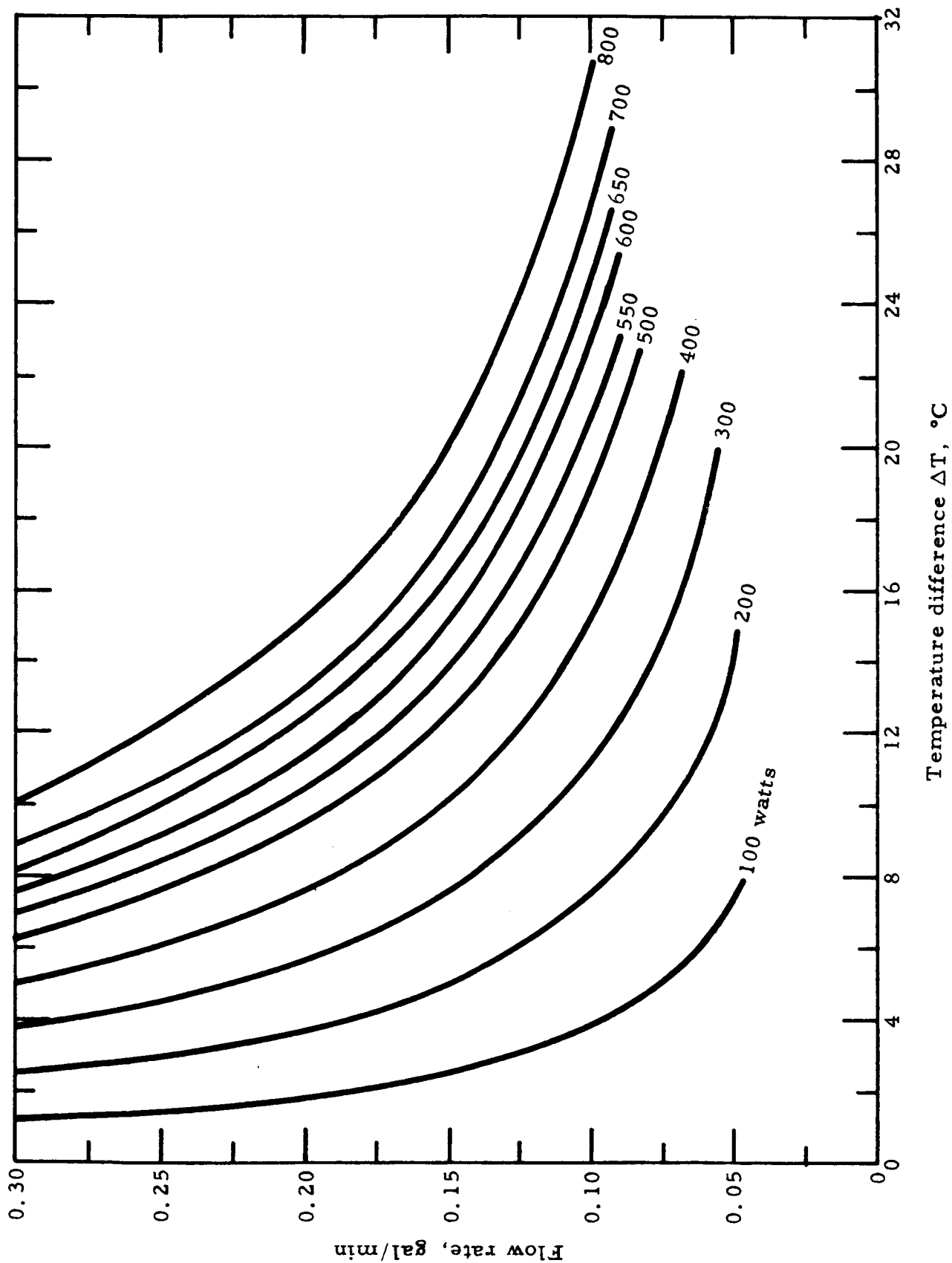Fig. II-1. Bottom view of dummy cavity, showing schematic locations of thermocouples.

Fig. II-2. Temperature rise vs flow rate.

SECTION VII

OPERATING LOG

Operating Log

Dummy Cavity

No.	Time Started	Time Stopped	Purpose of Test	Remarks on Operation	Accumulative Operating Time

164